

University Of Hertfordshire

MSc by Research Degree Thesis

Development of an off the shelf methanol maser telescope

**Author : N.L Chanka
(15043754)**

Supervisor: Dr. M.Thompson

Co-supervisor: Prof. W.Martin

**Centre for Astrophysics Research
School of Physics , Astronomy and Mathematics
University of Hertfordshire**

**Submitted to the University of Hertfordshire in partial fulfilment of the
requirements of the Degree of MSc by Research in Astrophysics**

October 2017

Declaration

I declare that no part of this work is being submitted concurrently for another award of the University or any other awarding body or institution. This master thesis contains a substantial body of work that has not previously been submitted successfully for an award of the University or any other awarding body or institution. Except where indicated otherwise in the submission, the submission is my own work and has not previously been submitted successfully for any award.

Signature of the author: N L Chanka **Date :** October, 2017.

Acknowledgements

Firstly, I would like to express my sincere gratitude to the **Newton Fund-UK** through the Development in Africa with Radio Astronomy (DARA)- Project for funding my MSc studentship at the University of Hertfordshire.

Secondly, I would like to thank my two supervisors: Dr Thompson Mark and Prof Martin William for their aspiring guidance, friendly advice, assistance and dedication in every step throughout the project. Their continuous guidance and support really helped me in all the time of the research and writing this thesis. In particular, I would also like to take this opportunity to thank Prof Martin William for the tools and the lab space he provided for my research work. I would not have imagined having better supervisors for my MSc research than these two supervisors.

Thirdly, my sincere thanks goes to the members of the Centre for Astrophysics Research (CAR) for their support during my research work. Besides the members of CAR, I would like to extend my sincere gratitude to Dr Macleod Gordon and Dr Nicholson George for their guidance and suggestions on my research when I visited Hartebeesthoek Radio Astronomy Observatory (HartRAO).

Most importantly, I am really grateful to God for an awesome opportunity and for the loving family who really supported me through encouragements and prayers. Without all these people's priceless time, none of this work could have happened.

Abstract

Methanol masers are some of the brightest radio sources in the sky with flux densities exceeding several hundred or a thousand of Janskys. This implies that they are very accessible to *small (meter class)* and low-cost radio telescopes, which can then be used to educate and provide hands-on experience with the fundamentals of a radio telescope and an insight into the realm of radio astronomy techniques to students and members of the public interested in radio astronomy. The 12.2 GHz methanol maser line in particular is accessible to Ku band satellite TV receivers and so it could be possible to construct a very low cost (a few hundred dollars or less) methanol telescope out of off-the-shelf satellite TV components. This could then be deployed widely as a teaching tool in schools or colleges, bringing radio astronomy to the wider public. This research work is to design, build, and commission an off-the-shelf methanol telescope. Readers of this work will learn a variety of technical skills in radio astronomy from hardware to software, and ultimately learn how to use a small telescope to monitor bright methanol masers and other astronomical radio sources. One of the most important part of this study is that we have demonstrated how to design, construct, and use a low cost portable radio telescope, which can help students and individuals interested in making small radio telescopes of their own and use them to do cheap radio astronomy experiments. The entire telescope system has room for improvement that can be achieved by doing away with low-cost. Therefore, a bit of investment could solve a number of problems that were encountered in this study due lack of a proper telescope mount and drive system. An inexpensive telescope mount and drive system could be the best solution for easy pointing and tracking of a source, since our meter class radio telescope is not that sensitive which is caused by the size of its antenna. Hence, we are limited to the brightest radio sources.

Key words: 12.2 GHz methanol masers, off-the shelf methanol telescope, and Ku-band.

List of Abbreviations

The following listed abbreviations will be written in full the first time it appears within the main text.

ADC	Analogue to Digital Converter
AM	Amplitude Modulation
ATNF	Australia Telescope National Facility
AVN	African Very (Long Baseline Interferometer) Network
BPF	Band Pass Filter
BWFN	Beam Width to First Null
DARA	Development for Africa with Radio Astronomy
dB	Decibels
DC	Direct Current
DSP	Digital Signal Processing
F	Noise Factor
FM	Frequency Modulated
FWHM	Full Width at Half Maximum
GMT	Greenwich Mean Time
HarTRAO ...	Hartebeesthoek Radio Astronomy Observatory
HPBW	Half Power Band Width
IF	Intermediate Frequency
ISM	Interstellar Medium
JD	Julian Date
Jy	Jansky [$1 \times 10^{-26} W m^{-2} Hz^{-1}$]
k	Boltzmann's constant ($1.38 \times 10^{-23} [JK^{-1}]$)
K	Kelvin
LCP	Left Hand Circular Polarisation
LMST	Local Mean Sidereal Time
LST	Local Sidereal Time
LNA	Low Noise Amplifier

LNB	Low Noise Block
LO	Local Oscillator
MASERs	Microwave Amplification by Stimulated Emissions of Radiation
MSPs	Mega Samples Per Second
NF	Noise Figure
NRAO	National Radio Astronomy Observatory
RA	Right Ascension
RF	Radio Frequency
RMS	Root Mean Square
RFI	Radio Frequency Interference
RCP	Right Hand Circular Polarization
SDR	Software Defined Radio
SF-50	Satellite Finder
SKA	Square Kilometre Array
SSB	Single Side Band
STRI	Science and Technology Research Institute
TV	Television
UTC	Universal Time Coordinated
VSWR	Voltage Standing Wave Ratio

Contents

1	Introduction	1
1.1	Problem statement	2
2	Theoretical background	4
2.1	Astrophysical Masers	4
2.2	Methanol masers	4
2.2.1	The significance of studying methanol masers	6
2.2.2	Methanol maser sources	7
2.3	The feasibility of detecting methanol molecular line at 12.2 GHz	7
2.3.1	Antenna size	7
2.3.2	Spectrometer	8
2.3.3	Full Width to Half Maximum (FWHM)	9
2.3.4	Geometrical Area	10
2.3.5	Aperture Efficiency	10
2.3.6	Antenna Gain	11
2.3.7	Effective Area	12
2.3.8	Beam Solid Angle	12
2.3.9	Power received from radio sources	14
2.3.10	Brightness of the Source	14
2.3.11	Antenna Temperature and Flux density	15
2.3.12	System Temperature	16
2.3.13	Radiometer Sensitivity	18
2.3.14	Integration Time	19
2.4	Drift Scan Technique	20
2.4.1	Azimuth and Elevation	21
2.4.2	Right Ascension and Declination	22
2.4.3	Sidereal and Solar time	23
3	Design and development of the telescope	24
3.0.1	Materials and equipment	24
3.0.2	The design of the methanol maser radio telescope	25
3.0.3	Satellite television dish	25
3.0.4	Low Noise Block- Down-converter	26
3.0.5	In-Line Amplifier	29
3.0.6	Satellite Finder	30
3.0.7	Airspy- software defined radio device	30
3.0.8	DisEqC 1.2 motorised H-H motor	31
3.0.9	Power supply and other components	32
3.0.10	Cabling of the system	35
3.0.11	Computer	35
3.0.12	The complete system of the methanol telescope	35
4	Signal Digitization	37
4.1	Radio astronomy-SDR data logging	38
4.1.1	Radio astronomy observation with Airspy-receiver	38
4.2	Data Recording and Processing with GNU-Radio	39

4.2.1	Digital signal processing and recording with GNU-Radio Companion	39
4.2.2	GQRX Receiver	41
4.3	Data logging with simple_ra software	42
4.3.1	Spectral data processing	42
4.3.2	Continuum data processing	44
4.3.3	Comma Separated Variables (CSV)-data processing	45
5	Commission and calibration of the methanol maser telescope	47
5.1	Commissioning of the telescope	48
5.1.1	Ku band geostationary satellites	48
5.1.2	Solar drift scan	50
5.1.3	Solar drift scan with the methanol maser telescope in Ku band	51
5.2	Calibration of the methanol telescope	53
5.2.1	Antenna beam width	53
5.2.2	Antenna beam solid angle	55
5.2.3	Measured effective area	56
5.2.4	Measured antenna solar Temperature	56
5.2.5	Solar Brightness Temperature	57
5.2.6	System Temperature	57
5.2.7	Measured flux density of the Sun	59
5.2.8	Measurements of the brightest methanol masers	60
5.2.9	Analysis of the measured bright methanol masers	60
5.3	Research Limitations	66
6	Conclusions and proposed future work	68
6.1	Conclusions	68
6.2	Proposed future work	69
	Appendix A	70
	Appendix B	71
	Appendix C	101
	Appendix C	102

List of Figures

1.1	Shows South-Africa and other SKA- partner countries	1
2.1	The radio spectrum of astronomical sources	5
2.2	Shows a sketch of an antenna beam width of a radio telescope	10
2.3	A sketch of a parabolic offset antenna indicating the effective aperture	12
2.4	The beam pattern in polar coordinates	13
2.5	Illustrates the drift scan technique with a single radio telescope	20
2.6	shows the graph of the solar drift scan of the Brage Antenna	21
2.7	Shows the horizon coordinate system for an observer	21
2.8	The measuring of the celestial equator coordinates	22
3.1	Shows a complete schematic diagram	25
3.2	Shows the one-meter offset satellite T.V dish	26
3.3	Universal Ku-band LNB used in the development	27
3.4	Schematic diagram of the Universal Ku-band LNB showing the components inside the LNB	27
3.5	Shows the SVS- 2-02 basic in-line amplifier	29
3.6	Shows the signal meter (SF-50)	30
3.7	Shows an Airspy-Min SDR device used	31
3.8	Indicates the internal components of the Airspy	31
3.9	Illustrates the setting of the Elevation and Declination Angle	32
3.10	Shows the picture of a DisEqC 1.2 motor	33
3.11	Shows the DC-power injector used in this project	33
3.12	The schematic diagram of the DC-power Injector	34
3.13	Switchable DC power supply	34
3.14	Radio Frequency (RF) choke with current of 3A	34
3.15	Shows the picture of a complete hardware of the one-meter class	36
4.1	The digitization of an analogue signal by the SDR-device	37
4.2	Shows different signals observed in real time spectrum analyser	38
4.3	Image of the graphically programmed GNU-radio application	40
4.4	The frequency spectrum plot	40
4.5	Shows the waterfall plot window	41
4.6	Solar observation with a real time spectrum analyser of the GQRX	41
4.7	Is the real time spectral window that measures	43
4.8	shows an image of the square wave bandpass spectrum	43
4.9	The Gaussian of the processed continuum file of the solar drift scan	44
4.10	Shows the Gaussian of the continuum observation of the solar drift scan	45
4.11	Shows the Gaussian of the solar drift scan observed by the 1m UH	46
5.1	Shows the setup of the one-meter off the shelf radio	47
5.2	Shows the other parts of the telescope in the control room	47
5.3	Illustrates the setting up of the latitude and altitude	49
5.4	Shows the observed Astra1N geostationary satellite signal	49
5.5	Shows the observation of the broadband signal from the sun	50
5.6	Some of the magnetic compasses used in the research during observations	51
5.7	Multimode control system of the Simple_ra receiver	52

5.8	Full solar drift scan processed in excel	54
5.9	The results of the half drift scan of the Sun	55
5.10	The square wave bandpass spectrum	61
5.11	Square wave bandpass spectrum of the telescope showing	62
5.12	Illustration of how weak features of the observed signal	65
5.13	Shows the processed weak methanol maser signal	66
6.1	Full solar drift scan observation on a windy and rainy day	101
6.2	Full solar drift scan observation on a windy and rainy day	101
6.3	Observation site at the University	102
6.4	Observation site at the University	102

1. Introduction

Radio astronomy experiments can be considered to be one of the most expensive experiments in the field of astronomy, and generally out of the scope of children in schools and by individual members of the public (Mandal et al., 2016). This is because of the mechanical and economical challenges in the building of enormous radio telescopes that could observe distant astronomical radio sources with low intensities. Some schools and universities in developed countries like the United Kingdom (UK) operate small radio telescopes but these generally lack sensitivity to observe other weak astronomical radio sources apart from the Sun. Most universities in Africa have no radio astronomy facilities due to the radio telescope cost, size and complexity of the data. As a result, most students in African universities pursuing an undergraduate course in physics have no opportunity to do other experiments in astronomy apart from optical astronomy, although they spend several hours per week in physics laboratories. Optical astronomy is one of the most common branch of astronomy performed in schools and universities though it is inconvenient because of experiments done at night and depends more on the weather (Storey and Lloyd, 1993).

Since most African countries are not entirely affected by Radio Frequency Interference (RFI) as compared to other developed countries; lately, Africa has attracted a number of big projects in the field of astronomy that are currently being developed such as the Square Kilometre Array (SKA) and the African Very Long Baseline Interferometer Network (AVN) as shown in figure (1.1).



Figure 1.1: Shows South-Africa as the main host and the other SKA- partner countries. The white dots represents potential array stations of the SKA project <https://vivaafrika.wordpress.com>

Most of these African partner countries of the AVN and the *SKA* project shown in figure (1.1) are quite new in the field of radio astronomy. Therefore, promoting and developing radio astronomy in Africa is part of the objectives of the DARA-project, which is the *Development*

for *Africa with Radio Astronomy*. However, the main aim and objectives of my research work are to design, develop and commission a portable off the shelf radio telescope that could be used to promote radio astronomy in African schools, colleges and to the members of the public. This study has also focused on documenting an instructive guide as part of the thesis on how to build low-cost but high-performance small radio telescopes from commercially available domestic satellite television components.

The small radio telescope developed in this study, has an off-set feed with unblocked aperture, providing an aperture efficiency of 0.68 and with an angular resolution of 1.75° which is equivalent to 0.0305 radians. It is basically built from off the shelf television (T.V) components such as *1-metre satellite T.V dish, Ku-band Low Noise Block (LNB), Satellite finder, In-line amplifier, cheap personal computer, and the Software Defined Radio (SDR)* device. Additionally, the telescope is aimed to prove that a small radio telescope with low sensitivity operating at 12.178597 GHz could detect methanol molecular line. In order to achieve this, a universal Ku band LNB is used as the front-end receiver because of its frequency coverage range i.e. 10.70 - 12.75 GHz that can tune to 12.178597 GHz transition of methanol molecular line in massive star forming regions by using the Aispy-Mini SDR device as a real-time spectrum analyser.

Previous studies indicate that, methanol masers are some of the brightest radio sources in the sky that are produced by one of the most important astrophysical molecular lines in radio spectrum called *methanol molecular line* (Breen et al., 2011). These masers are found to have high flux densities of about hundreds or a thousand Janskys (Fish and Rogers, 2009), and it implies that they can be detected and monitored by a small off the shelf radio telescope operating in a Ku-band hence the name *Methanol Maser radio telescope*. Apart from that, this project focuses on educating people on how they could build their own off the shelf small radio telescopes and observe astronomical radio sources at a low cost. The telescope described in this study, is not only limited to observing methanol masers, but one can still do a number of cheap radio astronomy observations on different astronomical radio sources provided that the front-end receiver (feed horn) is changed to suit one's experiment. The observational capability of this telescope depends on how much one practices with the telescope. It has also been noted that the more you use it, the more you discover what you can observe with it.

1.1 Problem statement

Since methanol masers are considered to be intense and widespread in the Interstellar Medium (ISM) with high flux densities (Rohlfs et al., 2009). It is believed that astronomical methanol molecular line could be accessed by a one-meter class low-cost off-the shelf radio telescope. Therefore, in this study, we explore the possibility of accessing the methanol molecular line with a one-meter low-cost radio telescope. In particular, this study focuses on the possibility of detecting and monitoring the brightest 12.178597 GHz transition of methanol (CH_3OH). The main objectives of this study are addressed in order to promote cheap radio astronomy experiments based on software defined radio in African schools. So that next generation could embrace astronomy projects in Africa and other parts of the world.

Besides that, in this piece of writing, different chapters and sections have been covered to give the reader an insight on how to design, develop and commission an off-the shelf small radio telescope. The following is how the rest of this thesis is structured.

Chapter 1 will give the reader an overview of the entire research project by starting with

an introduction, research goals, problem statement and how the entire thesis is structured.

Chapter 2 gives the theoretical background of this study, by providing the reader with an insight on the feasibility of detecting the brightest methanol masers in massive star forming regions at 12.178597 GHz with a small off-the shelf radio telescope. This chapter also explains the astronomical radio observation techniques used in this study, and some other important equations that are used in the calibration of a single radio telescope.

Chapter 3, In this chapter I will guide the reader on how to develop a low-cost off-the shelf methanol maser radio telescope or small radio telescopes using satellite T.V components and other cheap materials. This chapter will also share and explain the design of the telescope developed in this research work, equipment and materials that made the project possible. Furthermore, I will explain the mechanism and the key components of the methanol maser radio telescope developed in this study.

Chapter 4, this chapter is divided into three major sections that describes signal digitization and the software used in this project such as Airspy Min-Soft Defined Radio, GNU-Radio with GNU-Radio companion, GQRX software and the *Simple.ra* software .The Chapter will start by explain digital signal processing from an ADC (software defined radio device) by the software installed on the computer.

Chapter 5, Involves the commissioning and calibration of the telescope using the solar drift scan and the calibration equations explained in *chapter 2*. Moreover, this chapter explains the observation techniques used in this study and how the detected signal (data) from the Sun can be of used in the calibration of the telescope. In the same chapter, I will also present the reader with the findings and outline the limitations of the current study on the measurements of the brightest methanol masers.

Chapter 6, will conclude the entire research work, and provide the reader with suggestions for the future work that could improve the operation of the telescope based on the limitations of this study outlined in chapter 5.

2. Theoretical background

2.1 Astrophysical Masers

An astrophysical maser is defined as a source of stimulated spectral line emission that occurs naturally in microwave portion of the electromagnetic spectrum. According to previous studies on natural masers, it has been indicated that astrophysical masers are very intense and highly beamed. Therefore, they are considered as some of the brightest radio sources in the sky (Preethi, 2016) & (Fish and Rogers, 2009). MASERs is an acronym for *Microwave Amplification by Stimulated Emissions of Radiation*, which are referred to as the very compact sites that are found within molecular clouds. In addition, there are other astronomical objects that may have masers in them i.e Comets, Planetary atmosphere, Stars, Nebular, Galaxies and Supernova remnants. So far astrophysical masers are known to arise from different types of molecules in space such as *Water (H_2O)*, *hydroxyl radicals (OH)*, *Methanol (CH_3OH)*, *Silicon monoxide (SiO)*, *Ammonia*, *Formaldehyde* and *Hydrogen atom* (Preethi, 2016). Some of these molecules shows the action of masers that are considered to be intense and commonly found in the Interstellar Medium (ISM) such as *water*, *hydroxyl radicals*, *silicon monoxide* and *methanol (CH_3OH)*. These astrophysical masers are known as the compact sources of high brightness temperature that often display narrow spectral line width, polarized emission and variability (Preethi et al., 2008). During the formation of these astrophysical masers, atoms are forced into an excited state and amplify radiation at a specific frequency. As a result, different types of masers are observed at different frequencies. However, In this study our main focus is on the 12.178597 GHz transition of methanol (CH_3OH), which is categorized as a class II methanol line (Fish and Rogers, 2009).

2.2 Methanol masers

Methanol masers have been categorised into two classes such as class I and class II. The classification of these masers depends on the transition that indicates maser action in the methanol molecule. These methanol masers are the most recently discovered intense and widespread masers in the Interstellar medium as compared to other types of masers (Rohlfs et al., 2009). The classification of either weak or strong maser depends on the spectral line radiation produced by a maser. According to Rohlfs et al. (2009), strong masers are known to produce intense spectral line radiation of OH and H_2O , while weaker masers are commonly found in interstellar medium. Moreover, the flux densities of methanol masers indicates the brightness of the source. The literature on the observed methanol masers has shown that detected methanol masers with high flux densities are considered as the brightest or strongest sources. In this research work, we mainly focussed on exploring the possibilities of detecting and monitoring of the 12.178597 GHz of methanol maser molecular line and other brightest astronomical radio sources with a small radio telescope operating in Ku-band. The sketch in figure (2.1) shows the radio spectrum of astronomical sources that can be observed by radio telescopes with different aperture.

The *red vertical line* in figure (2.1), marks the frequency at which the telescope is operating in Ku- band such as the one-meter methanol maser radio telescope developed in this study. Additionally, the *vertical axis* in figure 2.1 represent the flux densities of the sources, whereas the *horizontal lines* indicate the sensitivity that can be accomplished by the radio telescope of that diameter (Koppen, 2007).

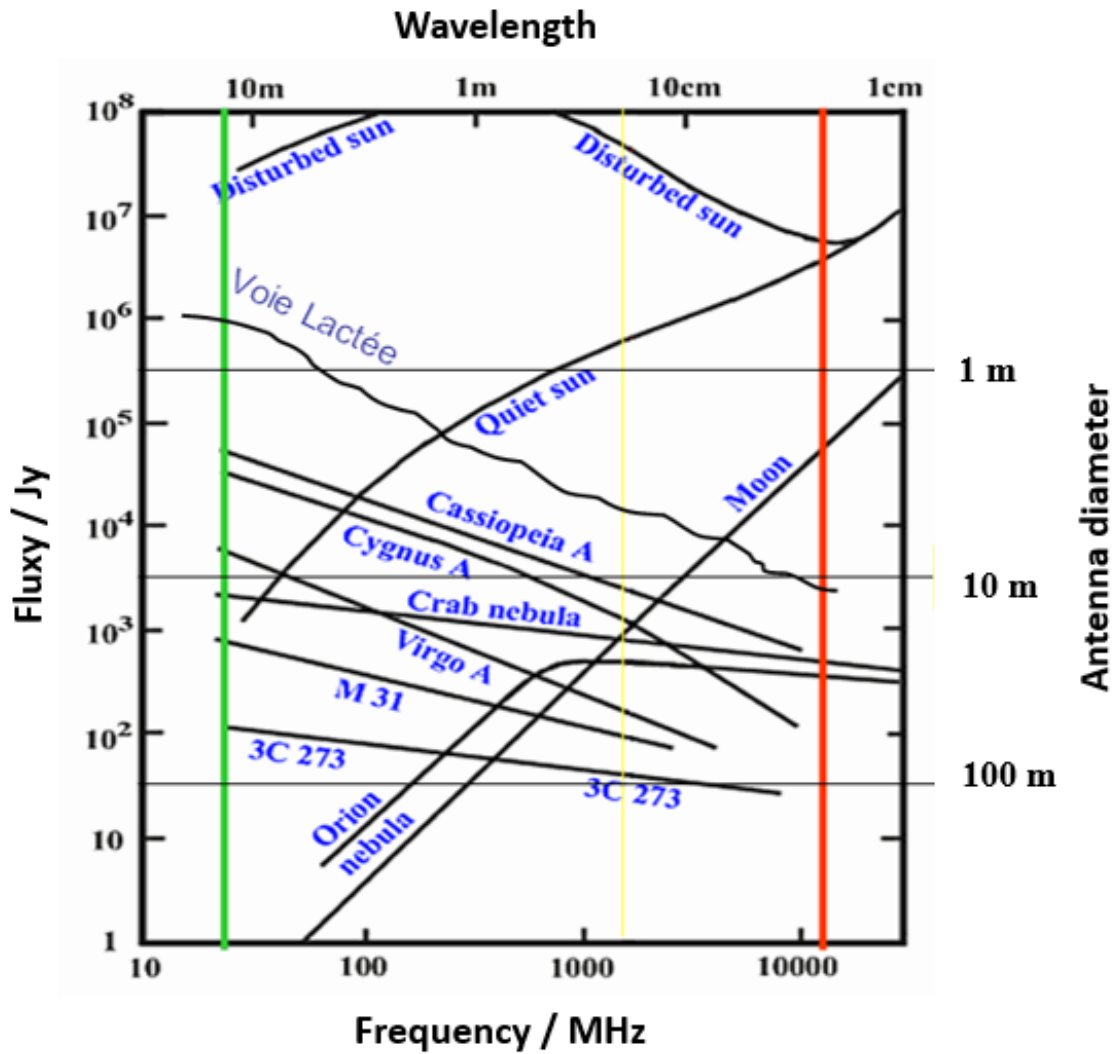


Figure 2.1: The radio spectrum of astronomical sources that can be observed by radio telescopes at different sensitivities marked with 1 m, 10 m, and 100 m (Koppen, 2007)

The class I and II are the only two types of methanol masers that are found in our galaxy. To start with the first class of methanol masers, these masers are mostly associated with sites of star forming regions and are usually found offset from regions where there other types of masers such H_2O and OH (Kurtz et al., 2004). In addition, the class I maser action are in the frequency of 25 GHz, 36 GHz and 96 GHz of methanol transition lines, and they are known to be collisionally pumped (Cragg et al., 1992). On the other hand, the class II methanol masers have been found to show action of strong masers in 6.6 and 12.2 GHz lines of methanol. These masers are often found associate with H II regions or close to the radiatively pumped (Sobolev, 2007). The main focus of this study is on the 12.2 GHz transition of methanol maser $2_0 - 3_{-1} E$, which is categorised as the class II methanol line. This means that the transition of the 12.2 GHz of methanol maser is formed in the presence of a strong radiation fields. Moreover, the 12.2 GHz methanol masers have been studied to be closely associated with the infrared sources OH and the massive star forming regions such as the H II regions (Breen et al., 2011). The nomenclature $2_0 - 3_{-1} E$ of Methanol (CH_3OH) is the energy level which is given by J_K , where k is either a positive or negative value. On the other hand, $J_K = 2_0 - 3_{-1} E$, where E is the energy level (Rohlfs et al., 2009).

Class I and Class II were first called *class A and B*, until *Menten.K.M* introduced the use of notations of class I and II. This was to avoid the confusion of the classes with A and E symmetry of CH_3OH species (Menten, 1991). The 6.6 GHz and 12.2 GHz of methanol masers are found to be interrelated, in the sense that a complete sample of 12.2 GHz has been observed by targeting a complete sample of 6.6 GHz (Breen et al., 2011). The chances of detecting the 12.2 GHz of methanol masers without detecting the 6.6 GHz of methanol maser counterparts are a bit slim. Nevertheless, according to previous studies conducted on methanol masers, the 6.6 GHz methanol masers are mostly found to be stronger with high flux densities as compared to the 12.2 GHz of methanol masers. So far more than a thousand of 6.6 GHz of methanol masers have been found in our galaxy associating with astrophysical objects such as young massive star forming regions and they are highly studied as compared to the 12.2 GHz of methanol masers Breen et al. (2011). Breen (2016), states that, "the Southern galactic plane is the region to search for 12.2 GHz of methanol maser molecular line." This is because it has been noted that the 12.2 GHz methanol masers population follows the population of the 6.7 GHz, which are found in the Southern galactic plane.

The 6.6 GHz ($5_1 - 6_0A^+$) transition of methanol maser were the very first strong emission to be detected by *KarlMenten* in 1991 by using the 43 meter telescope of the National Radio Astronomy Observatory (NRAO) at the Green Bank (Menten, 1991). During the first observation of 6.6 GHz of methanol masers, the telescope had a system temperature in the range of 50 K - 70 K and it was operating at the frequency of 6668.518 MHz. The emission line detected by the 43-meter NRAO telescope was then analysed with an auto correlator with two split parts of 512 channels each. The auto correlator had two bandwidths of 0.625 MHz and 5 MHz with resolution of 0.055 kms^{-1} and 0.44 kms^{-1} per channel respectively (Menten, 1991).

On the other hand, the first detection of the 12.2 GHz transition of methanol maser emission were first reported in 2008. This detection was achieved by targeting 113 known 6.6 GHz transition of methanol masers using the 64-meter Australia Telescope National Facility (ATNF) with the receiver operating in the Ku band and the system temperature of 205 K. The telescope used in the observation was configured to 8192 channels with a bandwidth of 16 MHz for each recorded linearly polarized signal. The observed methanol masers were found to have flux densities in excess of the 5σ detection limit of 0.55 Jy and 30% of these detection were found to be new discoveries (Breen, 2016).

2.2.1 The significance of studying methanol masers

The following are some of the major significance of introducing the study of the astrophysical methanol masers with a low cost off the shelf radio telescope in connection with massive star formation.

- Methanol masers are part of other astrophysical masers that are considered excellent probes of high-mass star formation regions. They are considered excellent tracers of regions where massive star formation is taking place (Ellingsen, 2005), this is because methanol masers are associated with early stages of high mass star forming regions Sanna et al. (2015). In addition, they are also found with other massive star formation tracers such as OH and H_2O masers, strong IR sources, and Ultra Compact (UC) HII regions. Therefore, methanol masers can be used as a tool to study the early stages of evolution of massive stars (Pestalozz.R.M., 2007), and also detect the sites of high mass star formation
- According to Caswell et al. (1993), the study of the 12.2 GHz methanol masers has

shown that these masers vary on a time scales of three months by a factor greater than 10%. Hence, the variability of these methanol masers can be used to study the binary nature of massive star formation.

2.2.2 Methanol maser sources

The table (2.1) below summarizes some of the major brightest sources of the 12.2 GHz methanol masers that could be observed by a small radio telescope like the one developed in this study. In this research work, we focussed on a limited number of strong sources of the 12.2 GHz transition of methanol masers. This is due to our location (northern hemisphere) and the size of the telescope.

Brightest methanol masers at 12.2 GHz				
Source	Flux density	IAU Constellation	Type	Declination angle
NGC 6334	1000 Jy	Scorpius	Supernova remnant	+40°
NGC 7538	1000 Jy	Cepheus	Cluster associate with Nebulosity	+61°
NGC 869	793 Jy	Perseus	Open star	+57° 01'49.5
Great Orion Nebula	400 Jy	Orion	HII region	-5°23'28"
W3(OH)	900 Jy	Cassiopeia	Compact HII region	+61°38'

Table 2.1: Table of brightest methanol masers at 12.2 GHz, with flux densities of several 100 or 1000 Jy in the Northern hemisphere
(Batra et al., 1987) & (Koo et al., 1988)

2.3 The feasibility of detecting methanol molecular line at 12.2 GHz

In this section we will describe the theoretical feasibility of detecting and monitoring the brightest methanol masers in *massive star forming regions* at 12.178597 GHz using a small off the shelf radio telescope with a receiver operating in Ku-band. In addition, we will discuss some of the useful and important equations used in the calibration of radio telescopes in particular single telescopes.

2.3.1 Antenna size

The *size of an antenna* is a very important parameter in the field of radio astronomy, which determines the angular resolution and the sensitivity of the telescope. In this project, we have used a 1-meter offset satellite T.V dish in order to prove that a meter class telescope could observe a strong methanol molecular line. Besides the size of an antenna, it is quite important to consider the type of an LNB to use in an observation. This can be determined by knowing the frequency at which an astronomical radio source can be observed. Since one

of the ultimate aims of this project is to detect and monitor the 12.178597 GHz transition of methanol molecular line as stated in chapter one. A Universal Ku band LNB has been used in this study in order for the telescope to be able tune to strong methanol molecular line in radiative fields such as *massive star forming regions* (Fish and Rogers, 2009).

2.3.2 Spectrometer

The spectrometer required in the development of an off-the shelf system that can monitor the 12.2 GHz methanol masers, is expected to have sufficient bandwidth that can cover the Doppler-shifted velocity range of methanol in massive star forming regions (Fish and Rogers, 2009). Additionally, the frequency resolution of the spectrometer should also be able to resolve methanol molecular line. The spectroscopy used in this project is an Airspy-Mini hardware, which is a software defined radio device. It has the maximum bandwidth of 6 MHz but only 5 MHz can be used. More information on this device will be covered in **chapter 3** of this thesis. Apart from having the right feed and the size of the antenna for the telescope system. There some important few basic parameters of the spectrometer that need to be considered for spectral line observation, and these are:

- **Number of channels** of the spectrum analyser used in this study is determined by the software defined radio hardware (Airspy-Mini) and the software that supports the SDR device during observations such as the *simple_ra*. The number of channels are defined as a feature of the spectrum analyser that allows you to view the observed source. Each software defined radio device has a fixed number of channels over a given bandwidth controlled by the spectrum analyser receiver software i.e the *simple_ra*. Therefore, the total width velocity of an observed source is determined by

$$Total\ velocity\ coverage = \frac{BW}{v} \times c [km/s] \quad (2.1)$$

where

BW is the detector bandwidth

$c = 3.0 \times 10^8$ m/s is the speed of light

v is the frequency at which the telescope is operating.

The measured total velocity coverage and total number of channels can then be used to determine the channel width velocity of the spectrum, which is defined as

$$Channel\ width\ velocity = \frac{Total\ velocity\ coverage}{Number\ of\ channels} [km/s] \quad (2.2)$$

In order to determine the actual bandwidth per channel you use equation (2.3)

$$Bandwidth\ per\ channel\ (\Delta v) = \frac{BW}{Number\ of\ channels} [kHz] \quad (2.3)$$

The calculated *Bandwidth per channel* with other parameters can then be used to determine the Root Mean Square (RMS) noise per channel, which gives the Signal to Noise Ratio (SNR).

- In the case where the line is still resolved and you have more total number of channels than the required amount, a reduction in the number of channels and an increase in the channel width can be achieved by averaging over a number of channels. This could lead to the reduction of the RMS noise by a factor of the square root of number of

channels. Therefore, the effective number of channels can be determined by equation (2.4),

$$\text{Effective number channels} = \frac{\text{Total Number of channels}}{\text{Number of Averaged channels}} \quad (2.4)$$

and the new channel width can be found by dividing the *Total velocity* by the *effective number of channels* which is given by

$$\text{Channel width} = \frac{\text{Total velocity coverage}}{\text{Effective Number of channels}} \text{ [km/s]} \quad (2.5)$$

All these parameters discussed in this section, will be used in the analysis of the measurements of the methanol masers in **chapter (5.)**.

2.3.3 Full Width to Half Maximum (FWHM)

The FWHM is an acronym for Full Width to Half Maximum, which is sometimes referred to as the Half Power Band Width (HPBW) of radiation pattern of a circular antenna (Rohlfs et al., 2009) & (Gaylard, 2012). This parameter determines the beam angular resolution of the telescope by using equation (2.6).

$$\begin{aligned} FWHM &= HPBW \\ &= \text{Beam width}(\theta) \\ &= \frac{1.2\lambda}{D} \text{ [Radians]} \end{aligned} \quad (2.6)$$

where

D is the diameter of the telescope antenna in [m]

λ is the wavelength [m]

Let us determine the beam angular resolution of our telescope with the diameter (D) of 1 m and $\lambda = 0.025$ m. The wavelength (0.025 m) was determined by considering that, $\lambda = c/v$, where c is the speed of light $c = 3.0 \times 10^8$ m/s, and $v = 12.1785$ GHz is the frequency at which the telescope is operating. Using equation (2.6) which is the (FWHM) for a single dish telescope, the beam angular resolution of our telescope is determined as follows.

$$\begin{aligned} FWHM &= HPBW = \text{Beam width}(\theta) \\ &= \frac{1.2 \times 0.0246\text{m}}{1\text{m}} \\ &= 0.0295 \text{ Radians} \\ &= 1.70^\circ. \end{aligned} \quad (2.7)$$

Hence, the calculated beam angular resolution of the one-meter off-the shelf methanol telescope developed in this study is 1.70° at the wavelength of 0.0246 m.

In figure (2.2), the acronym *BWFN* is defined as the Beam Width between First Nulls, which is denoted by the two dots along the x-axis (Rohlfs et al., 2009). On the other hand, *EWMB* is an acronym for *Equivalent Width of the Main Beam*, which is defined by equation (2.8).

$$EWMB = \sqrt{\frac{12\Omega_M}{\pi}} \quad (2.8)$$

where Ω_M is the Main beam solid angle.

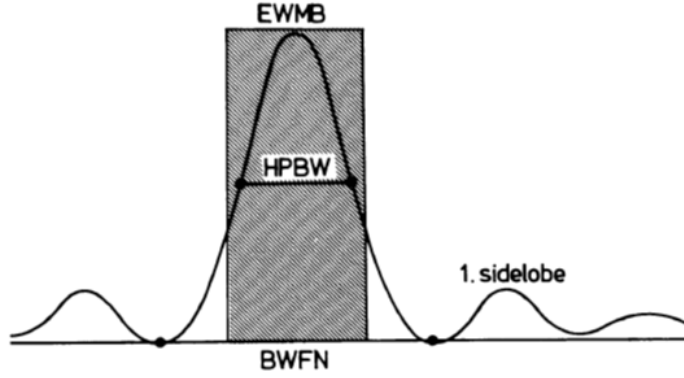


Figure 2.2: Shows a sketch of an antenna beam width (FWHM or HPBW) of a radio telescope with other parameters such as *EWMB* and *BWFN* (Rohlf et al., 2009)

2.3.4 Geometrical Area

The geometrical area of a radio telescope is defined as the physical area of the entire radio telescope antenna, which can be determined by using equation (2.9)

$$A_{geo} = \frac{\pi D^2}{4} \quad (2.9)$$

where D is the diameter of the antenna in meters. Given that, the manufacturer's quoted and measured diameter of our antenna is 1 meter. Therefore, let us use equation (2.9) to determine the geometrical area of our 1-meter radio telescope developed in this study.

$$\begin{aligned} A_{geo} &= \frac{\pi(1 \text{ m})^2}{4} \\ &= \frac{3.142 \times (1\text{m})^2}{4} \\ &= 0.786 \text{ m}^2 \end{aligned} \quad (2.10)$$

Therefore, 0.786 m^2 is the calculated physical area of the 1-meter antenna used in the development of the off-the shelf methanol maser radio telescope for this research work.

2.3.5 Aperture Efficiency

The aperture efficiency (η) of a radio telescope is defined as the ability of the telescope to detect incoming radiation from space. Previous studies indicate that, a typical radio telescope is expected to have an aperture efficiency in the range of 0.6 to 0.7 (Gaylard, 2006). The aperture efficiency of any type of a radio telescope is never 100%, whether it be a typical or an off the shelf radio telescope. This is caused by various factors that prevent the telescope from detecting all the incoming radiation from the source such as the model of the antenna, how the radio telescope is built, Spillover loss, Mismatch (VSWR) loss, and RF losses. However, the aperture efficiency of the telescope can either be determined by equation (2.11) or (2.12) provided that some of the parameters are known such as the effective Area (A_{eff}), geometrical area (A_{geo}), and the antenna gain (G) of the telescope.

$$\eta = \frac{A_{eff}}{A_{geo}} \quad (2.11)$$

Since the manufacturer's quoted gain of our antenna (G) = 40.3 dB $\equiv 1.07 \times 10^4$. Therefore, we can use equation (2.11) to determine the aperture efficiency of our telescope. Given that, the effective area of the telescope antenna is $A_{eff} = G\lambda^2/4\pi$, substituting it in equation (2.11) we will get equation (2.12).

$$\begin{aligned}\eta &= \frac{G\lambda^2}{4\pi A_{geo}} \\ &= \frac{(1.07 \times 10^4)(0.025 \text{ m})^2}{4\pi \times 0.786 \text{ m}^2} \\ &= 0.677 \\ &= 0.68\end{aligned}\tag{2.12}$$

Therefore, the calculated aperture efficiency of our small radio telescope is 0.68, which is within the expected range of the aperture efficiency of typical radio telescopes as stated earlier in this section.

2.3.6 Antenna Gain

The antenna gain of a radio telescope is sometimes referred to as the telescope system gain, which is directly proportional to the *aperture efficiency, physical area* of the telescope antenna and inversely proportional to the *square of the wavelength* as stated in equation (2.13).

$$G = \frac{4\pi A_{geo}\eta}{\lambda^2}\tag{2.13}$$

where A_{geo} is the physical area of the telescope antenna, η is the aperture efficiency and λ is the wavelength [m]. The antenna gain equation in (2.13) is determined by considering that

$$G = \frac{4\pi}{\Omega_A}\tag{2.14}$$

where the beam solid angle (Ω_A) = $\frac{\lambda^2}{A_{eff}}$. Recall that, equation (2.11) implies that the effective area of the antenna $A_{eff} = A_{geo} \times \eta$. Therefore, we can use equation (2.13) to illustrate how to determine the antenna gain of our telescope at the wavelength of 0.025 m.

$$\begin{aligned}G &= \frac{4\pi \cdot 0.786 \text{ m}^2 \times 0.677}{(0.025 \text{ m})^2} \\ &= 10698.9\end{aligned}\tag{2.15}$$

The calculated antenna gain in dimensionless can be converted into dB (decibels), which is defined as the Gain (G) of an amplifier in the engineering units given by equation (2.16).

$$\begin{aligned}Gain(dB) &= 10\log_{10}G \\ &= 10\log_{10}[10698.9] \\ &= 40.29dB \\ &= 40.3dB\end{aligned}\tag{2.16}$$

The antenna gain of a typical radio telescope with a good aperture efficiency of about 70 % (0.7) is expected to be in the range of 100 000 to 10 000 000 in dimensionless units, which is equivalent to 50 dB to 70 dB (Gaylard, 2012). However, the calculated and quoted antenna gain by the manufacturer of the antenna used in this study is less than the expected gain range for an ideal radio telescope antenna. The reduction in the antenna gain of our telescope is affected by the small amount of the aperture efficiency caused by the small size of the telescope antenna.

2.3.7 Effective Area

The effective area of a radio telescope antenna is defined as the area of an antenna that is effective in the collecting of the incoming radiation from radio sources (Kraus, 1986). The entire surface area of the telescope antenna is known not to be 100% efficiency. This means that the entire physical area of a radio telescope antenna does not detect all the incoming radio waves from the source, due to the design of the antenna used in the development of the telescope. Sometimes incoming radio waves are blocked from being detected by the antenna due to other parts of the telescope (Gaylard, 2006). Moreover, there is also spillover loss which is caused by the feed power pattern, some of the radiation does not contribute to the main beam as it falls outside the edge of the telescope dish. This has a great influence on the effective area and antenna efficiency of the telescope. According to the sketch in figure (2.3)

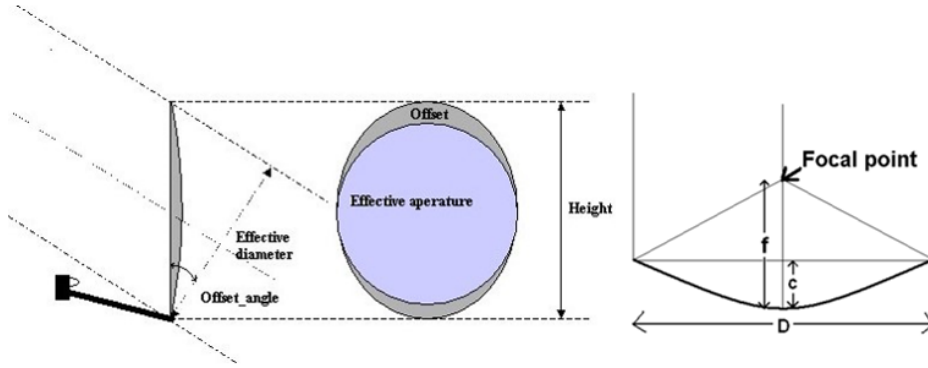


Figure 2.3: A sketch of a parabolic offset antenna indicating the effective aperture, offset angle and effective diameter (Antenna, 2017). On the right hand side, the figure shows the focal point, antenna diameter (D), focal length (f) and the depth of the antenna (c).

Effective diameter of a parabolic dish is defined as ($\text{Antenna height} \times \cos(\text{offset angle})$), which is equivalent to the antenna width and aperture diameter. Where $\text{offset angle} = (\text{Arc cos}(\text{antenna width} \times \text{Antenna height}))$. The focal length (f) of an antenna is another important parameter which is given by $f = D^2/16c$ [m].

The effective collecting area of the telescope antenna is given by equation (2.17), which is defined as the product of the physical or geometrical area of the dish and its aperture efficiency.

$$\begin{aligned} A_{eff} &= A_{geo}\eta \\ &= 0.677 \times 0.7855 \text{ m}^2 \\ &= 0.532 \text{ m}^2 \end{aligned} \quad (2.17)$$

This means that, only 68% of the measured physical area (0.7855 m^2) of the antenna used in this study is effective in the collection of the incoming radio emissions from space.

2.3.8 Beam Solid Angle

The beam solid angle for an antenna is an angular area that is measured in *radians*² or steradian (sr) (Kraus, 1986). The following equation in (2.18), describes the beam solid angle that has been subtended by an object with an angular radius of θ radians.

$$\Omega = 2\pi(1 - \cos\theta) \text{ [sr]}. \quad (2.18)$$

Let us consider the following two cases of the beam solid angle with a small angular radius and an isotropic antenna.

1. In the case of a small angular radius θ , the solid angle Ω is defined by equation (2.19)

$$\Omega = \pi\theta^2 \text{ [sr]}. \quad (2.19)$$

2. The second case is where an *isotropic* antenna used that sees the whole sky, and is considered to be equally sensitive to radio emissions from all directions Gaylard (2012). For this type of an antenna $\theta = \pi$, which implies that $\cos\theta = -1$. Using equation (2.19) and substituting $\cos\theta = -1$, Therefore, this shows that the entire sky has the solid angle of 4π [sr] as shown in equation (2.20)

$$\begin{aligned} \Omega &= 2\pi(1 - (-1)) \\ &= 4\pi \text{ [sr]}. \end{aligned} \quad (2.20)$$

The sketch in figure (2.4) shows the power pattern, main beam, and side-lobes in polar coordinates.

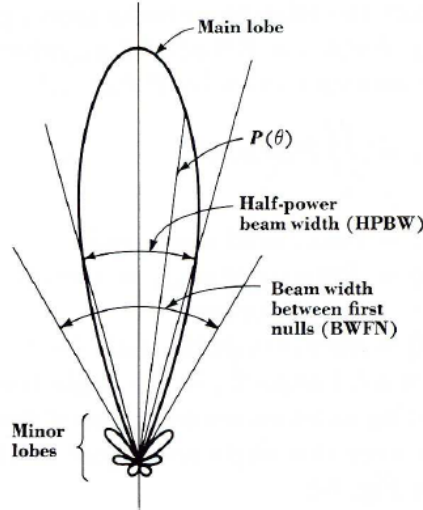


Figure 2.4: The beam pattern in polar coordinates showing measures of the Main lobe, HPBW, BWFN and Minor lobes Kraus (1986)

Therefore, the total beam solid angle is defined by equation (2.21)

$$\Omega_A = \iint_{4\pi} P_n(\theta, \phi) d\Omega \text{ [sr]}. \quad (2.21)$$

where

$P_n(\theta, \phi)$ is the antenna beam power pattern, which is defined as "the response of an antenna to incoming power as a function of the direction of the incoming electromagnetic wave as measured from optical axis of the antenna" DeWitt (2017). The main beam solid angle is achieved by integrating only the first minimum of the beam pattern, and hence the result is stated below

$$\Omega_M = \iint_{mainlobe} P_n(\theta, \phi) d\Omega \text{ [sr]}. \quad (2.22)$$

where Ω_M denotes the main beam pattern.

According to Kraus (1986), the beam solid angle of the telescope is also defined as the ratio of the square of the wavelength (λ) to the effective area (A_{eff}) of the telescope antenna.

$$\begin{aligned}\Omega_A &= \frac{\lambda^2}{A_{eff}} \\ &= \frac{\lambda^2}{A_{geo}\eta} [sr].\end{aligned}\tag{2.23}$$

where η , A_{geo} is the aperture efficiency and the geometrical area of the telescope antenna respectively as discussed earlier in this chapter.

2.3.9 Power received from radio sources

The amount of power received by the telescope from radio sources in the sky is determined by equation (2.24), which is defined as the power (W) received per unit bandwidth, in each polarization from an element of solid angle of the sky (Kraus, 1986).

$$W = \frac{1}{2} A_{eff} \iint_{\Omega} B(\theta, \phi), P_n(\theta, \phi) d\Omega [W Hz^{-2} \text{ per polarization}]\tag{2.24}$$

where

A_{eff} is the effective collecting area of an antenna [m^2]

$B(\theta, \phi)$ is the brightness distribution of radio emission across an antenna [$W m^{-2} Hz^{-1} sr^{-1}$]

$P_n(\theta, \phi)$ is the normalized power beam pattern of the antenna

$d\Omega = \sin\theta d\theta d\phi$ is the element of the solid angle [sr]

2.3.10 Brightness of the Source

The brightness (B) of an observed source is determined by considering the Planck's Law for a blackbody radiator, which is given by

$$B = \frac{2hv^3}{c^2} \frac{1}{e^{\frac{hv}{kT}} - 1} [W/m^2/Hz/rad^2]\tag{2.25}$$

Where : B is the brightness of the observed source

h is the Planck's constant which is given by ($6.63 \times 10^{-34} Js$)

v is the frequency in [Hz]

c is the speed of light = $3 \times 10^8 m/s$

$k = (1.38 \times 10^{-23} J/K)$ is the Boltzmann's constant

(T) = temperature [K].

When you are dealing with a centimeter wavelength regime $hv \ll kT$, therefore Taylor series is used to expand $e^{\frac{hv}{kT}} - 1$ to produce the Rayleigh-Jeans approximation for back-body radiation at radio wavelengths (O'Neil, 2001).

$$\begin{aligned}B &= \frac{2kTv^2}{c^2} \\ &= \frac{2kT}{\lambda^2} [W/m^2/Hz/rad^2]\end{aligned}\tag{2.26}$$

2.3.11 Antenna Temperature and Flux density

The antenna temperature (T_A) of a radio telescope is the parameter that describes how much radio emission is measured from the source. Its output measurement is in Kelvin (K) and it is also called the *antenna noise temperature* of the source (DeWitt, 2017). According to Gaylard (2012), the antenna noise temperature has no connection with the physical temperature of the telescope antenna, and it is easily determined by the different stated equations from depending on the type of an observed source. Using Rayleigh-Jeans approximation equation (2.26) for blackbody radiation at radio wavelengths, we can determine the antenna noise temperature

$$T_A = \frac{B\lambda^2}{2k} \quad (2.27)$$

Since the flux density of the source is given by $f_v = B\Omega_A$, therefore, we have the following equation as the antenna temperature

$$T_A = \frac{f_v\lambda^2}{2k\Omega_A} \quad (2.28)$$

where

f_v is the flux density of an observed point source

Ω_A is the beam solid angle and

λ is the wavelength [m]

The flux density (f) of an observed source is defined as the integral of the brightness over a source (Rohlfs et al., 2009), which is given by by equation ().

$$f = \iint_{source} B(\theta, \phi) d\Omega [Wm^{-2}Hz^{-1}] \quad (2.29)$$

For the case where the temperature over the emitter is not uniform, the flux density is defined as the integral of the temperature distribution over the object, which is given by the following equation

$$f_v = \frac{2k}{\lambda^2} \iint_{source} T(\theta, \phi) d\Omega [Wm^{-2}Hz^{-1}] \quad (2.30)$$

Considering that, the temperature distribution of the source is uniform across a solid angle. The flux density in equation (2.30) reduces to equation (2.32)

$$f_v = \frac{2kT_A\Omega_B}{\lambda^2} [Wm^{-2} Hz^{-1}] \quad (2.31)$$

Recall that $\Omega_A = \frac{\lambda^2}{A_{eff}}$, therefore, the total antenna temperature (T_A) for the general situation is given by equation (2.32), which determines the total antenna temperature in the main beam from different sources of radiation in all directions in proportion to the pattern response (Kraus, 1986).

$$\begin{aligned} T_A &= \frac{A_{eff}}{\lambda^2} \iint T_{source}(\theta, \phi) P_n(\theta, \phi) d\Omega [K] \\ &= \frac{1}{\Omega_A} \iint T_{source}(\theta, \phi) P_n(\theta, \phi) d\Omega [K] \end{aligned} \quad (2.32)$$

where

Ω_A is the antenna solid angle as stated earlier

$P_n(\theta, \phi)$ is the antenna power pattern.

In the case where a point source is observed $P_n(\theta, \phi) \sim 1$ over the solid angle, then the antenna temperature is defined by

$$\begin{aligned} T_A &= \frac{1}{\Omega_A} \iint_{\Omega_s} T_{source} d\Omega \\ &= \frac{\Omega_s}{\Omega_A} T_{avg} [K] \end{aligned} \quad (2.33)$$

where T_{avg} is the brightness temperature averaged over the observed source. But if the source is larger than the antenna beam size and the brightness temperature is constant (T_{const}). Then, the antenna temperature is given by

$$T_A = \frac{T_{const}}{\Omega_A} \iint_{source} P_n(\theta, \phi) d\Omega [K] \quad (2.34)$$

Note that if the source solid angle (Ω_s) is greater than the antenna beam size, then $T_A = T_{const}$, (O'Neil, 2001).

2.3.12 System Temperature

The system temperature (T_{sys}) of a radio telescope is defined as the addition of all the energy received by the telescope from several different radio sources during an astronomical observation (Gaylard, 2012). This implies that different radio sources are detected and recorded when the telescope is pointed in the sky. The detection of these emissions from different radio sources depends on the frequency or the wavelength at which the telescope is operating, and other factors. The combination of all the detected radio sources is called the System temperature which is given by the following equation (Gaylard, 2006).

$$T_{sys} = T_{cmb} + T_A + T_{at} + T_{vw} + T_g + T_R [K] \quad (2.35)$$

where

1. T_{cmb} is the Cosmic Microwave Background (CMB) radiation that is always detectable by radio telescopes. The literature on CMB indicate that, the CMB is known to be found in every direction the telescope is pointed in space, and it cannot be avoided (Gaylard, 2006) & (Rohlfs et al., 2009). The contribution of the CMB radiation to the system temperature of the telescope is highly influenced by the frequency at which the telescope is operating i.e. at 12 GHz we expect to have 2.5 K of CMB (DeWitt, 2017). Moreover, the brightness temperature of 2.7 K is the known amount of the blackbody radiation temperature of the cosmic microwave background Rohlfs et al. (2009).
2. T_A is the antenna temperature, which is defined as the output of the radio emission source measured by the telescope in Kelvin (K).
3. T_{at} is known as the atmosphere temperature that is contributed by the radiation from dry atmosphere during an observation. The amount of contribution of this radiation is about 1K (Kraus, 1986).

4. T_{wv} is the amount of the radiation contribution from water vapour in the atmosphere. The amount of water vapour temperature detected by the telescope depends on the humidity of the atmosphere. Previous studies has shown that at the frequency of 12 GHz, water vapour temperature in the range of 1-2 K in low humidity cases is detected by the telescope (Gaylard, 2006).
5. T_g is the contributed radiation from the ground temperature, which is received by the feed through the antenna side-lobes from the ground temperature of about 290 K. The amount of T_g contribution depends on how the telescope is pointed i.e. T_g contributes of about 5-15 K when the telescope is pointed straight up at zenith and increases when the telescope is pointing close to horizon (DeWitt, 2017). In addition, there is also contribution from spillover from the feed, which depends on the choice of the antenna or dish used in the development of the telescope.
6. T_R : O'Neil (2001), define T_R as the receiver noise temperature that is caused by amplifiers in the receiver that generates noise in the form of electronic noise.

Let the sky temperature (T_{sky}) be

$$T_{sky} = T_{cmb} + T_{at} + T_{wv} + T_g \text{ [K]} \quad (2.36)$$

Using the sky temperature T_{sky} stated in equation (3.37), the system temperature in equation (2.35) reduces to

$$T_{sys} = T_{sky} + T_A + T_R \text{ [K]} \quad (2.37)$$

where T_R is the Receiver Noise Temperature, which is defined by equation (2.38) Kraus (1986).

$$T_R = T_1 + \frac{T_2}{G_1} + \frac{T_3}{G_1 G_2} + \frac{T_n}{G_1 + \dots G_{n-1}} \text{ [K]}. \quad (2.38)$$

where $T_1, T_2 \dots T_n$ represent the noise temperature at different stages, from stage 1 to n of the receiver, while $G_1, G_2 \dots G_{n-1}$ represent the available power gain values of different stages starting with 1 to n-1 of the receiver measured in dimensionless units. Therefore, with the measured receiver noise temperature (T_R), we can determine the other three different but related noise of the system i.e noise factor (F), Noise Figure (NF) and the noise temperature. The noise factor of the receiver is defined by equation (2.39)

$$F = 1 + \frac{T_R}{290K} \quad (2.39)$$

The units for the noise factor of the receiver is dimensionless, and the relationship between the receiver noise factor and noise figure is given by equation (2.40)

$$NF = 10 \log F \text{ [dB]} \quad (2.40)$$

Substituting equation (2.39) into equation (2.40) we have the following

$$NF = 10 \times \log_{10} \left(\frac{T_R}{T_{Ref}} + 1 \right) \text{ [dB]} \quad (2.41)$$

The noise temperature of the receiver is the parameter that measures the temperature at which the resistor of the system input generates the same amount of noise measured at the output (Blattenberger, 2016). It can be determined by considering the relationship between

the noise figure and the noise temperature of the LNB (receiver), which is given by equation (2.42)

$$Noise\ Temp = T_{Ref} \times (10^{NF/10} - 1) [K] \quad (2.42)$$

where $T_{Ref} = 290K$ is the reference temperature unless otherwise specified. Since the manufacturer's quoted NF 0.1 dB of the LNB / receiver used in this study. We can then use it to determine the noise temperature of the receiving system of our small radio telescope by considering equation (2.42).

$$\begin{aligned} Noise\ Temp &= T_{Ref} \times (10^{NF/10} - 1) \\ &= 290K \times (10^{0.1dB/10} - 1) \\ &= 6.75K \\ &= 7K \end{aligned} \quad (2.43)$$

Therefore, 7 K is the noise temperature of the receiving system of the telescope in this study that includes the antenna at Input.

2.3.13 Radiometer Sensitivity

The input signal collected from the antenna during the detection of radio emissions from space is in the form of noise, which is then converted into a digital signal output by the ADC. The output voltage in each polarization shows fluctuations with a root mean squared size ΔT_{rms} (Gaylard, 2012)

$$\Delta T_{rms} = \frac{T_{sys}}{\sqrt{\Delta\nu\tau}} [K] \quad (2.44)$$

The size of fluctuations of the output voltage in each polarization is defined by equation (2.44), which states that ΔT_{rms} is directly proportional to the system temperature of the telescope that depends on the square root of the receiver bandwidth $\Delta\nu$ and the integration time (τ) (Gaylard, 2006). where (τ) is the integration time in seconds (s). The stated equation in (2.44) is referred to as the *radiometer sensitivity equation*. Let us consider a case where there is an averaging of n repeated scans, then radiometer sensitivity equation will be defined by equation (2.45)

$$\Delta T_{rms} = \frac{K_R T_{sys}}{\sqrt{\Delta\nu\tau n}} [K] \quad (2.45)$$

where

$K_R=1$, which is the sensitivity constant of the instrument for a single radiometer n is the number of records averaged, which leads to the reduction of the noisy fluctuations in the output signal (O'Neil, 2001).

For the case when there is a minimum change in antenna temperature ΔT_{min} , equation (2.46) and equation (2.47) are used to determine the ΔT_{min} and Δf_{min} respectively.

$$\Delta T_{min} = 3\Delta T_{rms} [K] \quad (2.46)$$

The above equation in (2.46), defines the smallest amount of change in antenna temperature ΔT_{min} , which is three times the rms noise (Kraus, 1986). On the other hand, the minimum detectable flux density (Δf_{min}) is given by equation (2.47), which depends on the effective area of antenna and system noise temperature.

$$\Delta f_{min} = \frac{3K_R k T_{sys}}{A_{eff} \sqrt{\Delta\nu \tau n}} \times 10^{26} [Jy] \quad (2.47)$$

where

Δf_{min} = the minimum detectable flux density measured in Janskys [Jy], ($1 \text{ Jy} = 1 \times 10^{-26} \text{ W m}^{-2} \text{ Hz}^{-1}$)

$K_R = 1$ [dimensionless] is the sensitivity constant for the receiver

T_{sys} is the system noise temperature measured in Kelvin [K]

Δv = detectable bandwidth per channel in Hz,

n is the number of records averaged

$k = 1.38 \times 10^{-23} [JK^{-1}]$, which is the Boltzmann's constant

A_{eff} is the effective area of the receiving antenna measured in m^2

With equations (2.44), (2.46) and (2.47), one can determine the amount of noise in the recorded data. Furthermore, we can also use the stated equations to predict the period it could take to observe radio sources of known flux densities as illustrated in the **subsection (2.3.14)** of this chapter.

2.3.14 Integration Time

The integration time (τ) is defined as the period over which the detected signal by the telescope is averaged. Given that, you know the system temperature, effective area of the antenna and the bandwidth of a single spectral channel; one can determine the time it could take to observe radio emissions from space by using equation (2.48) to obtain equation (2.49).

$$\Delta f_v = \frac{2kT_{sys}}{A_{eff}\sqrt{\Delta v\tau}} [Jy] \quad (2.48)$$

From equation (2.49) below, we can determine the period it could take to detect 1000 Jy of the 12.2 GHz of methanol maser molecular line with our telescope.

$$\tau = \frac{(2 k T_{sys})^2}{\Delta v (A_{eff} \times \Delta f_v)^2} \quad (2.49)$$

For example, let us assume that the small radio telescope developed in this research work has a system temperature of 100 K or less. This assumption is based on the literatures that have been written on small radio telescopes, and since the LNB used on this telescope has an excellent NF of 0.1 dB as quoted by the manufacturer although this might not be true. Considering that the calculated bandwidth for a single spectral channel is 1.466 kHz as shown in **section 5.29** of chapter 5, with an effective collecting area (A_{eff}) of 0.53 m^2 .

Firstly, making Use of equation (2.49), let us determine the period it could take to detect 1000 Jy of 12.2 GHz of methanol maser molecular line with our telescope. For a detection we require a Signal to Noise Ratio ($\frac{S}{N}$) > 3 . However, since we know the flux density of the source, we can determine the change in the flux density by $\frac{f_v}{\Delta f} > 3$ which is equivalent to $f_v = 3\Delta f_v$. Since the source of radio emission we want to detect has the $f_v = 1000 \text{ Jy}$, then $\Delta f_v = f_v/3 = 333.3 \text{ Jy}$. Substituting all the known valuables into equation (2.49)

$$\begin{aligned} \tau &= \frac{(2 \times 1.380 \times 10^{-23} \text{ W Hz}^{-1} \text{ K}^{-1} \times 100 \text{ K})^2}{1.468 \times 10^3 \text{ Hz} (0.53 \text{ m}^2 \times 333.3 \times 10^{-26} \text{ W/m}^2 \text{ Hz}^2)^2} \\ &= 1665 [s] \\ &= 27.7 \text{ minutes} \end{aligned} \quad (2.50)$$

Therefore, with our system it could take about 27.7 minutes of integration time or less to detect the 12.2 GHz of methanol molecular line with a flux density of 1000 Jy.

Secondly, let us consider determining the period it could take to detect a source with a lower flux density such as *Great Orion Nebula* with a flux density of 400 Jy using our small telescope. Since $f_v = 400 \text{ Jy}$, this implies that $\Delta f_v = f_v/3 = 133.3 \text{ Jy}$.

$$\begin{aligned} \tau &= \frac{(2 \times 1.380 \times 10^{-23} \text{ W Hz}^{-1} \text{ K}^{-1} \times 100 \text{ K})^2}{1.468 \times 10^3 \text{ Hz} (0.53 \text{ m}^2 \times 133.3 \times 10^{-26} \text{ W/m}^2 \text{ Hz}^2)^2} \\ &= 10,410 \text{ [s]} \\ &= 173 \text{ minutes} \end{aligned} \tag{2.51}$$

From the calculations above, we can conclude that it could take a longer period of integration to detect weaker sources than stronger sources. Hence, this research work focussed on stronger sources of methanol masers.

2.4 Drift Scan Technique

The drift technique is one of the oldest and common radio astronomical observation techniques that was even used by *Karl Jansky* in 1931, to discover radio emissions from the Milky way (Kraus, 1986). This observational technique involves the keeping of the telescope in a stationary mode to allow the desired astronomical radio sources to cross over the antenna beam at a particular time interval as illustrated in figure (2.5). The drift scan technique is considered as one of the cheapest radio astronomical observation technique as the Earth serves as the rotator. Therefore, in this study we have used this technique due to the budget concerns of the entire research work. In this study, in order to have a successful observation

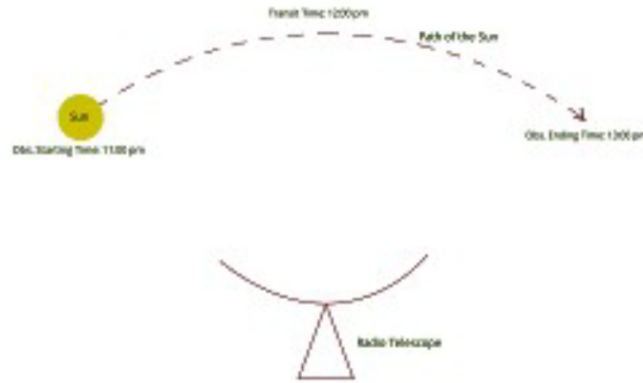


Figure 2.5: Illustrates the drift scan technique with a single radio telescope in a stationary mode Tarif (2016)

of any particular astronomical radio source of your interest with a drift scan, it is advisable to work hand in hand with the planetarium programs i.e. Stellarium software. This is to have the right coordinate system of the desired source in your local sky. Furthermore, the solar drift scan has been used to calibrate the telescope developed in this study, and for more information about the drift scan technique see **section (5.1)** of chapter (5). From this astronomical observation technique, the data recorded by the telescope is intensity of the source, which can be plotted as *antenna temperature (K) against time (s)* as shown in figure (2.6). According to previous studies on the solar drift scan, one can determine a number of important parameters in radio astronomy such as: *the antenna beam of the telescope, time*

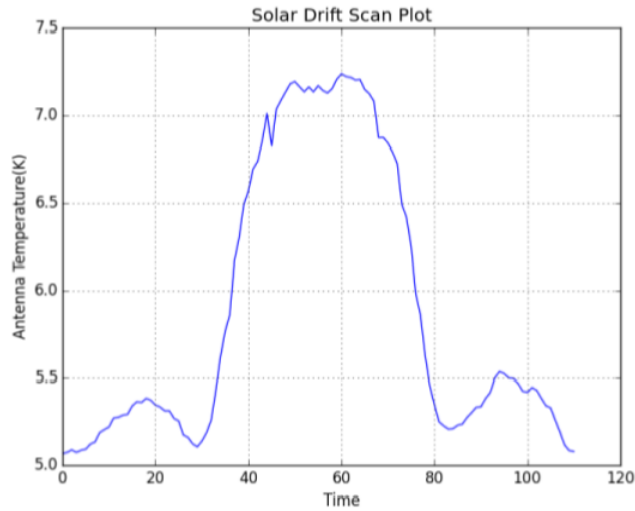


Figure 2.6: shows the graph of the solar drift scan of the Brage Antenna of the SALSA radio telescope Tarif (2016)

taken for the source to cross over the antenna beam, background noise from the receiver and system temperature as illustrated in chapter 5. However, there are few basic radio astronomy fundamentals on observational techniques, which you need to understand. In the next subsections of this chapter, we will explain some of the concepts to help the reader have a clear understanding on the observation techniques used in this study. Since we have used a simple equatorial type of amount mount, it is quite important understand the *horizon and celestial equator coordinate systems*.

2.4.1 Azimuth and Elevation

The azimuth and elevation angles in astronomy are defined as the apparent position of an astronomical object in the sky relative to a specific observation point (Rouse, 2017). This observation point is the location where the telescope is located for observation purposes, in our case the observation point is at the University of Hertfordshire Hatfield-United Kingdom. To start with, the azimuth is an angle measured clockwise degree from the true North as

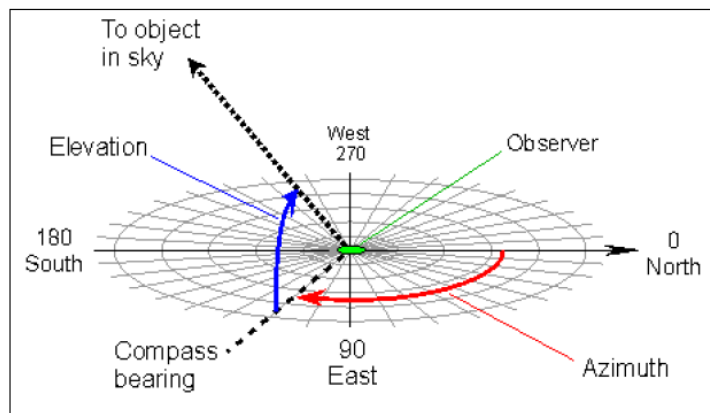


Figure 2.7: Shows the horizon coordinate system for an observer

illustrated in figure (2.7). The measured azimuth angles ranges from 0° *North* through 90° *East*, 180° *South*, 270° *West* and 360° *North*. as indicated in figure(2.7). The elevation angle is measured between the observation point and the object in the sky from the reference frame of the observer by first considering the compass bearing on the horizon relative to the true North. This angle is sometimes referred to as the *altitude angle of an observed object* or *the angle above the horizon* as shown in figure (2.7). The measured elevation angle of an astronomical object above the horizon ranges from 0° *on the horizon* to 90° at the zenith (Michael, 2003). The *horizon* is defined as an imaginary circle on the observer equidistant from the zenith and nadir as shown in figure (2.7) (Pillay, 2012).

2.4.2 Right Ascension and Declination

The Right Ascension and Declination coordinates are known as the celestial equatorial coordinate system for astronomy, which needs to be fully understood. To begin with, the Declination angle (Dec) of an object is defined as the distance in degrees measured from the celestial equator along the meridian (Greenwich Park, England) through the object (star) (MacRobert, 2017), as shown in figure (2.10). The measurement of the declination angle of

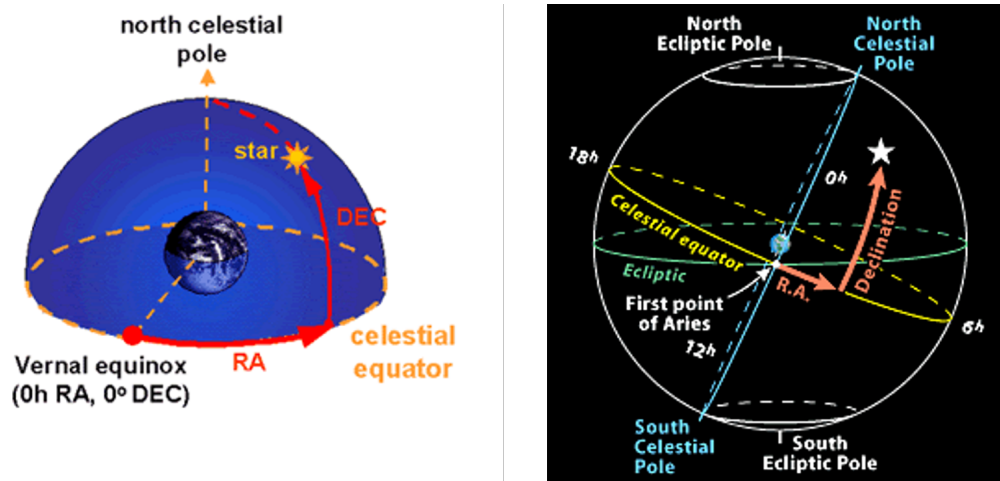


Figure 2.8: Shows the celestial equator coordinates (Declination and Right ascension) MacRobert (2017)

an object involves the consideration of the North and South of the celestial equator. Additionally, the measured declination angle of an object ranges from 0° *at celestial equator* to $+90^\circ$ *at the North celestial pole* and from -90° at the South celestial pole as shown in figure (2.8).

The Right Ascension (R.A) coordinate of an object is an angle measured in hours, minutes and seconds [HH:MM:SS], which is equivalent to the longitude of the Earth (MacRobert, 2006). This equatorial coordinate system is important as it gives the object's transit time in observer's local meridian time. The measured time of the right ascension of an object is in the range of 0 hour to 24 hours, along the celestial equator towards east from the point of Aries as shown in figure (2.8). In the case where the right ascension coordinate is equal to 0 hours and $Dec = 0^\circ$, is referred to as the *first point of Aries*, which is the position of the sun in the sky at the time of the vernal equinox. The vernal equinox is known to be the point where the sun crosses the celestial equator transiting South to North during the northern hemisphere summer and the southern hemisphere autumnal equinox (MacRobert, 2017).

2.4.3 Sidereal and Solar time

The sidereal time is also known as the astronomer time that is measured with respect to the apparent motion of the fixed stars in the sky due to the rotation of the Earth. This parameter is very important to astronomers as it helps them to point their telescopes without considering the location of Earth in its orbit (Crockett, 2012). On the hand, the solar time is defined as the measured time with respect to the Sun. The difference between the sidereal time and the solar time is determined by how long it takes for the Sun and a star to return to Greenwich meridian. Additionally, the Sun is known to take a longer time to return to the Greenwich meridian than a star.

Let us consider the 365.2422 number of mean solar days in a year that the Earth takes to complete one orbit, which has 360° . Therefore, on average the Earth's movement is defined as

$$\begin{aligned} \text{Earth's movement} &= \frac{360^\circ}{365.2422 \text{ days}} \\ &= 0.9856473^\circ \text{ per day around the sun.} \end{aligned} \quad (2.52)$$

Since the Earth rotates 15° in an hour, then 1° is equivalent to 4 minutes, which implies that 0.9856473° translates to 3 minutes 56 seconds. This tells the observer that, in order to observe a source from outside the solar system it would be observed to be present 3 minutes and 56 seconds earlier everyday due to the Earth's rotation (Millar, 2006). Furthermore, Solar day is defined as the time between successive transits of the sun, which is 24 hours. On the other hand, the sidereal day is the time between successive transits of Vernal Equinox that is 23 hours 56 minutes 04 sec. In addition to the astronomer time, it also important to understand parameters that are common in most planetarium software i.e. Stellarium.

1. The Local Mean Sidereal Time (LMST) is the addition of the current Greenwich Mean Sidereal Time (GMST) and the observer's longitude measured positive to the East of Greenwich meridian. The measured positive longitude of the observer is converted from degrees to hours using the following equation.

$$LMST [h] = GMST[h] + Longitude[^\circ]/15 \quad (2.53)$$

2. The Hour Angle (HA) of an astronomical object is defined by the following equation in . This hour angle is related to the time measured relative to the stars called the Sidereal time.

$$HA = LMST - R.A \quad (2.54)$$

where

RA is the Right Ascension angle

HA is the Hour Angle of an object that can be in either the East (negative) or West (positive) of the observer's zenith meridian. If the calculated hour angle is negative this indicates as the time until an object crosses the zenith meridian, while the positive HA indicates as the time since the object has crossed the observer's zenith meridian.

3. Design and development of the telescope

Radio telescopes are considered as the most sensitive and largest instruments in the field of astronomy, but the mechanism behind them is quite simple (Bogusław and Szymon, 2012). This means that with simple tools, equipment, and materials one can construct a functional off-the shelf radio telescope and do some cheap radio astronomy experiments. Nevertheless, this chapter demonstrates and guides the reader on how to design and build a small radio telescope using commercially off-the shelf available satellite T.V components and other cheap materials.

3.0.1 Materials and equipment

The following is the list of basic materials, equipment, and major satellite T.V components used in the construction of the one-meter off-the shelf radio telescope for this research work.

- One-meter Satellite T.V antenna
- Universal Ku-band LNB (10.70-12.75 GHz)
- Motor (DisEqc motor1.2 motorized H-H Motor)
- Tripod (base of the telescope)
- Satellite Finder (SF-50)
- Software Defined Radio (SDR)-device Airspy-Min
- In-line Amplifier
- Compass (Analog or Digital)
- 50 meters of RG6 coaxial cable
- F-type connectors and adapter
- SMA male connector
- Radio Frequency (RF) Choke
- DC-Power Injector
- Multi-meter
- Wire cutter
- Soldering gun, solder flux
- Screwdrivers
- Electric tape
- Power supply (Customized power supply)

- Computer

All the basic components and materials used in the development of the telescope are commercially available at an affordable price from second hand shops that sells electronics and satellite T.V components, and they can also be obtained from online auction sites such as Amazon, eBay etc. In addition, some of these components can be picked from the trash in a good condition for the telescope construction. Although it is not advisable to pick sensitive components from the trash, this might cause problems on the telescope in the near future. In this study, the University and my supervisors provided most of the materials, components, and tools used in the construction of the telescope.

3.0.2 The design of the methanol maser radio telescope

The sketch in figure (3.1) shows the schematic diagram of the methanol maser radio telescope developed in this study. This design has so much room for improvement to suit one's budget. In this study, we focused on constructing a low cost off-the shelf small telescope based on software-defined radio. Therefore, the research work had a limited budget.

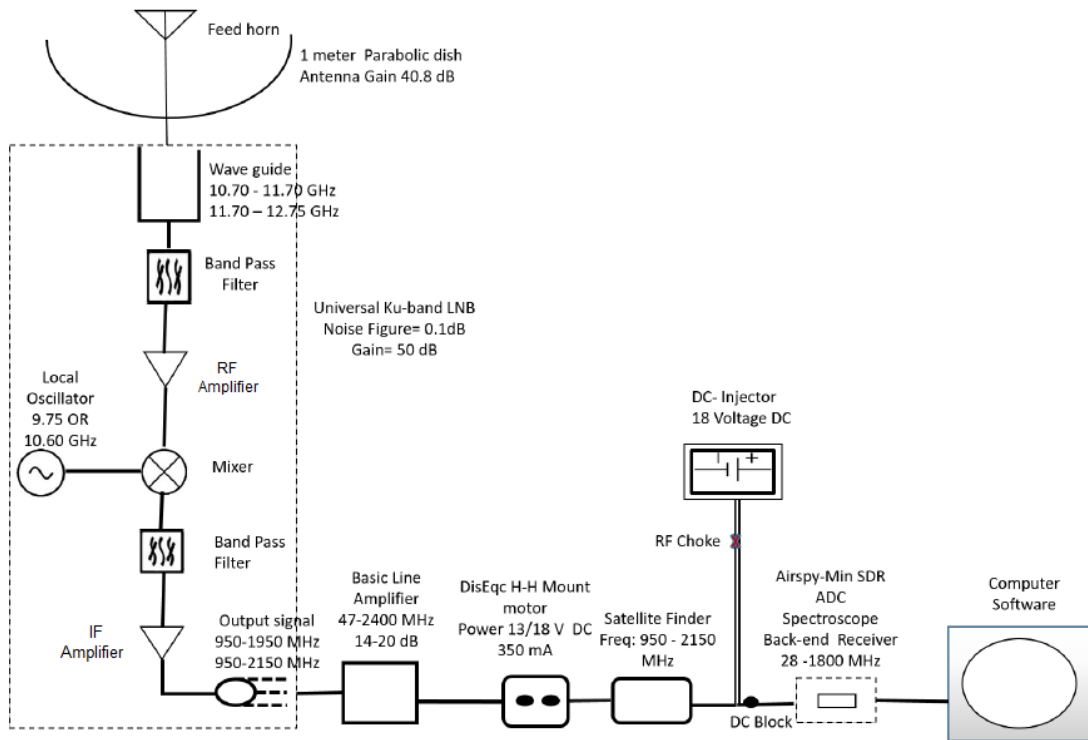


Figure 3.1: Shows a complete schematic diagram of our off-the shelf methanol maser telescope developed in this study

However, before putting the parts together it is important to understand the function of each component used in the development of the telescope as shown in figure (3.1).

3.0.3 Satellite television dish

A satellite television dish is sometimes referred to as an antenna, which is used to collect and transfer radio waves by having it pointed in the right direction of the selected part of the sky (Bogusław and Szymon, 2012). The parabolic antennas are commonly used in the field

of radio astronomy, the reason behind is because of their gain to detect very weak signals. Additionally, the size of an antenna is a very important parameter in the development of the telescope, and it is selected based on different factors such as location of the telescope, gain and the angular resolution required to detect astronomical radio sources (Pillay, 2012). In general, radio telescope antennas are usually enormous in size in order to provide enough sensitivity to detect signals from distant astronomical radio sources that emit extremely weak and faint signals (Kraus, 1986). The size of the antenna used in this study is a one-



Figure 3.2: Shows the one- meter offset satellite T.V dish with a universal Ku-band LNB used in this research work

meter offset dark grey aluminium parabolic dish, with a quoted gain by the manufacturer of 40.3 dB at the frequency of 12.75 GHz, and the weight of 6.1 Kg. The main function of the satellite T.V dish is to receive and reflect incoming radiation from space onto the feed-horn, which consists of the front-end receiver (Low Noise Block-down converter) in the centre (Bogusław and Szymon, 2012).

3.0.4 Low Noise Block- Down-converter

An LNB is an acronym for *Low Noise Block*, which is the central element found in the feed-horn on the front of the satellite T.V dish as shown in figure (3.2) (Jean, 2016). In this study, we will refer to the LNB as the front-end receiver that provides signal amplification to the received signal without adding much noise (Joshi, 2014). In general, the LNB filters out some of the unwanted frequencies in the signal from the antenna and down-converts it to a lower frequency band called the *Intermediate Frequency* (IF), which is sent down to the back-end receiver via a coax cable. In order to achieve the aim of this study, a universal Ku band LNB has been used in the development of the telescope due to its frequency coverage as discussed briefly in **chapter 2**. The quoted input signal by the manufacturer of the dual universal Ku-band LNB is in the range of 10.70-12.75 GHz and it is divided into two switchable frequency bands such as the *Low Frequency band and High Frequency band* with a Local Oscillator (LO) of 9.75 GHz and 10.60 GHz (Primesat.eu/lbns, 2017). These features makes this LNB an ideal component for this experiment, as it can be used for the detection of the methanol molecular line at 12.2 GHz within its high frequency band. The *low-frequency band* of the universal Ku band LNB covers the frequency in the range of 10.70



Figure 3.3: Universal Ku-band LNB used in the development of the methanol maser telescope

- 11.70 GHz that mixes the detected signal with a Local Oscillator frequency of 9.75 GHz. Therefore, the output signal called the intermediate frequency at this stage is expected to be in the frequency range of 950 -1950 MHz. On the other hand, the *high-frequency band* of the universal Ku-band LNB covers the frequency range of 11.70 GHz - 12.75 GHz and then mixes the detected signal with a local Oscillator of 10.60 GHz. The output signal during this process in the high frequency band is expected to be in the tuning range of 1100-2150 MHz which is sent to the back-end receiver for further processing. However, the following

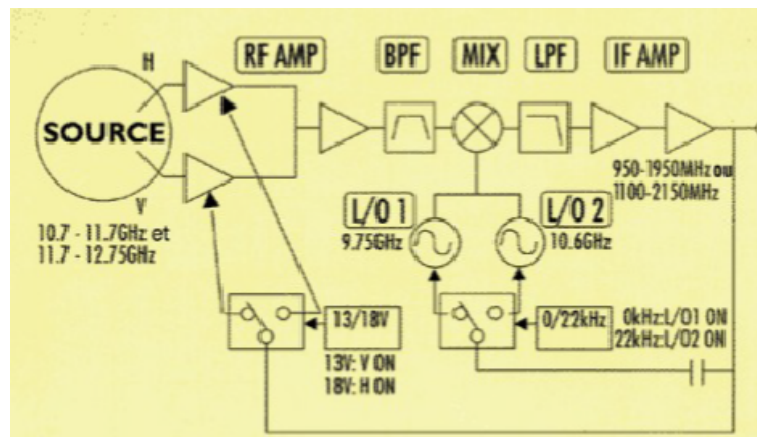


Figure 3.4: Schematic diagram of the Universal Ku-band LNB showing the components inside the LNB

is how the the detected Radio Frequency (RF) signal is processed by the universal Ku band LNB to produce the intermediate frequency that sent for further processing by other parts of the telescope. Once the signal is detected by the antenna, it is transferred to the part of the Ku-band LNB called the wave guide. Thereafter, the RF signal goes through a number of signal processing stages before it is sent for the digitization process by an ADC of the Airspy-Mini device as indicated in figure (3.1).

1. The source is a small pin located in the wave guide that picks up the received signal from the antenna, and send it for Radio Frequency Amplification (RF Amp) process-

ing stage. During the RF amplification processing stage, the signal is amplified and transferred to the Band Pass Filter (BPF) (Jean, 2016).

2. The Band Pass Filter (BPF): is the part of the LNB where the received signal from the antenna is filtered by allowing only the intended microwave signal to pass to the next stage (Eric, 2016). This means that only certain frequencies of the detected signal are allowed through to the next stage of the signal processing called the Mixer and Local Oscillator. The output signal from the Band Pass Filter is always found to be in the high frequency (GHz), which needs to be lowered by the Mixer for easier portability by the coaxial cable.
3. Mixer and Local Oscillator (LO): The processing of the signal at this stage depends on whether the input signal is in the high frequency band or low frequency band. The filtered signal from the Band Pass Filter of the Ku band LNB is then mixed with the LO frequency which depends on the frequency band of the detected signal by the antenna (Jean, 2016). In general, this process involves the subtraction of the frequency of the input signal with the Local Oscillator frequency. In order to have a better understanding on how the Local Oscillator of the universal Ku band LNB determines the output signal (IF), let us consider the following two examples:

- First of all, let us consider the input signal of the 12.40 GHz which is in the high frequency band of the Ku band LNB, the output signal is determined as follows

$$\begin{aligned}
 IF &= \textit{Input Signal} - LO \\
 &= 12.40 \textit{ GHz} - 10.60 \textit{ GHz} \\
 &= 1.8 \textit{ GHz} \\
 &= 1800 \textit{ MHz}
 \end{aligned} \tag{3.1}$$

Since the input signal is in the high frequency band of the LNB, the Local Oscillator frequency used in this process is the 10.60 GHz. Therefore, 1800 MHz is the intermediate frequency that is sent to the Low pass filter of the LNB and later on to the back-end receiver.

- The second scenario is where you have the input signal in the low frequency band of the Ku- band LNB such as 10.75 GHz. In this case, the LNB switches to the Local Oscillator frequency of 9.75 GHz to determine the intermediate frequency.

$$\begin{aligned}
 IF &= \textit{Input Signal} - LO \\
 &= 10.75 \textit{ GHz} - 9.75 \textit{ GHz} \\
 &= 1.0 \textit{ GHz} \\
 &= 1000 \textit{ MHz}
 \end{aligned} \tag{3.2}$$

Therefore, in this case 1000 MHz is the output signal that is sent to the Low Pass Filter.

Let us put the two previous examples into practice, since the detection of the methanol molecular line at 12.2 GHz is one of the major aims of this study. This means that the input signal should be switched into the high frequency band of the Ku-band LNB. Additionally, In order to be able to tune to the 12.2 GHz of methanol molecular line with the software defined radio device, the LNB LO has

to be considered in the process, and this is determined as follows

$$\begin{aligned}
 IF &= \text{Input Signal} - L O \\
 &= 12.2 \text{ GHz} - 10.60 \text{ GHz} \\
 &= 1.6 \text{ GHz} \\
 &= 1600 \text{ MHz}
 \end{aligned}
 \tag{3.3}$$

Therefore, tuning to the 12.2 GHz of methanol molecular line in massive star forming region, is achieved by tuning the software defined radio device on 1600 MHz using the supported software such as the Airspy-Mini receiver or simple_ra receiver.

4. The Low Pass Filter (LPF) is the stage that allows only the low intermediate frequency generated by the Mixer to pass to the intermediate frequency amplification.
5. The Intermediate Frequency Amplifier (IF Amp) amplifies the low intermediate frequency processed by the low pass filter and then send the signal to the receiver in the control room in the frequency range of 950-2150 MHz (Eric, 2016).

In general, LNBS are designed to select signals according to the frequency and polarisation such as Right Hand Circular Polarization (RCP) or Left Hand Circular (LCP) (David et al., 2008). Universal Ku band LNBS are linearly polarized and have a switchable Local Oscillator. This means that a universal Ku band LNB can receive signals from all linearly polarized radio sources in Ku-band. The polarity of the Ku band LNB can be changed by alternating the DC supply voltages by either 13 volts or 18 volts. For instance, 13 volts allows the Ku band LNB to receive vertically polarized signal, while 18 volts makes it receive horizontally polarized signal (David et al., 2008). It is important to know whether the source is vertically or horizontally polarized in order to know how much DC to supply to the LNB . The switching of the LO frequency between the high and low frequency band is achieved by a 22 kHz present or absent in a coaxial cable to the LNB. For more information on the switchable local oscillator and polarity changing in a Ku band LNB see www.satsig.net/lnb/explanation-description-lnb.htm. However, it is very important to consider using a lower noise figure or a larger dish to have a better signal to noise ratio. The lower the noise figure of the LNB the better the output signal, which means that special electronics techniques are used in the LNB in order to have less noise in the signal output (Jean, 2016).

3.0.5 In-Line Amplifier

The In-Line Amplifier is a device that receives a low microwave signal from the LNB and boost its amplitude to a measurable level (Marcus, 2012). If the telescope is running on a



Figure 3.5: Shows the SVS- 2-02 basic line-amplifier with the manufacturer quoted gain of 14 - 20 dB, and the frequency range of 47-2400 MHz

long coaxial cable, it is important to use two or more in-line amplifiers that could offer the

gain in the range of 10-20 dB, although these in-line amplifiers are found to have very poor noise figure. In this study, we have used commercially off-the shelf available SVS-2-02 basic in-line amplifier with the gain in the range of 14-20 dB, which is capable of amplifying the signal from the LNB in the frequency range of 47-2400 MHz. According to the design of our telescope, the SVS-2-02 basic in-line amplifier is connected right after the LNB as shown in figure (3.1).

3.0.6 Satellite Finder

The satellite finder is a device that is usually used for orienting satellite dishes towards geostationary satellites (Lashley, 2010). It measures the strength of the signal in decibels (dB), therefore, it is referred to as the *satellite signal meter*. In this study, we have used commercially available off-the shelf analog signal meter called the SF-50 as shown in figure (3.6) that serves as a square law detector. This device notify the observer whether the LNB



Figure 3.6: Shows the signal meter (SF-50) that serves as a square law detector

is working or not by measuring the strength of the signal from the LNB (Bogusław and Szymon, 2012). The measurement of the signal strength by the signal meter is achieved by checking the display on the meter and the sound it emits when a strong signal is detected. This gives a great advantage of using this device on the telescope for outreach and education purposes, as it emits a sound according to the strength of the detected signal. The SF-50 signal meter used in this project receives the signal from the LNB in the frequency range of 950-2150 MHz and then send it to the back-end receive (Airspy-device) via a coaxial cable. It requires the power source of 13 to 18 volts, which is supplied via the same coaxial cable, connected to the DC power injector as shown in figure (3.11).

3.0.7 Airspy- software defined radio device

The Airspy-Mini is a Software Defined Radio (SDR) device that I personally define as a multipurpose device in the field of amateur radio astronomy. In this project, the Airspy-Mini serves as the ADC, back-end receiver, and radio spectrometer. Furthermore, the Airspy-Mini device has inbuilt components such as the *modulator, demodulator, amplifier, mixer, filter, and IF-amplifier* that can be implemented on a computer by means of software hence the name *Software Defined Radio*. The software defined radio device used in the development of our telescope has a tuning range of 24-1800 MHz, 12-ADC and 3 MHz or 6 MHz of the bandwidth. The 6 MHz is the maximum bandwidth offered by the Airspy-Mini device which



Figure 3.7: Shows an Airspy-Min SDR device used in this study, with a tuning range of 24-1800 MHz www.airspy.com.

can be adjusted by the software implemented on the computer such as the *Airspy real time spectrum analyser*, *GQRX receiver* and the *Simple-ra receiver*. The tuning range of 28-1800

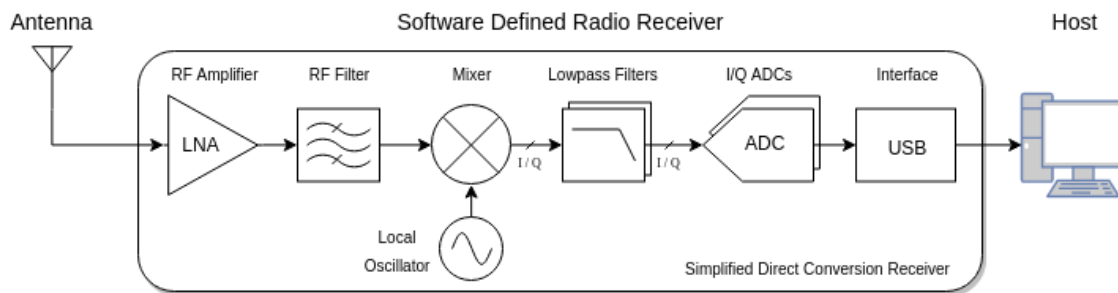


Figure 3.8: Indicates the internal components of the Airspy Mini device

MHz of the Airspy-Mini made it an ideal device for this project. Since it can be used to tune to the methanol molecular line within the frequency range of 950-1800 MHz. Apart from that, the device is found to be compatible with most of the radio applications used in this study i.e. GNU-radio, GQRX-receiver, and *Simple.ra* receiver. The other advantage of this device is that, one can either use it on Linux or windows machine (www.airspy.com, 2017). The block diagram in figure (3.8) shows the internal components of the Airspy Mini device.

3.0.8 DisEqC 1.2 motorised H-H motor

The DisEqC 1.2 motorised H-H motor used in the development of the telescope mount is meant for tracking satellites in the sky. In this project, we have used this motor for different purposes such as holding the one-meter offset antenna on a tripod, for easy accuracy in pointing during an observation as shown in figure (3.9). Furthermore, it also serves as an easy power connection between the LNB and the rest of the parts of the telescope to avoid complicated power connections. The motor used in this project runs on the LNB 's current of 0.3 A and 18 volts DC that is passed on to it through the satellite finder and the in-line amplifier. The following are some of the major considerations you need to take note, when setting up the DisEqc 1.2 motor, for more information check <http://www.satcruiser.com>

1. Firstly, make sure that the mast of your tripod used as the base of the telescope is vertical enough.

2. Secondly, the mast of the tripod must be stable enough to hold the weight of the DisEqC 1.2 motor and the antenna of the telescope.
3. Last but not the least, make sure the size of the motor is capable of supporting the size of your antenna.
4. The coaxial cable from the LNB to the back-end receiver (Airsby-Mini) in the control room must be as short as possible in order to prevent signal loss.
5. After that, you can start by setting up the mast and then attach the DisEqC motor to it as shown in figure (3.9).

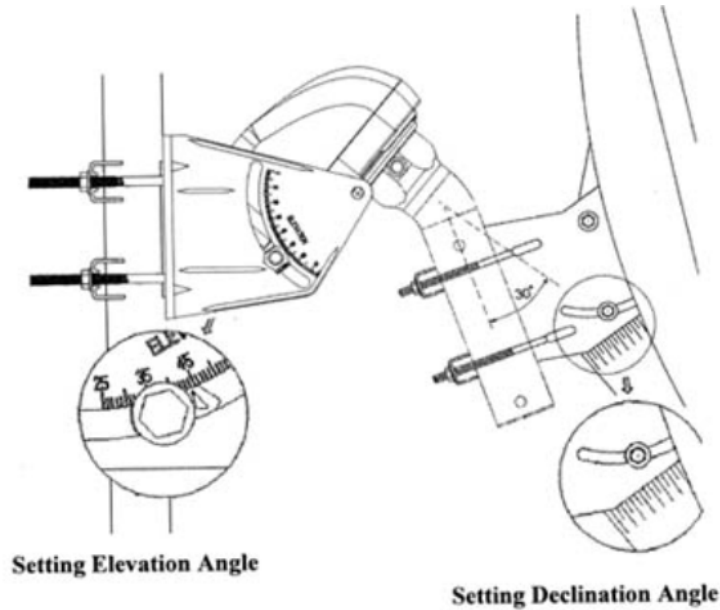


Figure 3.9: Illustrates the setting of the Elevation and Declination Angle on the DisEqC 1.2 H-H motorised motor

6. Before setting up the latitude of your location on the telescope, make sure that the dish motor is at zero degree on the mast.
7. Then set up the Latitude angle of your location on the part of the motor that indicates LATITUDE, to help the motor move the antenna in the right direction during observations. This is achieved by adjusting the inclinometer latitude scale on the side of the motor following the latitude of the location as illustrated in figure (3.9), in our case the location is $(51.7618^{\circ}N, 0.2468^{\circ}W)$.
8. Thereafter, the rest of the angles can also be manually adjusted for an accurate pointing at the source as illustrated in **chapter 5**. The altitude and azimuth angle of an astronomical radio source can be obtained from the planetarium software installed on the computer.

3.0.9 Power supply and other components

There are several ways of powering the telescope built in this study. On the other hand, there are major factors you need to consider before developing the power supply. For the system



Figure 3.10: Shows the picture of the DisEqC 1.2 motor used in this study holding the dish

described in this study, it needs about 13 -18 volts of direct current to power on the LNB, satellite finder, and the DisEqc 1.2 motor. The RFI from an external power supply needs to be prevented from interfering with the IF signal from the LNB. The following are the major components used in the development of the power supply suitable for our system. Since all the components of our system are controlled via one coaxial cable, we decided to use a DC-power injector with a DC- block as shown in the figure (3.11). The main purpose of using the power injector with a DC-block is to prevent direct current from damaging the Airspy-device that is connected direct to the computer as show in figure (3.15). The DC-power injector



Figure 3.11: Shows the DC-power injector used in this project

used in this setup was chosen due its capability of receiving and transmitting signal in the frequency range of 5-2200 MHz. Additionally, it also prevents direct current from interfering with the signal that goes to the Airspy-Mini device. According to the schematic diagram in figure (3.1), the DC-power injector draws power from an external power source called the DC power supply as shown in figure (3.13). The RF signal from the antenna to the LNB is transmitted through the DC power injector by the coupling capacitors (David et al., 2008). Considering that the part labelled *DC* in figure (3.12) is the part that is connected to an external power supply to draw power for the satellite finder, DisEqc motor and the LNB. Apart from that, the part labelled *RF + DC* is defined as the connector only for the LNB, Satellite finder and the motor. It supplies power to the LNB and transmits the RF from LNB to the part labelled *RF*. The RF part in figure (3.12) connects the rest of the system

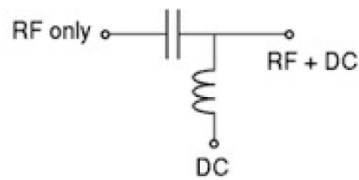


Figure 3.12: The schematic diagram of the DC-power Injector used in this study (David et al., 2008).

to the back-end receiver as illustrated in the schematic diagram of this telescope. Its main function is to transfer only the signal from the LNB to the Airspy-Mini software defined radio device for digitization.



Figure 3.13: Switchable DC power supply

The other major component used in the development of the power supply is the *Radio Frequency (RF) choke*, Its main function is to prevent radio frequency interference supplied by the external power supply from interfering with the signal from the LNB. The picture in figure (3.14) shows the RF choke used in the building of the power supply for the telescope. The RF choke is connected in the middle of the positive wire of the coaxial cable connected



Figure 3.14: Radio Frequency (RF) choke with current of 3A

to the external power supply and the DC- power injector, as in indicated in figure (3.15). The choice of the RF choke used in the development of the telescope power supply depends on the current needed for components like the LNB.

3.0.10 Cabling of the system

The entire system of the methanol maser radio telescope shown in figure (3.15) is cabled with the RG6 coaxial cables with 70 Ohms, F-type and SMA connectors. Due to the cost concerns of the this research project, the RG6 coaxial cables, F-type and SMA connectors, are found to offer a good quality at an affordable price. Moreover, RG6 coaxial cable is known to have a great advantage when the system is running on a long cable (Marcus, 2012). In this study, the entire system is controlled on one coaxial cable, which runs from the LNB to the software-defined radio-hardware connected to the computer in the control room.

3.0.11 Computer

In this study, a computer is defined as a machine where the entire system software is installed. It plays a vital role in helping radio astronomers to view and understand what they have observed with their telescope, and this is achieved by using sophisticated software that could record, process and analyse data (Marcus, 2012). The data collected by the satellite T.V dish is sent to the control room through a coaxial cable lands on the computer, and the computer acts as the display and interface where most of the activities are controlled. In this project, we have used a personal computer to record, process and analyse data with software compatible with the software defined radio device. Once the Airspy software is installed on a computer successfully, the plugging in of the Airspy-device onto the computer turns it into a back-end receiver for the telescope. In order to have successful cheap radio astronomy experiments based on software defined radio, a computer with the following specifications or better is needed Marcus (2012).

- A dual-core system
- Running at 2.8 GHz or better
- A computer with a spare USB-2.0 port for an SDR-device i.e Airspy-Mini
- A computer with 2GB Ram or better that can support GNU-radio software and its applications

However, in this study, we have performed some cheap radio astronomy experiments based on software-defined radio on two different computers running on different operating systems such as *Windows and Linux operating system*. Since the entire system of our telescope is controlled through a single coaxial cable connected to the computer, therefore, the computer is considered as the major component of the methanol maser radio telescope.

3.0.12 The complete system of the methanol telescope

After putting all the major and minor components together, we now have a complete methanol telescope that needs to be powered and tested. The picture in figure (3.15) shows a complete hardware of the methanol maser radio telescope designed and built in this study. Now since we have constructed a complete hardware of the methanol telescope, the next chapter will focus on the software part of the entire system.

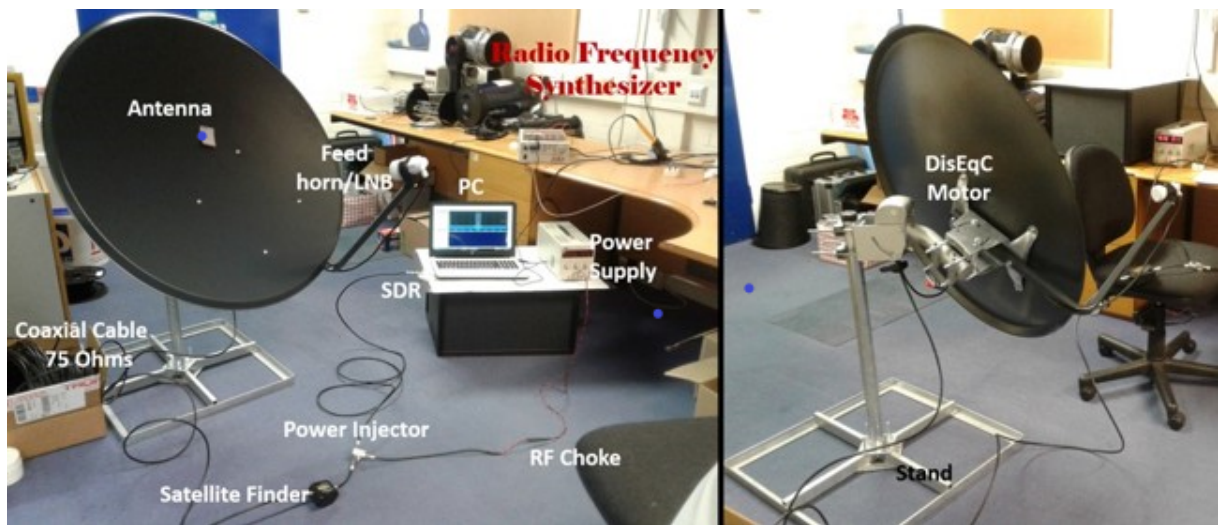


Figure 3.15: Shows the picture of a complete hardware of the one-meter class off-the shelf methanol maser radio telescope in the control room, indicating all the major components.

4. Signal Digitization

Signal digitization with the system developed in this study, involves the transformation of an analogue signal into a digital signal by an Analogue to Digital Converter (ADC), which is part of the Airspy-software defined radio device. The digitization of the detected signal by the telescope is very important in the field of radio astronomy, this is because an analogue signal cannot be recognized, recorded, or processed on a computer until it has been digitized. The block diagram in figure (4.1) illustrates how the detected radio emissions by the antenna are converted into *digital signals* by the system developed in this study. In addition, this

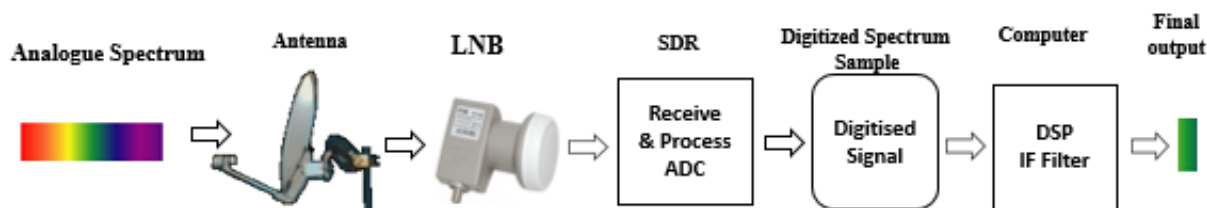


Figure 4.1: The digitization of an analogue signal with a small radio telescope based on software defined radio device (Laufer, 2015)

illustration depicts a good example of a typical radio astronomy experiment with an off-the shelf radio telescope based on software defined radio. The entire process in figure (4.1) illustrates how the observed signal by the antenna gets on the computer via a cheap software defined radio device (Airspy-Mini) for further digital signal processing (Laufer, 2015). In general, the software defined radio hardware acts as the intermediate component between the antenna and the computer. It receives radio waves from the antenna in the form of an analogue signal and then converts them into a digital signal that can be recognized by the computer.

For example, let us consider a very simple analogy of the colour spectrum as shown in figure (4.1) to illustrate the digitization process of the detected radio signal by our telescope. Assume that you tune the radio telescope at a particular frequency to detect a known source, which is denoted by the green part in the analogue spectrum. Instead of the telescope detecting only the green part, it picks up the entire analogue spectrum at the frequency the telescope is operating. Thereafter, the detected signal (analogue spectrum) by the antenna is sent to the LNB for amplification and down-conversion as explained in **chapter 3**. The output (IF) signal produced by the LNB is then sent to the ADC, to read the analogue signal and digitize it for further signal processing on the computer (Laufer, 2015). The digitization of the analogue signal received by ADC depends on the bandwidth of the software-defined radio-device used in development of the telescope. After the digitization process by the Airspy-Mini, a chunk of digitized (I/Q) data is sent to the computer at the sample rate of 3 MSPS or 5 MSPS for recording or further Digital Signal Processing (DSP). With the digital signal processing software installed on the computer, the detected signal from the source of your interest (the green part) can then be extracted from the digitized spectrum with the help of *digital IF algorithm* as illustrated in figure (4.1).

4.1 Radio astronomy-SDR data logging

Cheap radio astronomy experiments based on the software-defined radio device with our telescope can either be done on a computer running on Windows or Linux operating system. In this chapter, we will discuss some of the amateur radio astronomy software compatible with the Airspy-device and how they are used to perform cheap radio astronomy experiments on both Linux and Windows operating system.

4.1.1 Radio astronomy observation with Airspy-receiver

The Airspy-Mini software defined radio device provides a real time spectrum analyser called *Airspy-receiver*, which is implemented on the computer in the form of a software. This receiver has a number of interesting functions that can be used for recording and visualization of the observed source in real time.

The SDR-device used in this project receives the signal from the LNB in the range of 28-1800 MHz, which is then processed as a chunk of Radio Frequency (RF) spectrum of about 3 MHz or 5 MHz of bandwidth www.airspy.com (2017). It has been noted that in the received chunk there might be other signals from other radio sources as shown in the observation experiment with an Airspy Mini-receiver in figure (4.2). With a real time spectrum analyser

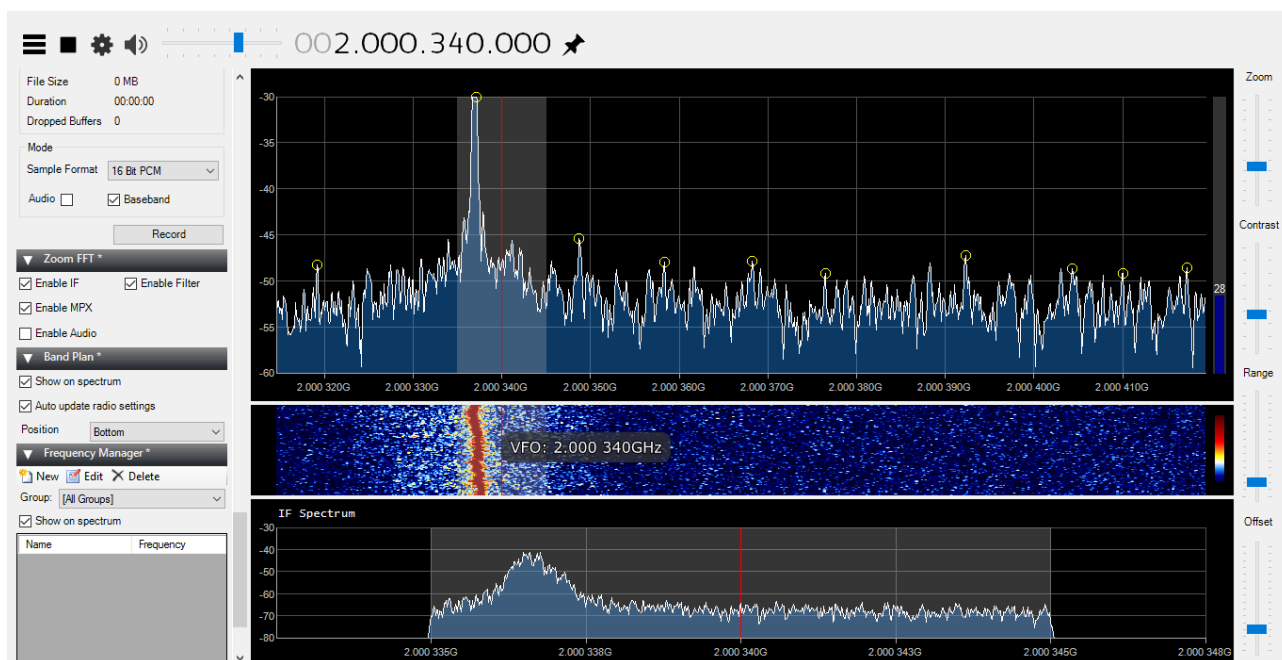


Figure 4.2: Shows different signals observed in real time spectrum analyser at the frequency of (12.200340 GHz) with the Airspy-Mini receiver

provided by the software-defined radio-device, one is able to visualize all the components of a received signal by using the FFT plot and the waterfall window plot as shown in figure (4.2). All the peaks shown in figure (4.2) represent different signals from other radio sources that were detected at a particular frequency. The Airspy-real time spectrum analyser is quite important for this project, as it can be used to demonstrate to students the effects of Radio Frequency Interference (RFI) in real time observation. This means that, you will be able to see other detected signals when the telescope is pointed in some parts of the sky targeting a known source.

4.2 Data Recording and Processing with GNU-Radio

Amateur radio astronomy experiments based on software defined radio have increased in the past few years due to an incredible flexibility of the software defined radio device (Laufer, 2015). Software defined radio-devices save money from buying a number of different items of hardware, that are used in the transfer of the signal from hardware into software for further processing (Marcus, 2012). The GNU-radio is a free software that is considered to be a signal processing framework, which depends on software defined radio devices (Gnuradio.org, 2016). This signal processing frame work is used to control the software defined radio hardware used in the development of the telescope, by using the GNU-radio companion block called *Osmocom block*. The Osmocom block is one of the most powerful block of the GNU-radio companion, which is implemented on the computer as a software. Its main function is to connect the software defined radio-hardware with other GNU-radio software applications (Seeber, 2014). Without having the Osmocom block installed on a computer, radio astronomy experiments based on the SDR-device with GNU-radio applications could not be possible. Therefore, it is important to have it installed first on a computer before considering the use of any GNU-radio application. The guidelines on the installation and the use of the Osmocom block can be found at <http://sdr.osmocom.org/trac/wiki/GrOsmoSDR>. Lately, the use of the GNU-radio applications in conducting cheap radio astronomy experiments based on software-defined radio have also increased. This is because the GNU radio applications are easy to use and have a collection of signal processing blocks that are useful in the building of radio receivers within the GNU-radio companion. Furthermore, the GNU radio software provides hands on experience on the processing of the received digital signals from the SDR-device (Airspy) by using one of the radio receivers compatible with the GNU-radio software such as the *GQRX receiver and the simple_ra receiver*.

4.2.1 Digital signal processing and recording with GNU-Radio Companion

The GNU-radio companion is one of the most important and powerful component of the GNU-radio software (Gnuradio.org, 2016). It allow the user to graphically program GNU-radio applications such as *simple_ra receiver* or *real time spectrum analyser* that provides features like *frequency spectrum plot*, *spectrum waterfall plot*, *constellation plot* and *scope plot* (Seeber, 2014). Graphically programming in GNU-radio involves the connecting of the GNU-radio blocks found within the GNU- radio companion as illustrated in figure (4.3), which is achieved by having the Osmocom block as the key component. More information on how to install and use GNU-radio companion on Linux and other operating systems can be found at <http://www.gnuradio.org/>. The following are some of the main features of a real time spectrum analyser developed in GNU-radio companion.

1. The *frequency spectrum plot* measures the signal amplitude in dB against frequency in MHz. Therefore, it is sometimes referred to as the frequency domain spectrum analyser (Seeber, 2014). With the real time spectrum analyser shown in figure (4.4), an observed source of our interest is found in the middle of the spectrum analyser, while the left and right hand side of the spectrum analyser represent the lowest and the highest frequency respectively. This means that the frequency at which you are observing the source is found in the middle of the spectrum analyser.
2. The *waterfall real time spectrum analyser* is one of the common feature of the GNU-radio applications. It measures the signal frequency against time as indicated in figure

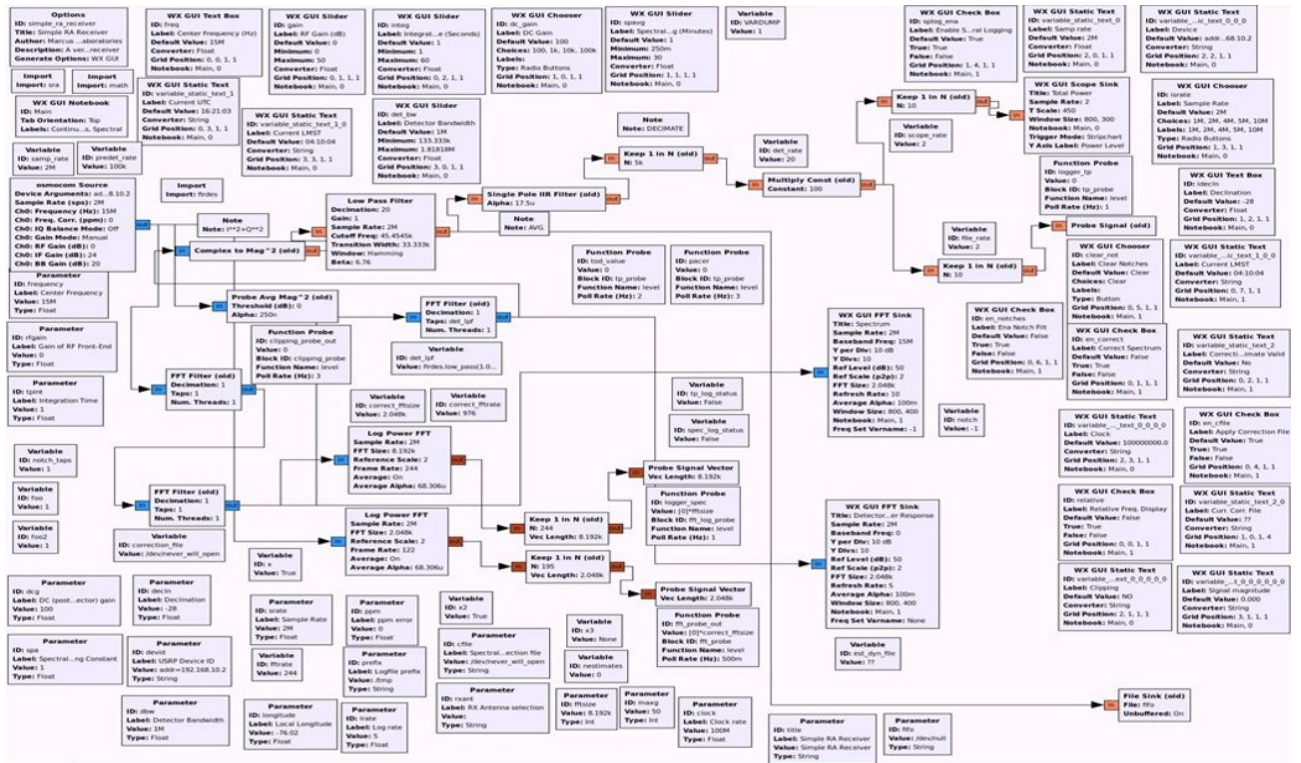


Figure 4.3: Image of the graphically programmed GNU-radio application of the simple_ra <https://www.google.com/amp/slideplayer.com/amp/7446123/>.

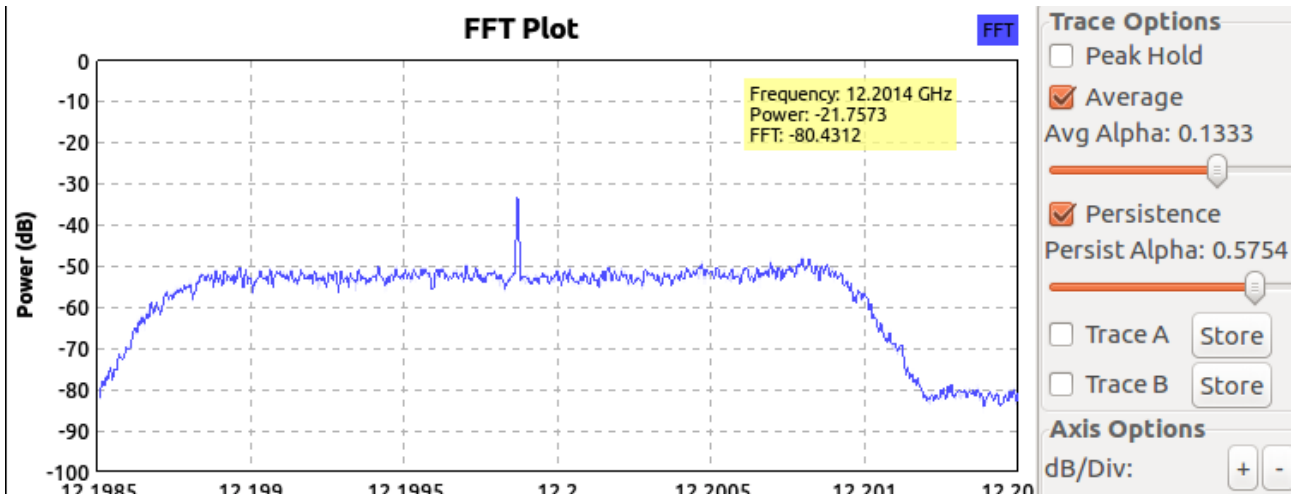


Figure 4.4: The frequency spectrum plot showing the measured signal amplitude in dB against frequency in MHz

(4.5), and it is referred to as the waterfall plot window. The waterfall plot is sometimes called the *frequency domain analysis*. With these two real time spectrum analysers, one can visualize the strength and the components of the detected signal in both plots as shown in figure (4.6). In radio astronomy, waterfall plots are very useful in the study of various objects such as Fast Radio Bursts (FRBs), Pulsars, Rotating Radio Transients etc.

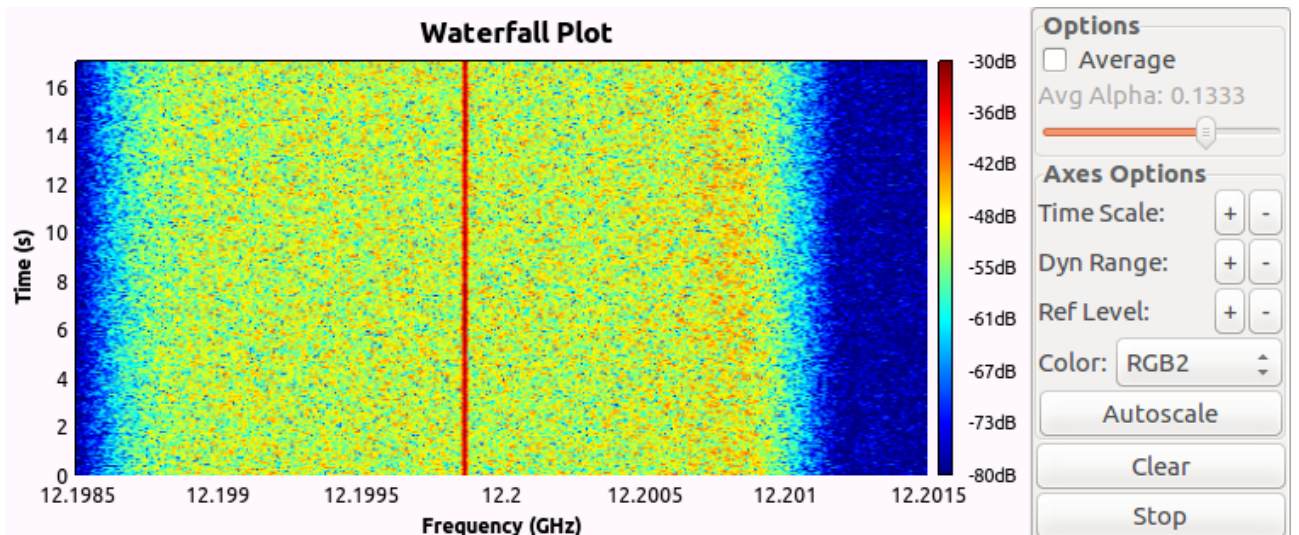


Figure 4.5: Shows the waterfall plot window with a strong detected signal in the middle

4.2.2 GQRX Receiver

The GQRX is an open source software based on software defined radio device developed by *Alexandru Csete*. It is also implemented on a computer as a software receiver that works with GNU-radio and Qt tool kit (Alexandru, 2016). Additionally, the GQRX software has been proven to be compatible with different software defined radio devices such as *Funcube Dongle*, *RSTL-SDR*, *Airspy*, *HarckRF*, *BladeRF*, *RFSpace*, *USRP* and *SoapySDR* (Alexandru, 2016). The GQRX receiver provided by the GQRX - software has similar features of that of the Airspy-receiver on a machine running on Windows OS, the only difference is that it allow the input of the Local Oscillator frequency of the LNB used as the front-end receiver of the telescope. This receiver can also receive signals in *Amplitude*

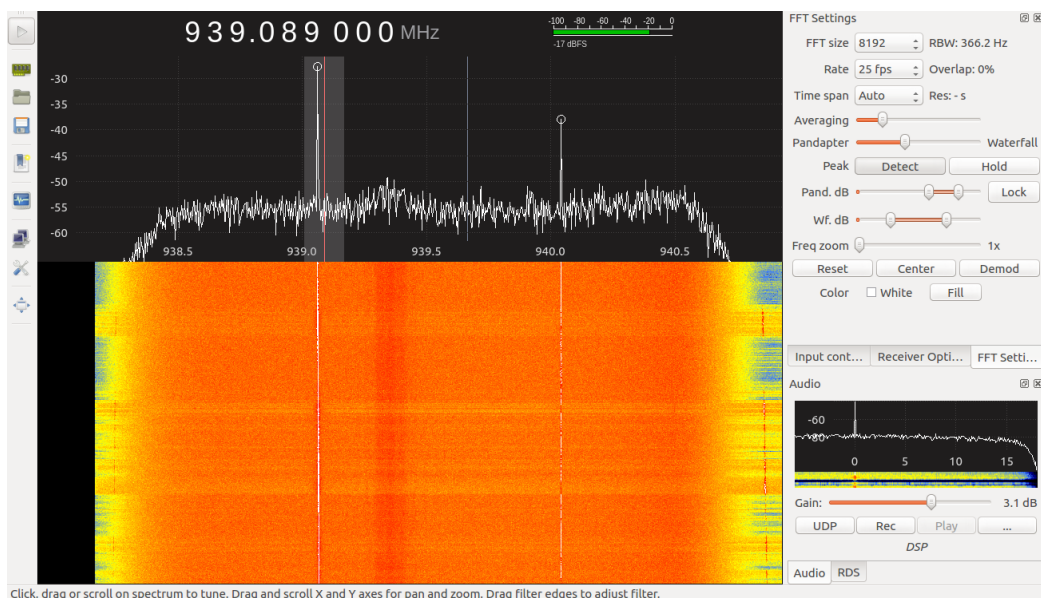


Figure 4.6: Shows a real time spectrum analyser of the GQRX receiver during the Solar observation with the 1 m off-the shelf UH telescope

Modulation (AM), Frequency Modulation (FM) and Single Side Band (SSB) with an audio output (Laufer, 2015). However, the GQRX software with a software defined radio-hardware works well on Linux and Mac system supported by the Osmocom block, which has been discussed earlier in **section (4.2)** of this chapter. In this study, we have experimented with simple radio astronomy observations with the GQRX-receiver and the Airspy-receiver, and one of them is shown in figure (4.6) that shows the solar observation in real with the GQRX receiver. One of the advantages of using the receiver provided by the GQRX-software is that, you are able to visualize the detected signal in both the FFT and the Waterfall display in real time. The observed signal by the telescope is recorded in WAV format and can be replayed later with the GQRX receiver. For more information about the GQRX-software follow <http://gqrx.dk>

4.3 Data logging with simple_ ra software

The `simple_ra` application is defined as a simple radio astronomy receiver with a collection of tools based on a digital single processing framework called the GNU-radio. This application is an open source application that is compatible with a number of software-defined radio devices. It was first developed in GNU- radio companion by *Marcus. D. Leech* in 2007, in order to support and promote cheap radio astronomy experiments based on software-defined radio. The `simple_ra` application is sometimes referred to as an integrated receiver that allow a single dish radio astronomy observation by collecting both total power and spectral data in real time (Marcus, 2013). With the `simple_ra` application, one can do observations such as continuum of total power, pulsar monitoring and spectral observations. The usage of the installed `simple_ra` receiver application on a Linux system can be achieved by typing a command `simple_ra` in the terminal and pressing Enter. This is a general command, but since we have used an Airspy device in this study, therefore the command should be written as `simple_ra -devic airspy=0 -srate 3.0e6 -freq 1.60e9` where `-srate` represent the sample rate and `-freq` is the frequency. Further information on how to install and use the `simple_ra` application can be found at <http://www.sbrac.org/files/install-gr-ratools>. The computer system requirements of this application is similar to that of the GNU-radio as discussed earlier in **section 3.0.11** of chapter 3.

4.3.1 Spectral data processing

The processing of spectral data observation recorded by the `simple_ra` receiver may produce very useful graphs of particular spectral features in the data set. During a spectral observation in the spectral mode of the `simple_ra` receiver, the real time spectral window shows the signal amplitude (dB) against frequency (MHz) as shown in figure (4.7). In this study, spectral data processing is achieved by taking note of the following simple steps.

1. Spectral data processing involves the processing of data files with a file name in the format of `spec-YYYYMM-HH.dat` (Marcus, 2013). An example of the recorded spectral data set in this study is shown in **appendix B (B.1.0)**. This data set contains data recorded in both UTC and LMST. For more information on the recorded spectral data set, see **appendix B (B.1.0)**.
2. The recorded spectral data set is averaged over a period of time from where you can choose the period you would like to process. Therefore, the processing of the spectral data set is achieved by typing in the command line `process_simple_specdat -u`

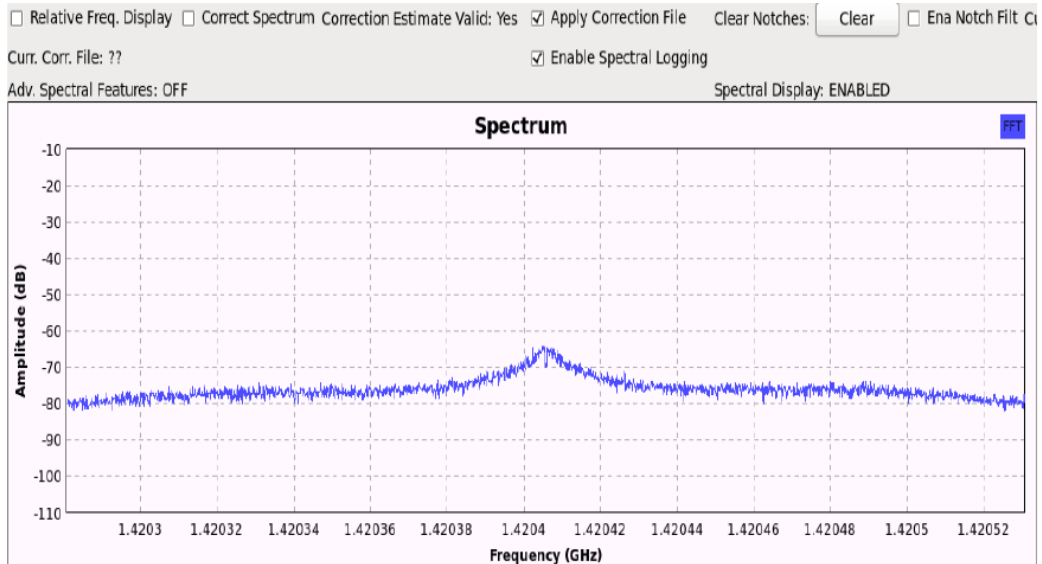


Figure 4.7: Shows the real time spectral window that measures the amplitude of the signal against frequency

HH:MM:SS HH:MM:SS -t "title of an observation" a \$HOME/simple_ra_data/spec-20170523-15.dat in the terminal, where HH:MM:SS HH:MM:SS is the time- period you would like to process from the recorded data set.

3. The graph produced by this process is always in a Portable Network Graphics (PNG) format as shown in figure (4.8).

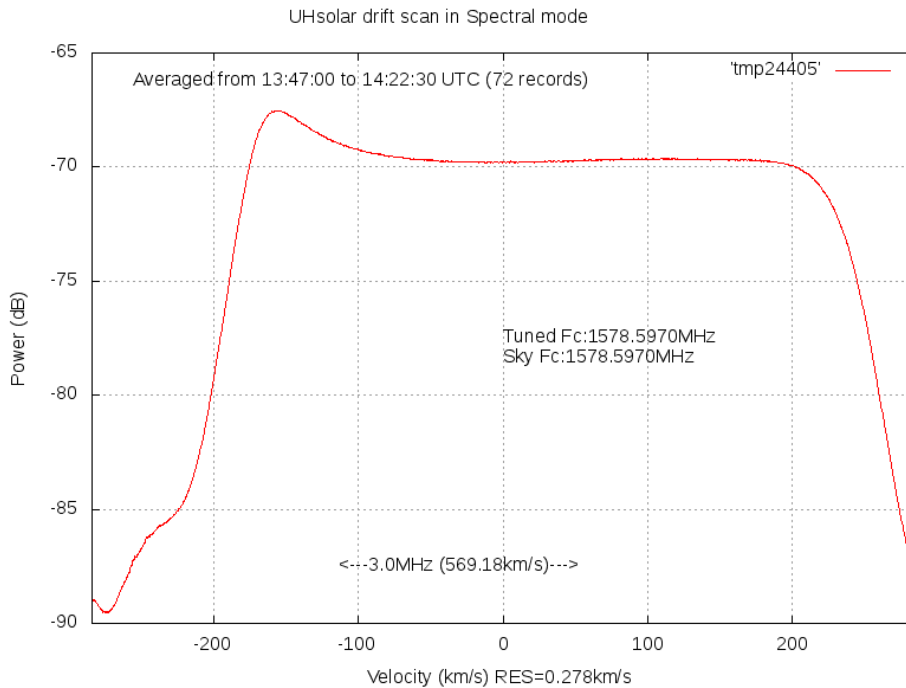


Figure 4.8: Shows an image of the square wave bandpass spectrum of our off the shelf telescope

4.3.2 Continuum data processing

1. The processing of continuum logged files is achieved by processing of data files of the continuum observation, which is recorded by the simple_ra receiver with a file name in the format of *tp-YYYYMM-HH.dat*.
2. This process is simply done by typing the command `process_simple_tpdat -u HH:MM:SS -t "observation title" -f sun_drif.png -r $HOME/simple_ra_data/tp-20170523-16.dat` in the terminal provided that you are in the right directory of the recorded data.
3. The results of the continuum data processing produce a graph in PNG format as shown in figure (4.9), which can be set in the command line during the processing.

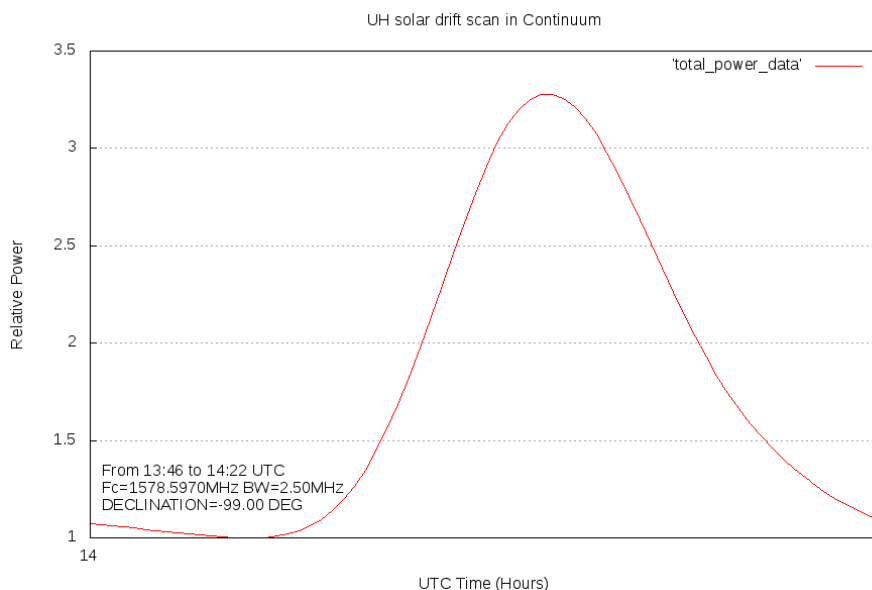


Figure 4.9: Shows the Gaussian of the processed continuum file of the solar drift scan observed by the 1 m UH off the shelf telescope

4. During a continuum observation with the simple_ra, the observed data files are also recorded in Comma Separated Variables (CSV) format at the same time-period, although the *tp-YYYY-MM-HH.dat* is known as the standard format for recording data files in the continuum mode (Marcus, 2013).
5. Data files recorded in the continuum mode have parameters such as the Centre Frequency (Fc) in MHz, the detector Bandwidth (BW) in MHz, the current Declination (Dc) angle, the Julian date(jdate) and the Right Ascension (RA) as shown in one of the logged files in **appendix B (B.1.2)**.
6. According to figure (4.10), it shows a full drift scan of the sun observed by the 1 meter UH off the shelf methanol maser telescope in continuum mode on the 9th June, 2017 at 14:22 hours UTC.

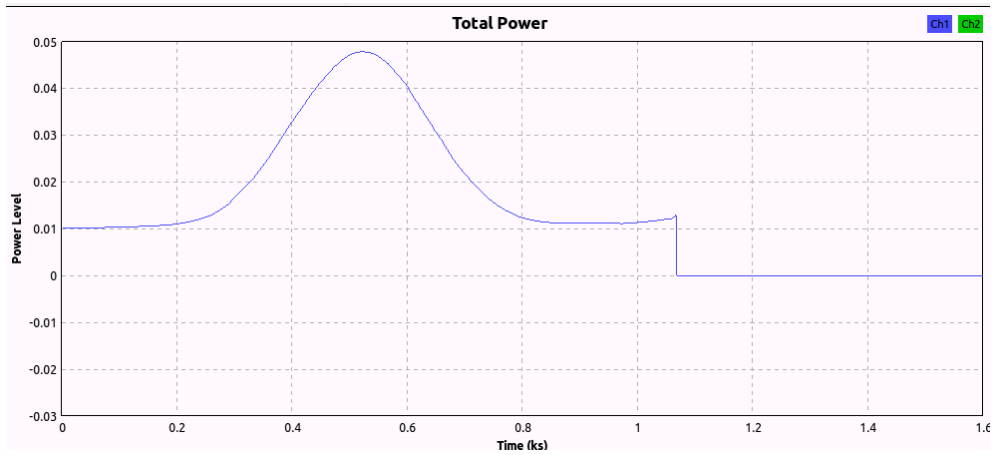


Figure 4.10: Shows the Gaussian of the continuum observation of the solar drift scan observed with the 1 m UH off the shelf telescope

4.3.3 Comma Separated Variables (CSV)-data processing

The `simple_ra` receiver automatically produces the CSV-data files when an observation is done in the continuum mode. These files can easily be processed in python program, matlab or Excel. The following is how the CSV-data set of the solar drift scan was processed in Excel

1. In this study, the CSV data files are recorded with a file name as (CR_YYYYMMMDD_experiment name.csv), and saved on the computer in a folder called `Simple_ra` named after the `simple_ra` receiver.
2. First of all, open the recorded data set of an observation in CSV-format.
3. Import the text file into Excel and select the time-period you would like to process from the recorded data.
4. From the imported data, you can plot the graph of the observed source as power [dB] against time [UTC] as shown in figure (4.11)
5. One of the advantages of using Excel in the processing of the CSV-data files is that, It is user friendly and one can select the time- period to process from the data set that has been recorded for a long period.
6. Further information about the `simple_ra` application can be read from a free guide written by *Marcus D Leech* http://github.com/patchvonbraun/simple_ra.

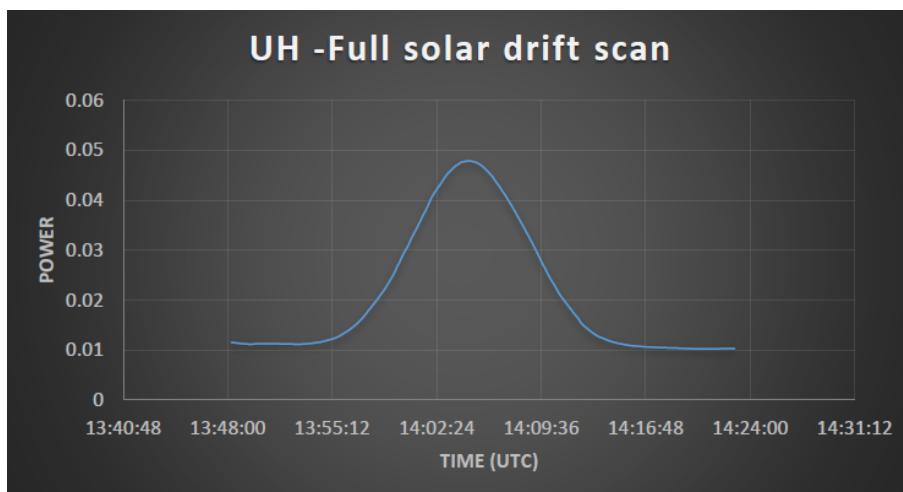


Figure 4.11: Shows the Gaussian of the solar drift scan observed by the 1m UH off the shelf telescope at the University of Hertfordshire and processed in Excel

5. Commission and calibration of the methanol maser telescope

This chapter is divided into two main sections that explains the commission and the calibration of the telescope developed in this study. It will also discuss some of the major radio sources used in the testing and the calibration of our telescope. The entire hardware of the



Figure 5.1: Shows the setup of the one- meter off the shelf radio telescope up the roof of the STRI building at the University of Hertfordshire

1-meter radio telescope was mounted up the roof of the Science and Technology Research Institute (STRI) building at the University of Hertfordshire with a 30-meter coaxial cable running down to the control room as shown in figure (5.1). The picture in figure (5.2) shows



Figure 5.2: Shows the other parts of the telescope in the control room

the other parts of the methanol maser radio telescope in the control room at the University of Hertfordshire. The two computers shown in the picture run on two different operating systems with different logging software installed on them. For the sake testing the telescope on different operating systems, the Airspy-Mini SDR-device is plugged on one of the computers depending on the type of an observation the observer would like to perform. The Airspy-Mini software defined radio device is an important component of the methanol maser radio telescope, which connects the rest of the telescope system shown in figure (5.1) to the computer for data logging, processing and visualization of the detected signal as discussed in **chapter 3 and 4**. A switchable power supply of 13 or 18 Volts DC is needed to control the polarization of the Ku band LNB as explained in **section 3.0.4** of chapter 3. In this study, this process is achieved by using a switchable DC power supply generator shown in figure (5.2) indicated as power supply.

5.1 Commissioning of the telescope

The following are some of the astronomical and man-made radio sources that were used to test the telescope. Since our telescope operates in the Ku-band, locating of the geostationary satellites and observing the Sun in Ku band were some of the activities used to investigate the observational effectiveness of the telescope. These observational experiments were accomplished by using different real time spectrum analysers and data logging software installed on the two computers shown in figure (5.2)

5.1.1 Ku band geostationary satellites

The observation of the Ku band geostationary satellites was the first observational experiment that was performed in this study to test the performance of the entire telescope system.

- This observational experiment was achieved by first checking the azimuth and altitude of the Astra geostationary satellites, which were found to be 144.969° and 25.062° respectively according to the latitude of Hertfordshire.
- In addition, the azimuth and altitude of the source are very important coordinates for easy pointing of the telescope of this kind at the source provided that; the right latitude of the location is perfectly set on the latitude scale of the telescope.
- Thereafter, the altitude of the source is also manually set on the telescope as illustrated in figure (5.3). On the hand, the azimuth of the source is set by manually rotating the base of the telescope to the right azimuth angle, which is set by using one of the magnetic compasses shown in figure (5.6) or the ones on smart phones.
- After setting up the entire telescope, the telescope antenna was pointed to 144.99° towards East-South having the offset angle of the antenna and the altitude angle of the source into consideration.
- The telescope was able to detect a strong signal from *Astra1N* geostationary satellite at the frequency of 12.2000,340 GHz as indicated in the real time spectrum analyser in figure (5.4).
- During this observational experiment, the telescope had the latitude of our location and altitude angle of a source manually fixed as illustrated in figure (5.3), only the azimuth of the telescope was manually rotated in order to get the best signal.



Figure 5.3: Illustrates the setting up of the latitude and altitude angles on the telescope system

A number of these geostationary satellites are in orbit above the Earth and are found to be orbit above the equator. In order to observe geostationary satellites above the equator, it is quite important to put the celestial equator into consideration when determining the altitude to look for satellites, which is determined as follows

$$Altitude = (90^\circ) - (Latitude) \quad (5.1)$$

This might give you a rough altitude angle to search for geostationary satellites (DeWitt, 2017). Note that, during the detection of geostationary satellites in spring and autumn equinox the sun could be considered as RFI. The reason behind is that during the spring and autumn, the Sun is found to shine above the equator (Boguslaw and Szymon, 2012). During

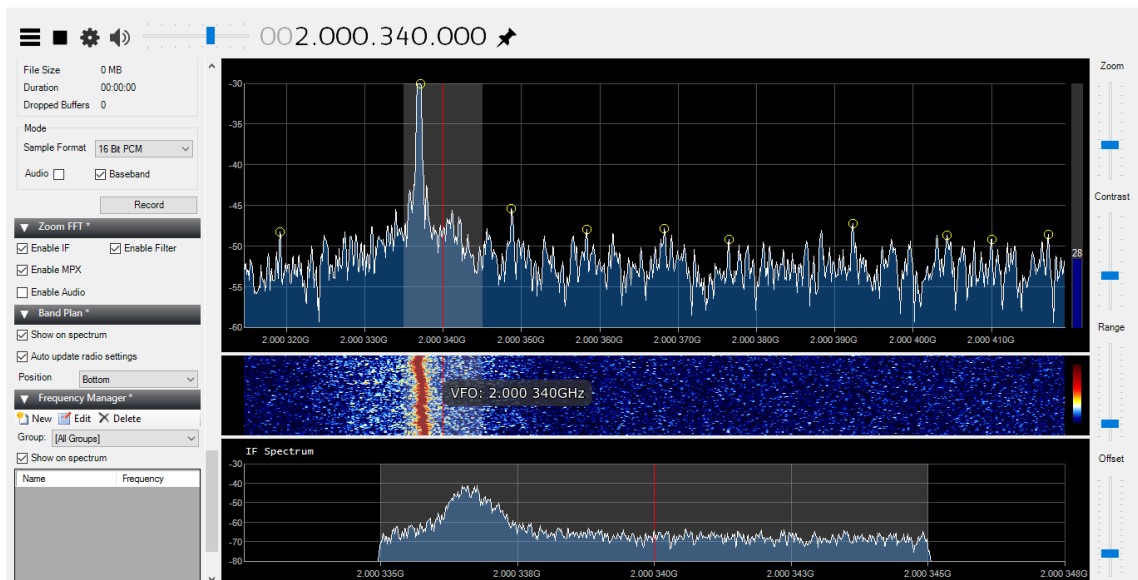


Figure 5.4: Shows the observed Astra1N geostationary satellite signal at the frequency of 12.200340 GHz in the Airspy-Mini real time spectrum analyser. The signal shown in this figure indicates the narrow band from a geostationary satellite in Ku band

this experimental observation, we used the Airspy-real time spectrum analyser as shown in

figure (5.4). This is because we really wanted to visualize the strength of the signal detected from Astra1N in both the FFT plot and the waterfall plot. On the other hand, we also wanted to test the performance the telescope when observing a narrow band and a broadband radio sources with the Airspy-Mini receiver and the GQRX receiver in real time. Geostationary

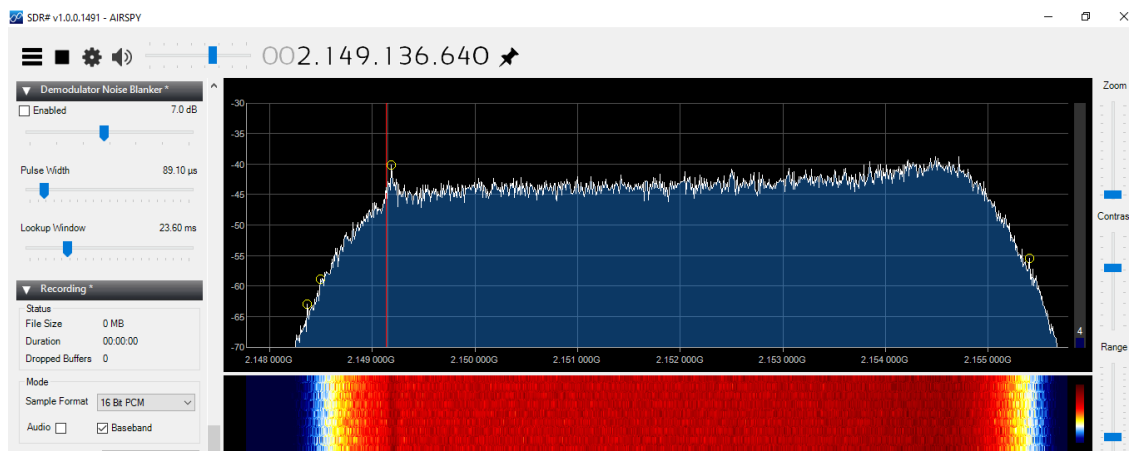


Figure 5.5: Shows the observation of the broadband signal from the Sun in the Ku band. The observation of the broadband signal with an Airspy-Min real time spectrum analyser requires the observer to pay attention to two things such as: *to take note of the increase and decrease in the power level of the FFT plot when the source passes across the antenna beam, and also the colour of the waterfall plot changes from light to darker as shown in the figure above.*

satellites are believed to be easy to observe because of their emission of narrow beams, hence they are sometimes referred to as the *narrow beam transmitter*. The entire observation of the geostationary satellites by the telescope in this project was achieved by pointing the telescope antenna in the right direction with the help of the magnetic compass as shown in figure (5.6). The first successful experimental observation of the geostationary satellite proved that our telescope is capable of performing some astronomical radio observations in the Ku band. Nevertheless, the solar drift scan was the second observational experiment that was performed in the commissioning and testing the performance of the telescope developed in this study.

5.1.2 Solar drift scan

The Sun is an important astronomical object in the Solar System, in this study not only we tested the performance of telescope using the Sun but we also used it to calibrate the telescope system. From a successful drift scan of the Sun we can calibrate important parameters of the entire radio telescope system such as *Antenna beam (HPBW)*, *System temperature*, *the sensitivity of the telescope*, *the Gain of the telescope* and *the solar flux density* detected by the telescope. In addition, with a solar drift scan, you can determine the antenna solar temperature and the surface temperature of the Sun measured by the telescope and compare it with the measured temperature by professionals on the same day.

Solar observation with a one-meter offset radio telescope operating in the Ku band is not easy as compared to the detection of satellites like the geostationary satellites. In the Ku band frequencies, the Sun's angular diameter is 0.53° , which is the same as the actual visual diameter of the Sun (Lashley, 2010). The Sun's surface has enormous temperature of about



Figure 5.6: Some of the magnetic compasses used in the research during observations

6000 K, although in the sky it only appears to be 0.5° (Koppen, 2011a). However, the radio emissions from the Sun that are observed by the telescope are unpolarised and known to be produced by the low regions of solar atmosphere above the photosphere (Koppen, 2011b).

5.1.3 Solar drift scan with the methanol maser telescope in Ku band

The Solar drift observation can be divided into two categories such as a full drift scan or half drift scan depending on how long you would like to perform the observation. In this section, we will discuss the procedure on how to perform a successful full or half-solar drift scan using our one-meter off-the shelf radio telescope. One of the most important factor you need to take note is the movement of the Sun, in the northern hemisphere the Sun rises in the East, reaches its peak due South and sets in the West. But if you are in the Southern hemisphere, the Sun rises from the East, reaches its highest angle due North and sets in the West https://en.m.wikipedia.org/wiki/Sun_path. The following are some of the major steps one can follow in order to have a successful solar drift scan with our telescope.

1. Firstly, you need to make sure that the right latitude of the location is manually set on the telescope as illustrated in figure (5.3). In our case, the observation point with our telescope is at the University of Hertfordshire, which is in the Northern hemisphere at the latitude of 51.7618° N, and longitude of 0.2468° W.
2. Secondly, check the Sun's position from the planetarium program such as the Stellarium by taking note of the altitude, azimuth and the declination angle in your local sky at a particular time you would like to observe the Sun or other astronomical radio sources. The best time to do a Solar drift scan with this type of the telescope is at *noon*. This is because during the noon period the elevation angle of the Sun is constant, moving only in azimuth.
3. Once you finish setting up the entire telescope, make sure that it is fixed at the right

position for the Sun to drift through the antenna. This is achieved by having set the right latitude, altitude and azimuth angle on the telescope at a particular time the sun is transiting as illustrated in **section (2.4)**.

4. Thereafter, run down to the control room, power on the entire system and wait for the time to start the recording of the observation.
5. Start the Simple_ra receiver by setting the frequency, bandwidth, declination angle, and the sample rate at which you would like to record the observation of the Solar drift scan. This can be achieved by typing the command `simple_ra -devid airspy=0 -srate 3.0e6 -freq 1.60e9` in the terminal and pressing *Enter*.
6. Start taking data at an interval of 1 minute and with an integration time of 50 seconds that can be set using the control of the multimode simple_ra receiver as shown in the figure (5.7)

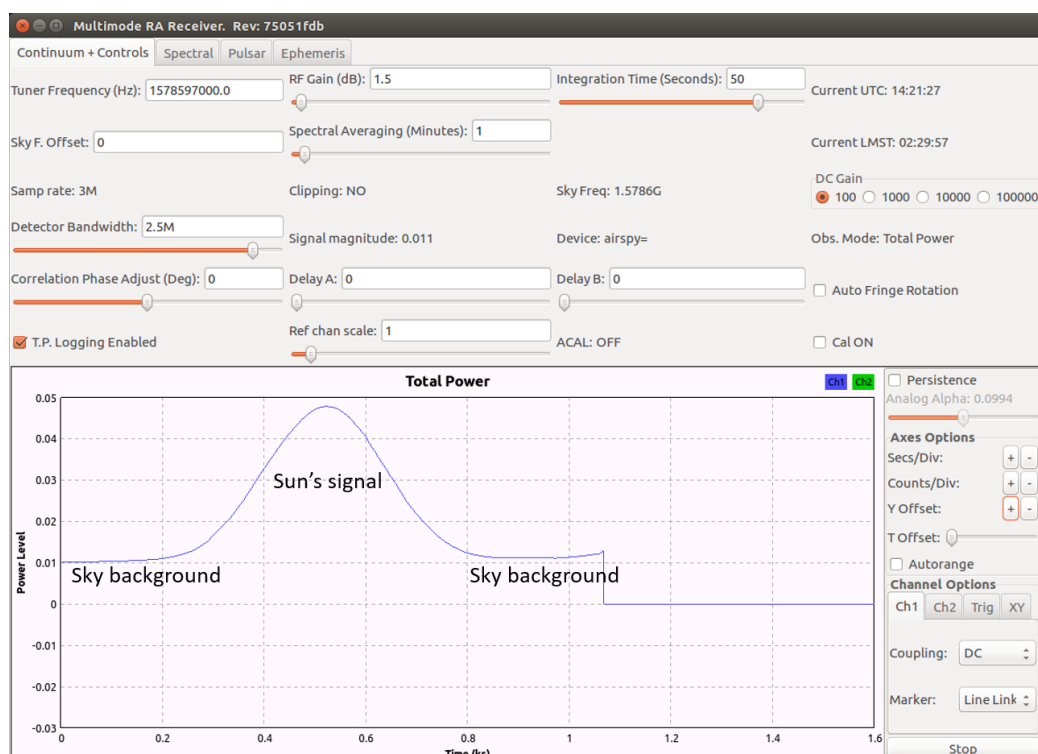


Figure 5.7: Multimode control system of the simple_ra receiver showing the drift scan of the Sun in real time

7. Make sure that you start the recording of the solar drift scan 15 minutes before the Sun drifts through the antenna beam and observe the change in the signal. The recorded data at this time will just be the blank sky.
8. Take note of the rise in the signal and wait for it to drop to its initial level, which is the sky background as shown in figure (5.7). You can also observe the change in the spectrum window of the simple_ra receiver, by taking note of the increase and decrease in the power level in dB during the observation .
9. Measure the constant level of the signal for about 5 minute after the rise.

10. The entire observation of the solar drift scan can be viewed in the continuum window in real time as illustrated in figure (5.7)
11. After 30 minutes of observing the blank-sky and the Sun you can stop the recording in the Simple.ra window in both the continuum and spectrum window.

For a half Solar drift scan, the procedure is almost the same as the full Solar drift scan, the only difference is that this time you only do a drift scan of the Sun for only 15 minutes, unlike the entire 30 minutes. The following is how it could be done.

1. Locate the highest peak of the Sun by moving the telescope in one direction, which is the azimuth direction with the help of the magnetic compass.
2. After the Sun is located, move the telescope few degrees to the West and start the recording until the signal drops to the constant level as shown in figure (5.7).

The recorded data files by the simple.ra receiver can be found in a folder called simple_ra in different file formats as explained earlier in **section (4.3)** of chapter 4. The data files of the recorded observations, are just numbers as shown and explained in **appendix (B)** respectively. In order to make sense of the recorded numbers in the data files, different programs are used to process the data and later analyse the results.

5.2 Calibration of the methanol telescope

The calibration of a radio telescope is very important in the field of radio astronomy, although the results may not be consistent with some of the parameters such as the system temperature of the telescope (O’Neil, 2001). This could be caused by a number of factors such as the response of the entire telescope to weather and atmospheric conditions (Joardar et al., 2010). This section describes how the system developed in this study was calibrated using simple techniques that are used in the calibration of other single dish radio telescopes. In order for one to fully understand the calibration of a radio telescope, it is important to understand and recall most the equations discussed in **chapter 2**. Most of the mathematical equations used in the calibration of our telescope have been covered in detail in **chapter 2**.

5.2.1 Antenna beam width

The antenna beam width of our telescope was calibrated by considering the results from the Solar drift scan, which was observed with our telescope at the University of Hertfordshire on the 9th June, 2017 at 13:46:35 PM. The logged files of the Solar drift scan were processed in Excel and the results are shown in figure (5.8) and (5.9) respectively. In this study, we used figure (5.8) of the solar drift scan to measure the time it took for the Sun to drift through the antenna beam, by considering half of the maximum value of the full Solar drift scan as illustrated in figure (5.8). According to the measurement, It was found that the Sun took 9.3 minutes to drift through the antenna starting at 14:00:05 to 14:09:25. Converting the measured time, it took the Sun to cross over the antenna beam into an angle: firstly, you need to determine the angular speed with which the Sun crosses the sky by considering the location of the Sun. If the Sun is on the celestial equator such as on the 21st March or 21st September the Sun moves at the speed of 15^o /hour which is equivalent to 0.25^o /minute. But if the Sun is above or below the celestial equator its speed depends on its declination angle, and hence the angular speed of the Sun is found to be a bit slower than 0.25^o / minute

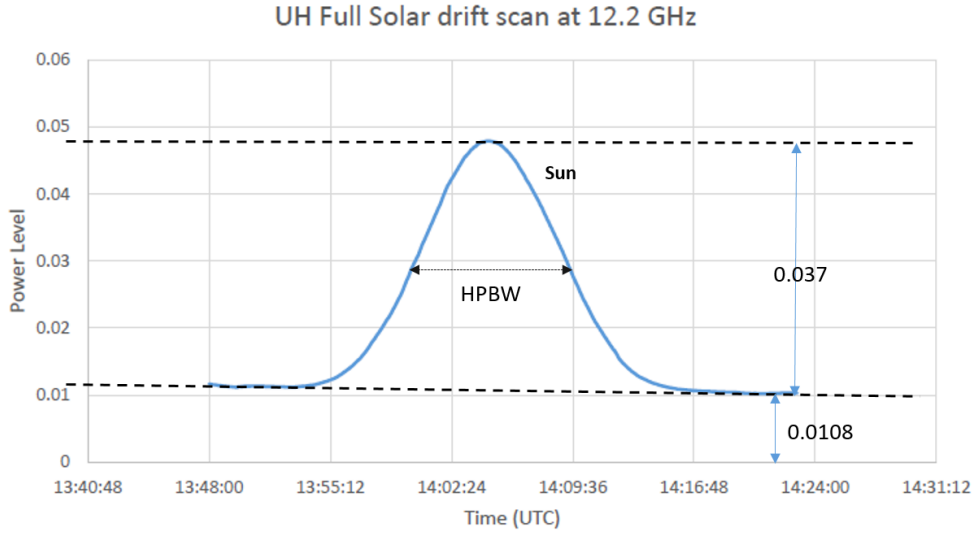


Figure 5.8: The full Solar drift scan processed in Excel showing power level against time (UTC)

(Jean, 2016). In this case, to determine the speed at which the Sun was moving during the observation, you must consider the declination angle at which the Sun was observed and use the following equation

$$\text{Angular speed} = 0.25^\circ/\text{min} \times \cos(\delta) \quad (5.2)$$

where δ is the declination angle at which the Sun was observed during the observation. Substituting the declination angle of 22.96° into equation (5.2), we have the following as the measured angular speed at which the Sun was observed

$$\begin{aligned} \text{Angular speed} &= 0.25^\circ/\text{min} \times \cos(22.96^\circ) \\ &= 0.23^\circ/\text{min} \end{aligned} \quad (5.3)$$

The calculated angular speed proved that the Sun moves a bit slower when it is observed above the celestial equator. Now since we have determined the angular speed of the Sun, it can be used to convert the measured time of 9.3 minutes from the drift scan into degrees

$$\begin{aligned} \text{HPBW} &= 0.23^\circ/\text{min} \times (9.3 \text{ min}) \\ &= 2.14^\circ \end{aligned} \quad (5.4)$$

The same principle can be applied to a half solar drift scan, you only need to double the time it took for the Sun to drift through the maximum half of the half drift scan as shown in figure (5.9). Let us consider the half-solar drift scan that was observed by our telescope on a rainy and windy day. Therefore, since it took 4.65 minutes to drift through the maximum half of the half solar drift scan. Using equation (5.5) and double the measured time, we will have the following as the measured HPBW

$$\text{HPBW} = 0.23^\circ/\text{min} \times (2 \times 4.7\text{min}) = 2.14^\circ \quad (5.5)$$

Applying deconvolution on the measured HPBW from the solar drift scan, we use equation (5.6) (Thompson, 2017). This is to reverse the effects of convolution on the recorded data during the observation.

$$\theta_A = \sqrt{\theta_m^2 - \frac{\ln 2}{2} \times \omega^2} \quad (5.6)$$

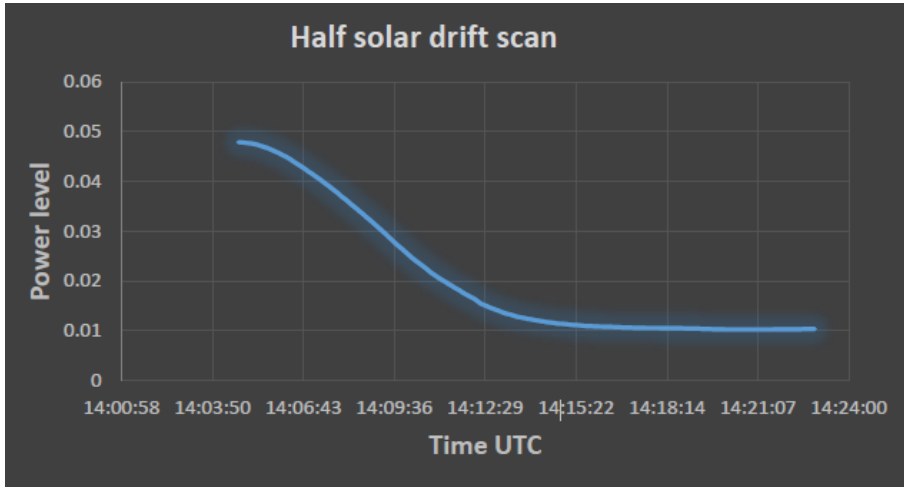


Figure 5.9: The results of the half drift scan of the Sun

where:

θ_A is the deconvoluted HPBW

θ_m is the mirror of HPBW= 2.14°

ω is the diameter of the Sun 0.5° at Ku band frequencies, which is the same as the visual diameter of the Sun (Lashley, 2010).

Substituting these values in equation (5.6), we get the following angle as the deconvoluted HPBW (FWHM)

$$\begin{aligned}
 \theta_A &= \sqrt{2.14^2 - \frac{\ln 2}{2} \times 0.5^2} \\
 &= 2.1^\circ \\
 &= 2.1^\circ \times \frac{\pi}{180^\circ} \\
 &= 0.0367 \text{ [radians]}
 \end{aligned} \tag{5.7}$$

The measured HPBW from the Solar drift scan is found to be larger than the expected value of about 1.70° , which was calculated in **chapter 2**. This difference in the measurements is believed to have been caused by the manufacturer's quoted values of some of the parameters of the antenna and receiver that were previously used in the calculation of the FWHM in **Chapter 2**. Moreover, the manufacturer's quoted Noise Figure of the LNB (0.1 dB) is believed not to be genuine. The other option of measuring the FWHM of our telescope is by observing a point source such as ASTRA satellite, provided that the mount accuracy is good enough.

5.2.2 Antenna beam solid angle

The antenna beam solid angle of this telescope was determined by considering the relationship between the beam solid angle and the measured FWHM, which is given by (Dale, 2014)

and (Koppen, 2011a).

$$\begin{aligned}
\Omega_A &= \frac{\pi}{4} \times (FWHM)^2 \\
&= \frac{\pi}{4} \times (0.0367)^2 \\
&= 1.058 \times 10^{-3} \text{ radians}^2 \\
&= 1.058 \times 10^{-3} \text{ sr}
\end{aligned} \tag{5.8}$$

Therefore, the measured antenna beam solid angle of 1.058×10^{-3} sr from the Solar drift scan, is close to the expected value of 1.137×10^{-3} sr, which was calculated in **chapter 2** at a wavelength of 0.0246 m.

5.2.3 Measured effective area

The measured effective area of the telescope was determined by considering the antenna beam solid angle from the antenna theorem $\Omega_A = \lambda^2 A_{eff}$ (Kraus, 1966). Hence, the effective area of the telescope antenna is given by

$$\begin{aligned}
A_{eff} &= \frac{\lambda^2}{\Omega_A} \\
&= \frac{(0.0246 \text{ m})^2}{1.058 \times 10^{-3}} \\
&= 0.572 \text{ m}^2
\end{aligned} \tag{5.9}$$

where:

$\lambda = 0.0246 \text{ m}$, is the calculated wavelength, since the Sun was observed at the frequency of 12.178 GHz

$\Omega_A = 1.058 \times 10^{-3}$ is the measured antenna beam solid angle

Therefore, the measured effective area (A_{eff}) of our telescope antenna from the solar drift scan is also close to the expected value of the effective area (0.532 m^2) calculated in **chapter 2**, although the measured value is found to be a bit bigger. Henceforth, additional calibrations tests will be needed in any future work.

5.2.4 Measured antenna solar Temperature

The antenna solar temperature ($T_{ant}(sun)$) detected by the telescope was measured by considering the following data from figure (5.8), which is the solar drift scan of the Sun.

- From the solar drift scan we determined the HPBW (FWHM) to be 2.14° .
- The measured background level of the blank sky $F_{sky} = 0.0108$, which includes the contribution from the Receiver, and the Blank sky temperature (sidelobes).
- The measured peak level of the Sun is 0.0478, which is the combination of the Receiver, Blank sky and that of the Sun. Therefore, the measured true signal level of the Sun is $S_{sun} = 0.0478 - F_{sky} = 0.0478 - 0.0108 = 0.037$
- The third measurement that was carried out right after the solar drift scan is the calibrator measurement (F_{cali}) using a near by STRI building wall. The measured power level from a near by STRI building wall is 0.027, which fills the main beam and much of the side-lobes. Therefore, the true signal level of the calibrator is determined by subtracting the measured blank sky level or background power level from the measured

signal level of the calibrator $F_{cali} = 0.027 - F_{sky} = 0.0162$, and this corresponds to the estimated calibrator's temperature (T_{cali}) of about 290 K.

Therefore, with the measured parameters from the solar drift scan we can now compute the Sun's antenna temperature using the following equation.

$$\begin{aligned}
 T_{ant(sun)} &= \frac{(S_{sun} - F_{sky})}{(F_{cali} - F_{sky})} \times T_{cali} \\
 &= \frac{(0.0478 - 0.0108)}{(0.027 - 0.0108)} \times 290K \\
 &= \frac{0.0370}{0.0162} \times 290K \\
 &= 663K
 \end{aligned} \tag{5.10}$$

Using the true measured power level of the maximum signal peak of the solar drift scan, the calibrator's signal and the blank sky level in the equation above, we got 662 K as the Sun's antenna temperature observed on the 9th June 2017 at the University of Hertfordshire with our small radio telescope.

5.2.5 Solar Brightness Temperature

The Solar brightness temperature is the parameter that describes the true temperature of the Sun measured by our methanol maser radio telescope at the frequency of 12.178 GHz at the University of Hertfordshire on 9th June, 2017. Since the measured antenna beam is larger than the Sun's angular diameter, we can determine the brightness temperature of the surface of the Sun by considering that the Sun's angular diameter at Ku band frequencies is 0.5° (Lashley, 2010). The true solar brightness temperature observed by the telescope is determined by equation (5.11). (Koppen, 2010)

$$\begin{aligned}
 T_{sun} &= T_{ant(sun)} \times \left(\frac{HPBW}{D} \right)^2 \\
 &= 663K \times \left(\frac{2.1^\circ}{0.5^\circ} \right)^2 \\
 &= 11695 K
 \end{aligned} \tag{5.11}$$

where:

D is the angular diameter of the Sun

$HPBW$ is the measured decolved antenna beam width.

This is the measured surface brightness temperature of the layer of the sun observed at the frequency of 12.178 GHz with our one meter off the shelf radio telescope. The measured brightness temperature of the Sun is believed to be detected from the transition layer of the Sun, which is the outer layers of the Sun between the corona and the chromosphere (Koppen, 2011b). In addition, the measured solar brightness temperature in this study is equivalent to what was expected to be measured in the Ku-band (Koppen, 2007)

5.2.6 System Temperature

The system temperature of a radio telescope is one of the important parameters in the calibration of the telescope system (Koppen, 2011a). It used to determine the overall sensitivity

of the telescope receiving system, which includes the receiver and the antenna of the telescope. This parameter can either be calculated or measured using various techniques such as Hot & Cold Loads using a microwave absorber, or a Switched Noise Diode. In this study, we have used a very simple method to measure the system temperature of our telescope, which is described as follows:

1. Let us consider the equation that involves the ratio (Y) of the measured power level ON the source (P_{ON}) to the measured power level OFF the source P_{OFF} driven from the solar drift scan in figure (5.8), which is given by

$$\begin{aligned} Y &= \frac{P_{ON}}{P_{OFF}} \\ &= \frac{0.0478}{0.0108} \\ &= 4.43 \end{aligned} \tag{5.12}$$

- Since we have used the measured power level ON the source of the signal of the Sun, which is equivalent to the measured Sun's antenna temperature (T_{Sun}) of 663 K, hence

$$\begin{aligned} Y &= \frac{T_{Sun} + T_{system}}{T_{sys}} \\ T_{sys} &= \frac{T_{Sun}}{Y - 1} \\ T_{sys} &= \frac{663K}{4.43 - 1} \\ T_{sys} &= \frac{663K}{3.43} \\ &= 193 K \end{aligned} \tag{5.13}$$

Where:

P_{ON} is the measured power level on the Sun as the source, which includes the emissions from the Receiver, Blank sky + side-lobes and the Sun.

P_{OFF} is the measured power level off the source, which includes the emissions from the Receiver and the Blank sky with Side-lobes

Y is the ratio given by 4.43.

Therefore, the measured system temperature of our small telescope is a bit high, in fact, it is almost double of the expected system temperature of a small radio telescope like the one developed in this study. We suspect that, thermal temperature from the walls of the STRI building that surrounded the telescope during the observation had much contribution. Moreover, this particular observation was carried out on a warm wet day just after the rains. It is also believed that the system temperature could have been affected by atmospheric influences that have effects on satellite communication on high frequencies (Zubair et al., 2011). The sun's output can vary significantly from day to day and over the Sun spot cycle, hence more calibrations of the solar drift scan will be needed in order to verify the measured system temperature and solar brightness temperature.

2. Apart from the Sun, we used the ground as a source that fills the entire antenna beam of the telescope and measured its power level of P_{ON} , and then measured the blank sky as (P_{OFF}). Therefore, the ratio between the two measurements is given by

$$\begin{aligned}
Y &= \frac{P_{ON}}{P_{OFF}} \\
&= \frac{0.027}{0.0108} \\
&= 2.5
\end{aligned} \tag{5.14}$$

- Since 0.027 is the measured power level of the calibrator which is equivalent to the assumed temperature of the ground of about 290 K. With all these data, we can determine the system temperature of the telescope by considering the following equation

$$\begin{aligned}
Y &= \frac{T_{cali}}{T_{sys}} \\
T_{sys} &= \frac{T_{cali}}{Y - 1} \\
&= \frac{290 \text{ K}}{2.5 - 1} \\
&= \frac{290 \text{ K}}{1.5} \\
&= 193 \text{ K}
\end{aligned} \tag{5.15}$$

Where:

T_{cali} is the calibrator temperature equivalent to 290 K

T_{sys} is the system temperature, which is the combination of the T_{Rec} and $T_{Blanksky+side-lobes}$

5.2.7 Measured flux density of the Sun

Since we have measured the antenna beam solid angle, effective area and the antenna solar temperature of the telescope. With all these parameters, one can determine the detected Solar Flux Unit by the telescope using equation (5.16) or (5.17). Let us start by determining the amount of power received from the Sun by the telescope during the solar drift scan

$$\begin{aligned}
P_{sun} &= 2kT_{ant} = 2 \times 1.38 \times 10^{-23} \text{ W s/K } T_{ant} \\
&= 2760 \times 10^{-23} \text{ W s/K } T_{ant} \\
&= 2760 \text{ W s/K } \times 663 \text{ K} \\
&= 1829880 \text{ Jy } m^2 \\
&= 183 \text{ SFU } m^2
\end{aligned} \tag{5.16}$$

where:

P_{sun} is the received power from the Sun,

2 is a factor that is taken into account that the emission from the sun is unpolarised

k is the Boltzmann's constant.

According to (Koppen, 2011a), 1 Solar Flux Unit = 10000 Jy and 1 Jy = 10^{-26} W s/m^2 . Therefore, using the measured effective area we can determine the Solar Flux detected by the telescope on 09/06/2017 at the frequency of 12.178 GHz and compare the results with

that of the professionals observed on the same day.

$$\begin{aligned}
 SolarFlux &= \frac{2kT_{ant}}{A_{eff}} \\
 &= \frac{183 SFUm^2}{0.572 m^2} \\
 &= 320 SFU
 \end{aligned}
 \tag{5.17}$$

Hence, 320 SFU is the measured Solar Flux Unit observed by our telescope, which corresponds to the SFU observed by other small radio telescopes in Ku-band frequencies (Sourav and Joydeep, 2011).

5.2.8 Measurements of the brightest methanol masers

The detection and monitoring of the brightest methanol masers in Ku-band with the telescope developed in this study, is one of the primary aims of this project. A limited number of the brightest 12.2 GHz methanol masers as mentioned in *chapter 2* were targeted in order to test whether our telescope is capable of detecting them due to its size and sensitivity. During the observations, we only focused on the brightest methanol masers that were apparent in the northern hemisphere at that time. The following are some of the brightest 12.2 GHz methanol masers that were targeted for measurements.

1. The NGC7538 is found in Cepheus constellation with flux density of about 1000 Jy. Since NGC7538 is one of the brightest Methanol maser visible in the northern hemisphere, we tried observing it at the frequency 12.178 GHz with an integration time of about 26 minutes. Longer period of integration was caused by the lower sensitivity of the telescope. In *chapter 2* we did some calculations on how long it could take to observe different bright methanol masers with different flux densities. After observing the source for about 35 minutes, the logged data files in spectral mode were processed and there was no sign of the detected signal from the NGC 7538 source. The experimental observations of this bright source were carried out on different days and time trying to prove that our telescope could detect the source. Unfortunately, the results of the observations were the same that showed no sign of a maser as shown in figure (5.10) of the processed telescope square wave bandpass spectrum.
2. Apart from the NGC7538, we tried observing a different bright methanol maser the NGC 869 with an intensity of 793 Jy. This source is found in Perseus constellation at a declination angle of $57^{\circ}, 01', 49.5''$. All the observations were done using the drift scan observational technique when the sources were transiting. In figure (5.11), we present the results of the processed logged files of the NGC 793 in spectral mode.

The square wave bandpass spectrum in figure (5.11) shows no sign of a maser but only noise, which implies that the aim of detecting and monitoring of the brightest methanol masers with our small telescope in Ku-band was not successful at this stage of the study. Therefore, this leads to another section that explains why we were unable to detect the brightest methanol masers with the one-meter off the shelf telescope.

5.2.9 Analysis of the measured bright methanol masers

The mathematical analysis on the measurements of the brightest methanol masers with our radio telescope is based on the results we got in **section 5.2.8** and some mathematical

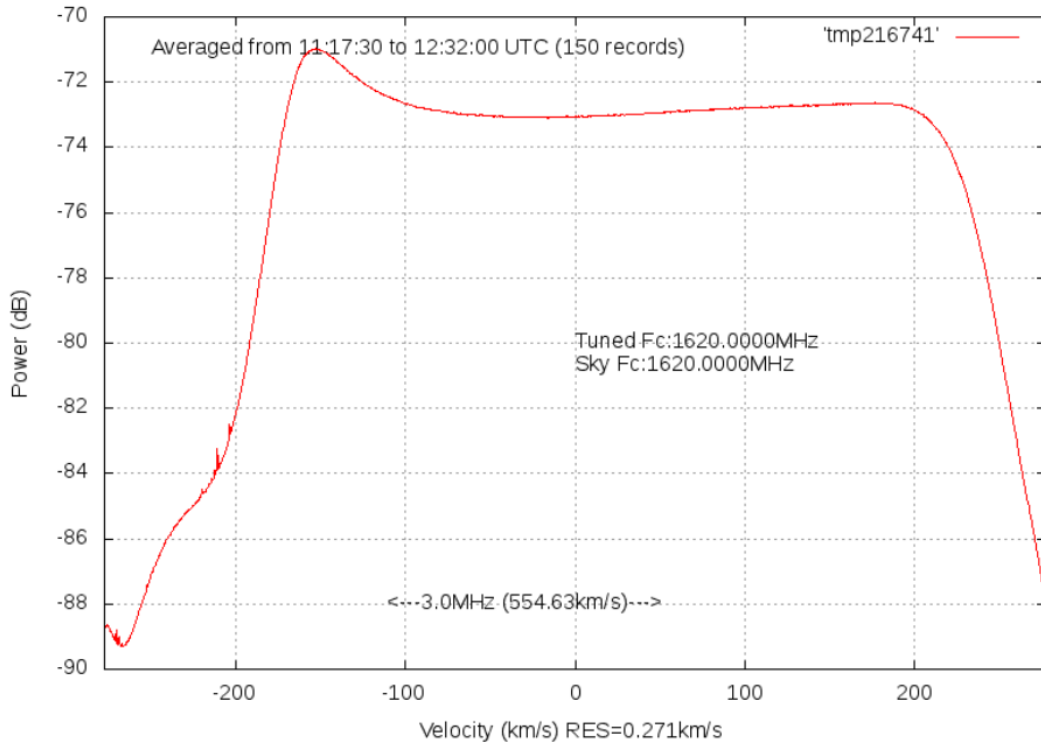


Figure 5.10: The square wave bandpass spectrum of the NGC 7538 source processed in spectral mode.

equations discussed in **chapter 2**. There are few important parameters of our radio telescope system, which can be determine from the measurements of the brightest methanol masers.

1. Number of channels determined by the Airspy-Mini device and the supported software (*simple.ra*) is one of the key feature in visualizing the detected signal of the bright methanol maser. From the results in figure (5.10) and figure (5.11), we can deduce that the Airspy-Mini soft defined radio device produced many channels, which contributed to the poor visualization of the detected signal of the bright methanol masers. Using equation (2.2) from **chapter 2** and data velocity from figure (5.12), we can show that during the measurements of the 12.2 GHz methanol masers, number of channels produced by the SDR device were more than what is required for this observation with a small telescope. Since the observations of the brightest 12.2 GHz methanol masers were done at the frequency of 12.178597 GHz with a detector bandwidth of 3 MHz, we found 554.63 km/s as the total velocity coverage of the spectrum and 0.271 km/s as the channel width velocity as indicated in figure (5.11). Hence, the total number of channels is given by

$$\begin{aligned}
 \text{Total Number of channels} &= \frac{\text{Total velocity coverage}}{\text{Channel width velocity}} \\
 &= \frac{554.63 \text{ km s}^{-1}}{0.271 \text{ km s}^{-1}} \\
 &= 2047
 \end{aligned} \tag{5.18}$$

The total number of channels produced during this observation were 2047 at a total velocity

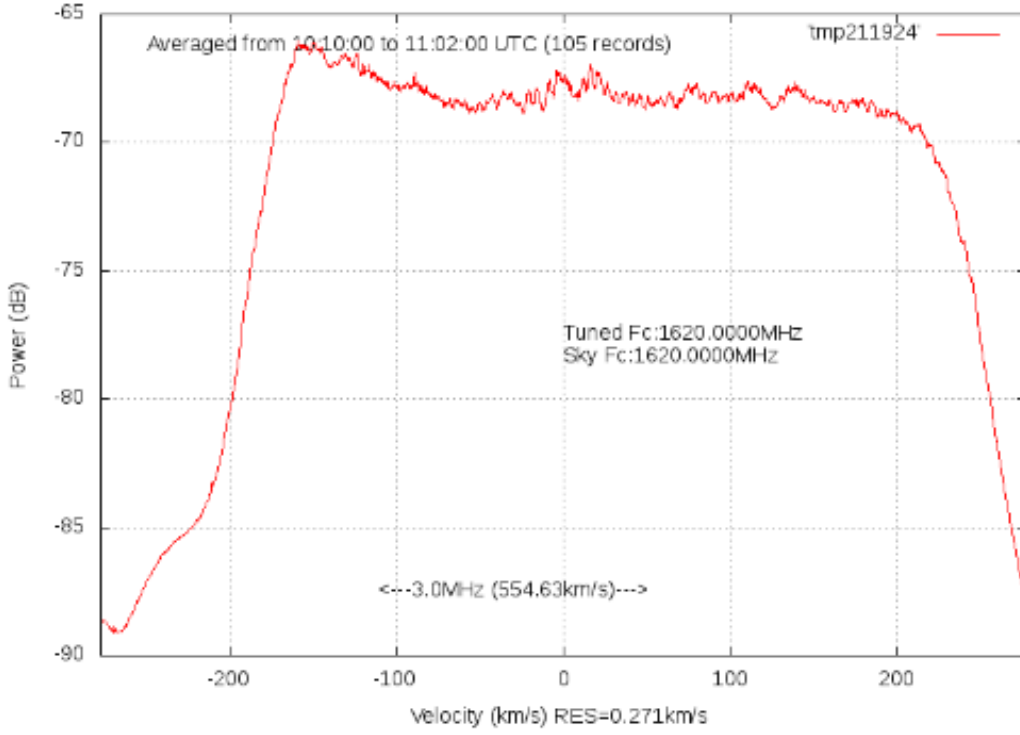


Figure 5.11: Square wave bandpass showing the processed logged files of NGC793 in spectral mode

of 74 km/s, which is calculated by using the following equation

$$\begin{aligned}
 \text{Total velocity coverage} &= \frac{BW}{v} \times c \\
 &= \frac{3 \times 10^6 \text{ Hz}}{12.2 \text{ GHz}} \times 3.0 \times 10^8 \text{ m/s} \\
 &= 74 \text{ km/s}
 \end{aligned} \tag{5.19}$$

Where:

BW is the detector bandwidth in Hz

v is the frequency at which the telescope is operating [Hz]

c is the speed of light [m/s]

The higher value of the total velocity coverage calculated above is believed to have been caused by the frequency of the Airspy device and not the actual detection of the methanol molecular line or an observed source. Using the calculated total channel velocity width of about 74 km/s, we can determine the width velocity per channel as follows

$$\begin{aligned}
 \text{Channel width velocity} &= \frac{\text{Total velocity channel}}{\text{Number of channels}} \\
 &= \frac{74 \text{ km/s}}{2047} \\
 &= 0.0366 \text{ km/s}
 \end{aligned} \tag{5.20}$$

Therefore, 0.0366 km/s is the calculated width velocity per channel. In order to determine

the actual bandwidth per channel use equation (2.3) which is given by

$$\begin{aligned}
 \text{Bandwidth per channel}(\Delta v) &= \frac{\text{Detector bandwidth}}{\text{Number of channels}} \\
 &= \frac{3 \text{ MHz}}{2047} \\
 &= 1.466 \text{ kHz}
 \end{aligned} \tag{5.21}$$

The number of channels can be reduced to increase the channel width, this is achieved by averaging the number of channels, which leads to the reduction of the RMS noise by a factor of the square root of the number of channels. Since in our case, the number of channels produced by the Airspy-Mini hardware is more than what is required in the detection of the methanol molecular line at 12.2 GHz with a small radio telescope. The best solution is averaging 16 channels that could reduce the number of channels by a factor of 4. Therefore, this could give us an effective number of channels, which is determined by the following equation

$$\begin{aligned}
 \text{Effective number channels} &= \frac{\text{Number of channels}}{\text{Averaging channels}} \\
 &= \frac{2047}{16} \\
 &= 128
 \end{aligned} \tag{5.22}$$

Hence, the new channel width will be 0.586 km/s which is determined by dividing the *total velocity* by the *effective number of channels* as illustrated

$$\begin{aligned}
 \text{Channel width} &= \frac{\text{Total velocity coverage}}{\text{Number of channels}} \\
 &= \frac{75 \text{ km/s}}{128} \\
 &= 0.586 \text{ km/s}
 \end{aligned} \tag{5.23}$$

- First, let us determine the period of time it could take for our one-meter radio telescope to observe a 1000 Jy source of the brightest methanol maser. Making use of equation (2.48), we get the following

$$\Delta f_v = \frac{2kT_{sys}}{A_{eff}\sqrt{\Delta v\tau}} \tag{5.24}$$

Where:

$T_{sys} = 193 \text{ K}$ the measured system temperature of our telescope

$A_{eff} = 0.572 \text{ m}^2$ is the measured aperture efficiency of our telescope

Δf_v is the change in flux density

Δv is the bandwidth per channel [kHz]

- Since the targeted source has the flux density (f_v) of 1000 Jy, and we know that for a detection we require a Signal to Noise Ratio ($\frac{S}{N}$) > 3 . Hence, the change in the flux density (333.3 Jy) was determined by considering that $\frac{f_v}{\Delta f_v} > 3$ which is equivalent to $f_v = 3\Delta f_v$. Using the above equation and substituting other parameters from the drift scan of the Sun and measurements of the brightest methanol masers, we get the

following

$$\begin{aligned}
\tau &= \frac{(2 \times 1.380 \times 10^{-23} W \text{ Hz}^{-1} K^{-1} 193K)^2}{1.466 \times 10^3 \text{ Hz} (0.57m^2 \times 333.3 \times 10^{-26} W/m^2 \text{ Hz}^2)^2} \\
&= 5324 [s] \\
&= 88.7 \text{ minutes}
\end{aligned} \tag{5.25}$$

Therefore, with our telescope it could take the integration time of 5324 seconds to observe a 1000 Jy source.

- Now we can determine how much can be measured from a 1000 Jy source with our one-meter radio telescope by using the following equation

$$\begin{aligned}
f_v &= \frac{2k\Delta T_A}{A_{eff}} \\
1000 \times 10^{26} W \text{ m}^{-2} \text{ Hz}^{-1} &= \frac{2 \times 1.380 \times 10^{-23} W \text{ Hz}^{-1} K^{-1} \times \Delta T_A}{0.572m^2} \\
\Delta T_A &= 0.21 K
\end{aligned} \tag{5.26}$$

- We can determine the RMS by considering the radiometer sensitivity equation

$$\begin{aligned}
\Delta T_{rms} &= \frac{T_{sys}}{\sqrt{\Delta\nu\tau}} [K] \\
&= \frac{190K}{\sqrt{1.466 \times 10^3 \times (5324 \text{ s})}} [K] \\
&= 0.069K
\end{aligned} \tag{5.27}$$

- Since $\Delta T_{rms} = \Delta T_{min}$, and $\Delta T_A \geq \Delta T_{min}$ (Kraus, 1986), then the signal to noise ratio is given by

$$\begin{aligned}
S/N &= \frac{\Delta T_A}{\Delta T_{min}} \\
&= \frac{0.21K}{0.069K} \\
&= 3.02
\end{aligned} \tag{5.28}$$

Hence, a 1000 Jy source could be observed with a signal to noise ratio of 3.02 in 88 minutes, which corresponds to RMS noise of 328 Jy per channel. However, with a drift scan this could be hard to do, hence tracking a source would be better. This is why we have proposed an inexpensive telescope mount and drive system.

- Comparing our findings with a bigger telescope like the 26-m of the Hartebeesthoek Radio Astronomy Observatory, with an aperture efficiency of 0.64 and diameter of 26-m with a system temperature of 100 K.

$$\begin{aligned}
\Delta T_A &= \frac{f_v A_{eff}}{2k} \\
&= \frac{1000 \times 10^{26} W \text{ Hz}^{-1}}{2 \times 1.380 \times 10^{-23} W \text{ Hz}^{-1} K^{-1}} \\
&= 123 K
\end{aligned} \tag{5.29}$$

With a bigger telescope, we can measure more from a source than we can measure with a small telescope.

From the methanol maser observations performed by our telescope and the calculations, I still believe that a small radio telescope could detect the brightest 12.2 GHz of methanol masers provided that it has a proper telescope mount and drive system. Although this could take a bit longer period with a small telescope like ours than it could take with a bigger telescope. Additionally, with all the parameters discussed in this section, it could be easier to detect very bright methanol masers with flux densities of about 1000 Jy as shown in table (2.1) such as NGC6334 and W3(OH), which both have the peak fluxes of about 1000 Jy with total velocity of 2 km/s and 3 km/s respectively (Koo et al., 1988). According to (Nicolson G, 2017), with 128 channels we could get the best sensitivity but the spectrum of the stated methanol masers would only fit about 3 or 5 channels respectively. This implies that, better resolution leads to worse signal to noise ratio. As a result, weaker features

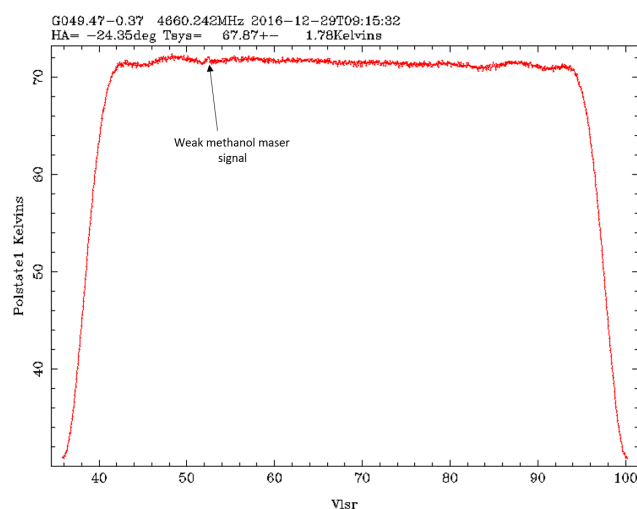


Figure 5.12: Illustration of how weak features of the observed signal of methanol masers disappear in Noise. The arrow in the square wave bandpass shows a weak observed maser that looks like noise at this stage of processing.

of the observed signals of methanol masers are likely to disappear into noise as illustrated in figure (5.12) of the weak 6.6 GHz methanol masers observed by the 26 m HartRAO radio telescope. This data was used for illustration sake of what we could possibly see with our small radio telescope, which is not that sensitive in the detection of weak signals. After further processing of the results shown in figure (5.12) by fitting Gaussians, you will have data shown in **Appendix A**, which indicates the number of Gaussian fits and other important parameters. The results of the processed data of the weak 6.6 GHz methanol maser observed by the 29-m telescope at Hartebeesthoek Radio Astronomy Observatory in 2016 is shown in figure (5.13).

However, the results shown in figure (5.12) and (5.13) illustrates what is expected to be observed from the 12.2 GHz methanol maser molecular line with a small radio telescope. This is because our one-meter off-the shelf radio telescope developed in this study is small and less sensitive. Therefore, some of the features of the detected bright methanol masers are likely to disappear in noise as shown in figure (5.12). This is why it is advisable to use big antennas or an interferometer to increase the sensitivity of the telescope.

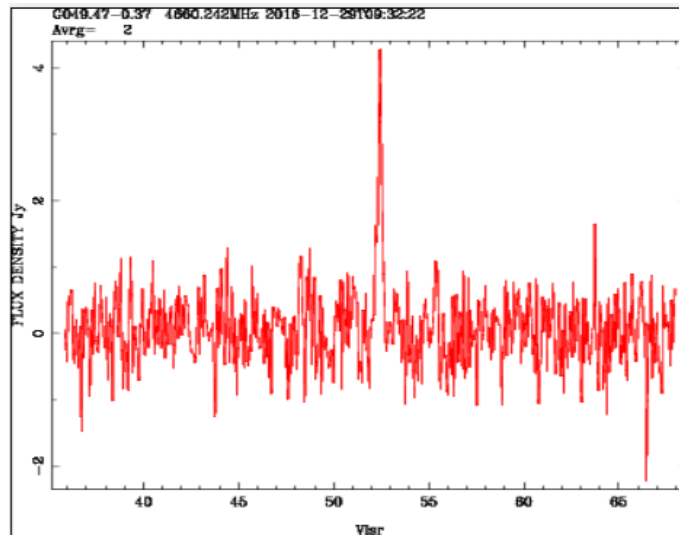


Figure 5.13: Shows the processed weak methanol maser that seem to disappear in noise as indicated in figure (5.12).

5.3 Research Limitations

Several problems were encountered in this study from hardware to software that are considered as the research limitations of this work. Therefore, the following are some of the main limitations to this study

1. The size of the antenna used in this project is quite small with low antenna gain. Hence, the telescope was not that sensitive in the detection of weak signals from distant astronomical radio sources. As a result, the telescope is only limited to observing strong astronomical radio sources in the Ku band. Increasing the size of the antenna from 1m to 2.5m with a good antenna gain could be a great solution to increase the sensitivity of the portable telescope in order to monitor methanol molecular line.
2. Since the entire research project was limited to the development of a low-cost off the shelf radio telescope. Therefore, the telescope system lacked a proper telescope mount and drive system that could be used to track and integrate on source. In this case, a cheap observational technique called the drift scan was used throughout the observations. From a drift scan we estimated that 2 degrees beam passes a point in the sky in less than 10 minutes, therefore integrating on a source for more than 10's of minutes using a drift scan could be a huge challenge. Hence, lack of a proper telescope mount and drive system is considered as one of the major limitation to this study that needs our attention.
3. Although previous studies indicate that radio astronomy experiments can be performed at any time of the day regardless of the weather. This is a bit challenging to small off-the shelf radio telescopes due to the reason that a number of challenges were encountered during experimental observations in bad weather such as *rainy, windy and stormy weather*. With a small radio telescope like the one developed in this study, it is quite difficult to perform radio astronomy experiments in rainy or stormy weather.

In general, small radio telescopes are disadvantaged to operate in bad weather since they are easily shaken and blown away by heavy winds, which could cause a short

circuit and poor observation of a targeted source as shown in **appendix C (c.1.0) and (c.1.2)**. In addition, bad weather causes so much problems such as lack of accurate pointing when there is too much wind. In order to have a successful solar drift scan as the one shown in figure (5.8) in the month of June on the roof of the University Hertfordshire STRI building, so much work has to be done to prevent the telescope from shaking and blown away by heavy winds. A proper stable base and mast of the telescope is required in order for the telescope to withstand stormy weather during observations. Moreover, this could allow radio astronomy experiments with small radio telescopes to be performed at any time of the day including in bad weather.

4. Pointing of the telescope in some directions at the University of Hertfordshire during observations was a bit limited. This is because the telescope was surrounded by building walls and roofs as shown in figure (6.3) and (6.4) in **appendix C (C.2.0) and (C.2.1)**. Therefore, sometimes we had to wait for a source to move in a better position of the sky away from the buildings for a better observation. For such observational experiments to be performed by students in schools, I suggest an open place for the telescope site would be better. Furthermore, some parts of the University are also avoided due to strong RFI that are detected by the telescope when it is pointed in some directions. Hence, astronomical radio sources in the sky are only accessed in some directions.
5. The setting up of the azimuth angle on the telescope during observations was a bit challenging as the magnetic compass used to find the right azimuth angle was affected by metals and roofing sheet on the site. In addition, inaccurate azimuth angle provided by the compass could lead to poor observation of the targeted source. Therefore, it is strongly advised to avoid metal materials to get close to a magnetic compass or instead you can use a digital compass on smart phones.
6. Lastly, the number of channels produced by the Airspy Mini and the associated software are more than the required number of channels for the observation of the methanol molecular line at 12.17859 GHz with a small radio telescope. It could be great if the software can control the number of channels in order to suit certain observations. From different observations performed in this study, we noted that the number of channels are determined by the spectrometer according to the detector bandwidth. Furthermore, the (*simple_ra*) receiver used during observations has a limited control for integration time, hence it is impossible to integrate on source for a longer period.

6. Conclusions and proposed future work

6.1 Conclusions

According to the experience and skills gained from this study, I have concluded that the size of the antenna, LNB (Noise Figure), Software Defined Radio device bandwidth, the telescope mount and drive system are the main key components that requires a major consideration in the development of a low-cost off the shelf small radio telescope. In addition, in order to have successful cheap radio astronomy experimental observations with this type of a telescope, a bit of investment is required in the buying of the stated key components. An inexpensive equatorial or polar mount and drive system that can accommodate 1m to 2.5m satellite television dish could solve a number challenges that were faced in this study. This is because accurate pointing and tracking of the source could lead to the success of this study.

However, in order to promote effective cheap radio astronomy experiments in African schools such as Colleges or Universities, proper documentations on small radio telescopes are required. It is a great idea for schools to have their own built small radio telescopes, so that students could have enough time to observe and study astronomical radio sources without being interfered by other astronomers. This could give a great advantage for students to perform observations at their own pace and learn how to build and repair their own small telescopes, unlike big telescopes owned by professionals in radio astronomy where you are given a limited time to use the telescope.

Theoretically, it is stated that a meter class low-cost radio telescope operating in Ku-band frequencies could observe methanol molecular line (Fish and Rogers, 2009). This implies that the small off-the shelf radio telescope should have a good sensitivity with an antenna gain of about 50 dB or better and aperture efficiency of about 0.7. In addition to that, accurate pointing is required that can be achieved by using an inexpensive proper mount and drive system. The telescope system spectrometer bandwidth should also be able to cover the Doppler shifted velocity range of methanol in massive star forming regions. Moreover, the LNB and the software defined radio device used in the development of the telescope system should be able tune to 12.17856 GHz of the methanol molecular line.

The following are some of the cheap radio astronomy activities based on software-defined radio that could be used to promote radio astronomy in schools with this type of a radio telescope

- Educating students on the development of their own small telescopes using satellite T.V components
- Expose students to the basics of microwave radio receivers.
- To educate students on the effects of RFI by observing geostationary satellites.
- Performing cheap radio astronomy observational techniques with the help of the planetary software.
- Perform Digital Signal Processing (DSP) on different spectrum analysers based on GNU-radio software such as GNU-radio companion based applications, the use of the SDR real time spectrum analyser, *Simple_ra* receiver and GQRX software.

Lastly, the entire set up of the telescope developed in this study has so much room for modification and improvement to suit one’s budget, technical radio astronomy knowledge, and skills. The testing of our telescope in this study responded well in the observation of the Sun and geostationary satellites in Ku band. This is due to the telescope large beam width, which is bigger than the measured sources. It was also noted that observing the Sun and geostationary satellites in Ku-band was quite easy using the drift scan method unlike the detection and monitoring of methanol masers. Based on observational results and calculations, we can conclude that with a proper cheap telescope mount, the observation of the brightest methanol masers with this telescope could be possible.

6.2 Proposed future work

The following are some of the major future work that I have proposed to improve this study.

1. The telescope system developed in this study has the right components that could make it observe brightest methanol masers if the pointing of the telescope is improved by purchasing an inexpensive equatorial or polar mount and drive system, that could be used for accurate pointing and tracking of sources. If the telescope is able to track a source, therefore we will be able to integrate on source unlike using the drift scan.
2. I propose trying the same set up used in this study with a bigger satellite T.V dish of about 2 to 2.5 meters with a good antenna gain of about 50 dB or better. This will increase the sensitivity of the telescope that could lead to better observations of weak signals and avoid focussing only on the brightest methanol masers. In addition to that, it could be a great idea considering the development of an interferometer of 3-one-meter antennas to increase the sensitivity and the gain of the telescope. Although, this may need a bit of investment in purchasing the telescope components. Later on, the simple interferometer could be used for educational purposes on cheap radio astronomy interferometer.
3. Measuring of the LNB’s *Noise Figure and L.O frequency* and SDR devices used in the development of low-cost telescopes needs to be considered. This is because most of the manufacturers falsely label most of the LNB’s and other components as a result; this might lead to inaccurate radio astronomy observations.
4. Since our telescope system function perfectly, another option could be the use of a different LNB i.e. 1.4 GHz LNB to study HI in the Milky Galaxy.
5. Total number of channels produced by the software defined radio-hardware at a certain bandwidth with the supported software (*simple_rareceiver*) should also be considered, in order to succeed with some of the sensitive radio astronomy observational experiments such as the monitoring of the methanol molecular line in the Ku-band. It has been noted that the SDR-hardware and the *Simple_ra* produced many channels during observations, which also contributed to unsuccessful detection of the methanol molecular line. It could be great to write some software or use Excel with the CSV-data, to average up data into broader channels. Therefore, with all the calculations performed in **section (5.2.9)**, it is believed that very bright methanol masers with flux densities of about 1000 Jy could be observed with this telescope provided that we have the right mount and drive system for easy pointing and tracking.

Appendix A

A.0 Fit Gaussians to the LCP and RCP data.

The G049.47-0.37 is a weak methanol maser of the 6.6 GHz that was observed by the 26 m radio telescope of the Hartebeesthoek Radio Astronomy Observatory (HartRAO) on 29/12/2016. We used this data in order to demonstrate how methanol masers observed by our small radio telescope could be processed and viewed. This is because our telescope is not that sensitive, hence most of the observed signals are likely to disappear in noise as shown in figure (5.12). The data below shows the number of Gaussian fits that were done during the processing of data using the LINES program developed by Michael Gaylard at HartRAO. In this case, we only had one Gaussian fit of a methanol maser as shown below in both Left-Circular Polarization (LCP) and Right-Circular Polarization (RCP).

A.1.0 Left-Circular Polarization (LCP)

G049.47-0.37 Scan 0 of 2016-12-29T09:32:22 Line 1 Best Fit Gaussian
Position = 52.430650 + - 0.013864
Height = 3.389790 + - 0.310336
Uncorrected width = 0.311397 + - 0.035097
Resolution = 0.075387
Corrected width = 0.302134 + - 0.035097 (spectra)
Signal / Noise = 22.598551
RMS of residue = 0.333959 expected = 0.423926
Baseline at 1.8822744309773234E-002

A.1.1 Right-Circular Polarization (RCP)

G049.47-0.37 Scan 0 of 2016-12-29T09:32:22 Line 1 Best Fit Gaussian
Position = 52.428092 + - 0.011337
Height = 3.574415 + - 0.300891
Uncorrected width = 0.265538 + - 0.023700
Resolution = 0.075387
Corrected width = 0.254612 + - 0.023700 (spectra)
Signal / Noise = 22.886265
RMS of residue = 0.321098 expected = 0.418062
Baseline at 7.8476434609455728E-004

Appendix B

(B.1.0) Spectral data file

The spectral file (spec-20170609-13.dat) contains data of the solar drift scan observation that was recorded by the simple_ra receiver in spectral mode with our one-meter radio telescope on 9/06/2017. This data has series of space-separated floating-point values, which represents the FFT magnitude in dB. In addition, the PARAMS line in the data file contains PARAMETERS such as the frequency, detector bandwidth, Declination and Julian date, Right Ascension, UTC, and LMST.

```
PARAMS 1578597000.00000 3000000.00000 -99.00000 2457914 12.00 13:47:00.0 01:55:24 [
-100.01
```

```
-99.74 -99.56 -99.59 -99.44 -99.25 -99.04 -98.93 -98.93 -98.95 -98.92
-98.83 -98.64 -98.43 -98.31 -98.33 -98.25 -98.07 -97.82 -97.79 -97.80
-97.75 -97.77 -97.74 -97.67 -97.59 -97.47 -97.33 -97.12 -97.06 -97.07
-96.83 -96.62 -96.59 -96.66 -96.71 -96.70 -96.56 -96.43 -96.35 -96.34
-96.23 -96.13 -96.07 -96.04 -95.97 -95.71 -95.49 -95.39 -95.31 -95.32
-95.27 -95.19 -95.23 -95.16 -94.99 -94.92 -94.84 -94.67 -94.57 -94.45
-94.35 -94.32 -94.27 -94.02 -94.00 -93.93 -93.78 -93.79 -93.86 -93.83
-93.72 -93.66 -93.63 -93.62 -93.48 -93.19 -93.07 -92.99 -92.87 -92.85
-92.76 -92.59 -92.48 -92.48 -92.38 -92.28 -92.20 -92.19 -92.09 -91.90
-91.82 -91.76 -91.76 -91.55 -91.47 -91.34 -91.20 -91.29 -91.34 -91.14
-90.87 -90.73 -90.77 -90.78 -90.62 -90.39 -90.36 -90.38 -90.26 -90.09
-90.18 -90.04 -89.79 -89.78 -89.73 -89.61 -89.59 -89.41 -89.19 -89.15
-89.13 -89.08 -89.00 -89.02 -88.91 -88.76 -88.69 -88.62 -88.38 -88.08
-87.97 -88.04 -88.04 -88.05 -88.21 -88.22 -88.02 -87.71 -87.63 -87.64
-87.50 -87.48 -87.47 -87.49 -87.43 -87.35 -87.16 -87.08 -87.11 -87.09
-86.93 -86.73 -86.80 -86.91 -86.85 -86.76 -86.67 -86.62 -86.48 -86.34
-86.34 -86.42 -86.33 -86.14 -86.01 -86.01 -85.98 -86.03 -86.06 -85.77
-85.63 -85.60 -85.43 -85.41 -85.49 -85.48 -85.37 -85.44 -85.42 -85.42
-85.40 -85.36 -85.33 -85.24 -85.21 -85.20 -85.25 -85.12 -84.90 -84.97
-85.04 -84.92 -84.85 -84.91 -84.89 -84.65 -84.39 -84.36 -84.45 -84.59
-84.58 -84.60 -84.59 -84.45 -84.42 -84.41 -84.40 -84.26 -84.03 -84.02
-84.10 -84.15 -84.21 -84.07 -83.90 -83.99 -84.04 -84.00 -83.95 -83.85
-83.90 -83.99 -84.01 -83.94 -83.79 -83.77 -83.79 -83.70 -83.61 -83.65
-83.62 -83.52 -83.52 -83.57 -83.58 -83.51 -83.35 -83.21 -83.35 -83.35
-83.31 -83.30 -83.37 -83.32 -83.25 -83.23 -83.35 -83.39 -83.31 -83.25
-83.12 -83.03 -82.96 -83.03 -83.17 -83.16 -83.17 -83.13 -83.05 -83.02
-83.16 -83.29 -83.23 -83.16 -83.08 -82.99 -82.85 -82.80 -82.90 -82.91
-82.92 -83.05 -83.14 -83.03 -82.94 -82.90 -83.05 -83.10 -82.82 -82.67
-82.87 -83.05 -82.91 -82.83 -82.84 -82.87 -82.86 -82.83 -82.76 -82.69
-82.84 -82.89 -82.75 -82.61 -82.62 -82.67 -82.58 -82.58 -82.68 -82.81
```

-82.77 -82.61 -82.59 -82.52 -82.49 -82.51 -82.61 -82.66 -82.55 -82.59
-82.52 -82.43 -82.51 -82.60 -82.54 -82.46 -82.53 -82.46 -82.60 -82.69
-82.61 -82.59 -82.62 -82.57 -82.56 -82.56 -82.65 -82.71 -82.60 -82.54
-82.71 -82.73 -82.69 -82.66 -82.50 -82.45 -82.54 -82.64 -82.67 -82.74
-82.57 -82.33 -82.33 -82.47 -82.43 -82.35 -82.33 -82.34 -82.39 -82.29
-82.39 -82.66 -82.60 -82.46 -82.44 -82.41 -82.49 -82.59 -82.50 -82.47
-82.39 -82.35 -82.38 -82.51 -82.62 -82.58 -82.40 -82.29 -82.40 -82.51
-82.52 -82.50 -82.47 -82.47 -82.47 -82.42 -82.33 -82.41 -82.43 -82.46
-82.59 -82.48 -82.36 -82.34 -82.32 -82.35 -82.35 -82.32 -82.42 -82.39
-82.22 -82.29 -82.53 -82.56 -82.50 -82.37 -82.28 -82.38 -82.46 -82.52
-82.49 -82.42 -82.36 -82.26 -82.19 -82.23 -82.42 -82.45 -82.41 -82.49
-82.58 -82.54 -82.53 -82.51 -82.38 -82.26 -82.33 -82.53 -82.54 -82.48
-82.55 -82.40 -82.35 -82.37 -82.35 -82.31 -82.32 -82.37 -82.41 -82.35
-82.30 -82.37 -82.36 -82.49 -82.49 -82.48 -82.54 -82.44 -82.27 -82.32
-82.35 -82.40 -82.56 -82.53 -82.48 -82.54 -82.58 -82.56 -82.53 -82.41
-82.27 -82.47 -82.51 -82.37 -82.35 -82.32 -82.30 -82.27 -82.26 -82.40
-82.45 -82.47 -82.59 -82.62 -82.50 -82.50 -82.38 -82.30 -82.32 -82.26
-82.30 -82.43 -82.38 -82.35 -82.45 -82.55 -82.54 -82.52 -82.45 -82.37
-82.38 -82.53 -82.57 -82.45 -82.50 -82.41 -82.36 -82.40 -82.38 -82.38
-82.39 -82.36 -82.41 -82.31 -82.33 -82.49 -82.44 -82.53 -82.52 -82.42
-82.37 -82.47 -82.46 -82.46 -82.56 -82.60 -82.55 -82.49 -82.44 -82.47
-82.50 -82.40 -82.32 -82.41 -82.43 -82.38 -82.44 -82.43 -82.40 -82.36
-82.37 -82.48 -82.50 -82.48 -82.55 -82.50 -82.40 -82.42 -82.43 -82.40
-82.31 -82.21 -82.28 -82.42 -82.50 -82.51 -82.51 -82.60 -82.53 -82.39
-82.35 -82.29 -82.19 -82.39 -82.54 -82.37 -82.34 -82.54 -82.60 -82.52
-82.40 -82.42 -82.41 -82.36 -82.30 -82.30 -82.39 -82.57 -82.57 -82.48
-82.58 -82.64 -82.66 -82.69 -82.49 -82.43 -82.40 -82.25 -82.28 -82.42
-82.41 -82.46 -82.50 -82.57 -82.61 -82.71 -82.64 -82.56 -82.43 -82.38
-82.39 -82.33 -82.33 -82.36 -82.49 -82.43 -82.38 -82.44 -82.41 -82.48
-82.46 -82.40 -82.48 -82.59 -82.57 -82.57 -82.47 -82.38 -82.37 -82.29
-82.31 -82.40 -82.47 -82.45 -82.39 -82.29 -82.26 -82.40 -82.53 -82.58
-82.49 -82.34 -82.42 -82.63 -82.64 -82.60 -82.58 -82.43 -82.40 -82.44
-82.45 -82.38 -82.28 -82.24 -82.32 -82.30 -82.34 -82.44 -82.41 -82.42
-82.65 -82.54 -82.42 -82.38 -82.37 -82.23 -82.32 -82.52 -82.50 -82.51
-82.53 -82.49 -82.46 -82.43 -82.46 -82.46 -82.36 -82.36 -82.44 -82.34
-82.14 -82.27 -82.41 -82.47 -82.44 -82.45 -82.50 -82.45 -82.46 -82.53
-82.50 -82.51 -82.43 -82.31 -82.45 -82.54 -82.46 -82.34 -82.30 -82.27
-82.36 -82.48 -82.49 -82.63 -82.61 -82.46 -82.31 -82.30 -82.42 -82.33
-82.33 -82.39 -82.41 -82.36 -82.38 -82.46 -82.37 -82.31 -82.31 -82.24
-82.16 -82.21 -82.36 -82.50 -82.52 -82.28 -82.17 -82.33 -82.42 -82.35
-82.30 -82.50 -82.51 -82.34 -82.17 -82.23 -82.34 -82.34 -82.38 -82.43
-82.39 -82.36 -82.43 -82.57 -82.61 -82.59 -82.55 -82.46 -82.41 -82.43
-82.35 -82.42 -82.44 -82.28 -82.19 -82.18 -82.19 -82.25 -82.26 -82.26
-82.41 -82.49 -82.46 -82.49 -82.34 -82.23 -82.28 -82.33 -82.50 -82.66
-82.68 -82.53 -82.37 -82.49 -82.42 -82.26 -82.29 -82.41 -82.51 -82.48
-82.36 -82.32 -82.38 -82.52 -82.51 -82.46 -82.52 -82.59 -82.55 -82.48
-82.43 -82.41 -82.40 -82.48 -82.53 -82.39 -82.40 -82.59 -82.56 -82.43
-82.35 -82.32 -82.40 -82.55 -82.56 -82.46 -82.50 -82.61 -82.62 -82.56
-82.40 -82.30 -82.33 -82.41 -82.46 -82.54 -82.53 -82.46 -82.43 -82.36
-82.45 -82.47 -82.33 -82.37 -82.45 -82.43 -82.48 -82.49 -82.56 -82.72

-82.60 -82.41 -82.42 -82.55 -82.60 -82.64 -82.61 -82.46 -82.46 -82.47
-82.52 -82.53 -82.44 -82.42 -82.40 -82.41 -82.54 -82.62 -82.59 -82.55
-82.38 -82.30 -82.39 -82.42 -82.51 -82.57 -82.59 -82.52 -82.63 -82.71
-82.46 -82.36 -82.42 -82.52 -82.76 -82.75 -82.37 -82.24 -82.40 -82.51
-82.52 -82.45 -82.42 -82.59 -82.45 -82.31 -82.40 -82.39 -82.36 -82.43
-82.54 -82.55 -82.49 -82.48 -82.51 -82.51 -82.49 -82.49 -82.42 -82.50
-82.80 -82.77 -82.61 -82.52 -82.51 -82.48 -82.34 -82.17 -82.30 -82.52
-82.61 -82.61 -82.55 -82.46 -82.49 -82.53 -82.53 -82.48 -82.48 -82.49
-82.59 -82.59 -82.50 -82.59 -82.63 -82.38 -82.25 -82.49 -82.76 -82.70
-82.70 -82.61 -82.47 -82.42 -82.52 -82.56 -82.45 -82.46 -82.47 -82.54
-82.51 -82.53 -82.57 -82.50 -82.43 -82.40 -82.34 -82.30 -82.34 -82.50
-82.63 -82.59 -82.52 -82.64 -82.67 -82.59 -82.49 -82.33 -82.20 -82.22
-82.29 -82.37 -82.48 -82.50 -82.57 -82.69 -82.66 -82.59 -82.58 -82.59
-82.44 -82.36 -82.48 -82.52 -82.46 -82.40 -82.51 -82.52 -82.50 -82.46
-82.36 -82.37 -82.48 -82.57 -82.76 -82.81 -82.74 -82.63 -82.49 -82.49
-82.43 -82.49 -82.70 -82.69 -82.59 -82.53 -82.51 -82.37 -82.27 -82.44
-82.67 -82.55 -82.51 -82.57 -82.60 -82.49 -82.46 -82.55 -82.56 -82.52
-82.48 -82.43 -82.55 -82.79 -82.76 -82.63 -82.53 -82.48 -82.47 -82.43
-82.52 -82.71 -82.90 -82.89 -82.72 -82.63 -82.62 -82.58 -82.59 -82.55
-82.38 -82.35 -82.48 -82.65 -82.72 -82.70 -82.64 -82.56 -82.56 -82.48
-82.29 -82.32 -82.47 -82.45 -82.39 -82.37 -82.35 -82.51 -82.79 -82.83
-82.67 -82.56 -82.64 -82.71 -82.63 -82.59 -82.63 -82.54 -82.54 -82.47
-82.48 -82.46 -82.34 -82.36 -82.50 -82.48 -82.41 -82.48 -82.58 -82.54
-82.39 -82.39 -82.48 -82.55 -82.61 -82.53 -82.39 -82.41 -82.46 -82.53
-82.52 -82.49 -82.55 -82.49 -82.36 -82.43 -82.40 -82.41 -82.56 -82.61
-82.57 -82.51 -82.42 -82.50 -82.64 -82.58 -82.57 -82.54 -82.48 -82.63
-82.62 -82.50 -82.46 -82.55 -82.71 -82.58 -82.54 -82.75 -82.78 -82.71
-82.72 -82.66 -82.70 -82.67 -82.54 -82.50 -82.68 -82.73 -82.53 -82.45
-82.44 -82.36 -82.46 -82.54 -82.42 -82.33 -82.35 -82.48 -82.50 -82.41
-82.39 -82.52 -82.66 -82.65 -82.56 -82.54 -82.56 -82.64 -82.56 -82.45
-82.43 -82.47 -82.63 -82.68 -82.71 -82.63 -82.47 -82.46 -82.59 -82.69
-82.64 -82.73 -82.77 -82.59 -82.46 -82.51 -82.54 -82.45 -82.41 -82.40
-82.41 -82.58 -82.68 -82.59 -82.40 -82.34 -82.44 -82.55 -82.57 -82.61
-82.58 -82.56 -82.72 -82.84 -82.70 -82.59 -82.60 -82.60 -82.48 -82.44
-82.50 -82.45 -82.37 -82.54 -82.68 -82.77 -82.78 -82.63 -82.53 -82.55
-82.45 -82.30 -82.25 -82.49 -82.68 -82.62 -82.54 -82.65 -82.56 -82.45
-82.51 -82.41 -82.31 -82.32 -82.40 -82.53 -82.55 -82.46 -82.44 -82.54
-82.59 -82.60 -82.70 -82.74 -82.72 -82.57 -82.49 -82.68 -82.72 -82.76
-82.74 -82.57 -82.44 -82.48 -82.58 -82.57 -82.65 -82.57 -82.46 -82.44
-82.36 -82.41 -82.47 -82.47 -82.45 -82.42 -82.57 -82.66 -82.60 -82.58
-82.65 -82.55 -82.31 -82.31 -82.47 -82.47 -82.34 -82.36 -82.48 -82.63
-82.54 -82.37 -82.46 -82.61 -82.49 -82.38 -82.42 -82.52 -82.56 -82.57
-82.51 -82.45 -82.44 -82.56 -82.69 -82.61 -82.57 -82.64 -82.60 -82.53
-82.49 -82.45 -82.48 -82.38 -82.34 -82.37 -82.26 -82.20 -82.33 -82.48
-82.41 -82.30 -82.29 -82.18 -82.18 -82.33 -82.42 -82.36 -82.51 -82.66
-82.56 -82.55 -82.66 -82.57 -82.34 -82.19 -82.18 -82.35 -82.38 -82.37
-82.44 -82.36 -82.32 -82.35 -82.54 -82.49 -82.41 -82.50 -82.52 -82.37
-82.39 -82.36 -82.23 -82.16 -82.25 -82.24 -82.28 -82.49 -82.50 -82.39
-82.43 -82.50 -82.47 -82.43 -82.45 -82.54 -82.59 -82.48 -82.39 -82.37
-82.30 -82.24 -82.27 -82.41 -82.56 -82.44 -82.27 -82.15 -82.26 -82.44

-82.52 -82.50 -82.47 -82.41 -82.31 -82.30 -82.35 -82.23 -82.27 -82.31
-82.24 -82.33 -82.43 -82.43 -82.43 -82.28 -82.25 -82.40 -82.54 -82.53
-82.36 -82.21 -82.23 -82.43 -82.41 -82.26 -82.39 -82.43 -82.33 -82.25
-82.15 -82.25 -82.36 -82.31 -82.36 -82.42 -82.34 -82.18 -82.19 -82.16
-82.14 -82.21 -82.08 -82.12 -82.25 -82.10 -82.07 -82.23 -82.25 -82.17
-82.21 -82.29 -82.24 -82.27 -82.31 -82.33 -82.19 -82.14 -82.05 -82.00
-82.18 -82.12 -82.06 -82.15 -82.17 -82.20 -82.33 -82.31 -82.23 -82.26
-82.28 -82.11 -82.06 -82.11 -82.16 -82.24 -82.22 -82.12 -82.00 -82.05
-82.05 -81.98 -82.08 -82.19 -82.14 -82.09 -82.05 -82.21 -82.23 -82.07
-82.00 -81.95 -82.02 -82.10 -82.05 -82.04 -82.05 -82.03 -81.98 -82.01
-82.05 -82.07 -82.05 -82.01 -81.95 -81.91 -81.90 -81.92 -81.92 -81.74
-81.73 -81.90 -81.98 -81.92 -81.88 -81.87 -81.88 -81.72 -81.71 -81.94
-82.10 -82.10 -81.94 -81.89 -81.89 -81.93 -81.86 -81.85 -81.99 -81.98
-81.96 -81.93 -81.90 -81.78 -81.75 -81.81 -81.73 -81.69 -81.62 -81.70
-81.90 -81.93 -81.90 -81.89 -81.73 -81.70 -81.61 -81.54 -81.45 -81.47
-81.60 -81.76 -81.76 -81.62 -81.65 -81.74 -81.85 -81.79 -81.61 -81.60
-81.57 -81.54 -81.56 -81.57 -81.44 -81.47 -81.58 -81.71 -81.76 -81.62
-81.52 -81.42 -81.39 -81.46 -81.49 -81.41 -81.40 -81.44 -81.34 -81.26
-81.37 -81.47 -81.58 -81.54 -81.36 -81.33 -81.34 -81.35 -81.36 -81.37
-81.34 -81.31 -81.34 -81.39 -81.43 -81.39 -81.34 -81.31 -81.32 -81.33
-81.19 -81.15 -81.21 -81.18 -81.12 -81.04 -81.04 -81.05 -81.00 -80.87
-80.89 -81.04 -81.03 -80.98 -80.97 -80.90 -81.02 -81.12 -81.02 -80.89
-80.86 -81.01 -81.10 -81.05 -80.98 -80.97 -80.94 -80.86 -80.82 -80.84
-80.91 -80.92 -80.88 -80.75 -80.77 -80.88 -80.88 -80.72 -80.55 -80.53
-80.52 -80.61 -80.67 -80.63 -80.59 -80.66 -80.69 -80.45 -80.37 -80.52
-80.62 -80.75 -80.72 -80.49 -80.35 -80.48 -80.55 -80.57 -80.50 -80.46
-80.66 -80.69 -80.46 -80.45 -80.44 -80.38 -80.41 -80.33 -80.35 -80.43
-80.40 -80.35 -80.44 -80.48 -80.39 -80.30 -80.47 -80.54 -80.37 -80.17
-80.17 -80.45 -80.50 -80.44 -80.32 -80.23 -80.17 -80.24 -80.39 -80.41
-80.41 -80.39 -80.48 -80.47 -80.33 -80.26 -80.21 -80.27 -80.37 -80.45
-80.50 -80.45 -80.30 -80.22 -80.24 -80.44 -80.57 -80.51 -80.35 -80.31
-80.28 -80.36 -80.56 -80.67 -80.68 -80.57 -80.51 -80.63 -80.82 -80.73
-80.56 -80.54 -80.56 -80.61 -80.62 -80.76 -80.79 -80.78 -80.89 -80.97
-80.91 -80.93 -81.07 -81.21 -81.30 -81.26 -81.18 -81.24 -81.29 -81.31
-81.26 -81.24 -81.51 -81.68 -81.80 -81.91 -81.88 -81.84 -81.83 -81.76
-81.94 -82.16 -82.11 -82.06 -82.14 -82.31 -82.47 -82.57 -82.67 -82.68
-82.82 -83.03 -83.22 -83.19 -83.19 -83.23 -83.31 -83.37 -83.27 -83.25
-83.35 -83.56 -83.78 -83.95 -84.04 -83.95 -83.94 -84.13 -84.36 -84.53
-84.65 -84.77 -84.80 -84.71 -84.77 -85.04 -85.11 -85.22 -85.38 -85.47
-85.56 -85.62 -85.72 -85.67 -85.69 -85.81 -85.94 -86.24 -86.53 -86.51
-86.35 -86.52 -86.89 -87.15 -87.14 -87.08 -87.26 -87.44 -87.54 -87.65
-87.84 -87.97 -88.00 -87.94 -87.97 -88.21 -88.43 -88.51 -88.62 -88.58
-88.52 -88.70 -89.00 -89.21 -89.32 -89.38 -89.44 -89.45 -89.47 -89.59
-89.67 -89.71 -89.88 -89.95 -89.95 -90.06 -90.20 -90.28 -90.42 -90.63
-90.79 -90.67 -90.60 -90.74 -90.93 -91.22 -91.33 -91.33 -91.36 -91.30
-91.41 -91.53 -91.66 -91.90 -92.09 -92.22 -92.26 -92.25 -92.35 -92.45
-92.52 -92.59 -92.68 -92.71 -92.70 -92.82 -92.93 -93.04 -93.18 -93.30
-93.29 -93.30 -93.37 -93.52 -93.55 -93.60 -93.70 -93.80 -93.85 -93.80
-93.64 -93.80 -94.09 -94.24 -94.24 -94.29 -94.37 -94.38 -94.50 -94.54
-94.60 -94.65 -94.55 -94.60 -94.71 -94.80 -94.83 -94.84 -94.89 -94.86

-94.80 -94.88 -95.10 -95.24 -95.20 -95.06 -95.01 -95.24 -95.37 -95.34
-95.39 -95.35 -95.31 -95.32 -95.43 -95.61 -95.77 -95.74 -95.55 -95.46
-95.57 -95.68 -95.69 -95.82 -95.92 -95.99 -95.91 -95.84 -95.82 -95.89
-95.96 -95.92 -96.12 -96.10 -96.01 -96.17 -96.19 -96.22 -96.22 -96.21
-96.06 -95.94 -95.99 -96.10 -96.17 -96.06 -96.13 -96.30 -96.30 -96.33
-96.29 -96.24 -96.31 -96.38 -96.35 -96.35 -96.32 -96.29 -96.38 -96.50
-96.59 -96.59 -96.52 -96.43 -96.41 -96.49 -96.50 -96.56 -96.57 -96.59
-96.58 -96.51 -96.48 -96.57 -96.72 -96.75 -96.59 -96.37 -96.56 -96.70
-96.66 -96.66 -96.70 -96.73 -96.95 -97.00 -96.88 -96.80 -96.82 -96.79
-96.86 -96.91 -97.06 -97.12 -97.06 -97.05 -97.24 -97.15 -96.89 -96.87
-96.92 -97.05 -97.19 -97.24 -97.11 -97.05 -97.13 -97.29 -97.23 -97.14
-97.15 -97.30 -97.44 -97.49 -97.53 -97.48 -97.42 -97.50 -97.59 -97.51
-97.51 -97.70 -97.83 -97.65 -97.46 -97.56 -97.78 -97.86 -97.78 -97.87
-98.01 -97.85 -97.87 -98.08 -98.09 -98.08 -98.11 -98.10 -98.13 -98.05
-98.00 -98.16 -98.07 -97.94 -98.16 -98.44 -98.61 -98.60 -98.39 -98.37
-98.59 -98.82 -98.91 -98.84 -98.73 -98.72 -98.80 -99.06 -99.10 -99.06
-99.15 -99.17 -99.20 -99.25 -99.22 -99.28 -99.32 -99.40 -99.45 -99.37
-99.42 -99.59 -99.71 -99.83 -99.87 -99.79 -99.72 -99.67 -99.75 -99.97
-99.89 -99.89 -99.98 -99.95 -99.97 -99.96 -100.08 -100.24 -100.40 -100.41
-100.30 -100.26 -100.22 -100.29 -100.47 -100.38 -100.42 -100.54 -100.51 -100.43
-100.39 -100.51 -100.72 -100.62 -100.51 -100.56 -100.66 -100.73 -100.77 -100.83
-100.74 -100.74 -100.72 -100.59 -100.44 -100.46 -100.58 -100.67 -100.58 -100.52
-100.56 -100.61 -100.67 -100.62 -100.57 -100.52 -100.37 -100.33 -100.20 -100.12
-100.25 -100.29 -100.23 -100.12 -100.21 -100.31 -100.38 -100.35 -100.23 -100.10
-100.00 -99.99 -100.06 -100.10 -100.10 -99.92 -99.93]

(B.1.2) Continuum data file

The continuum data file (tp-20170609-08.dat) below contains data of the solar drift scan recorded in the continuum mode with the simple_ra receiver. This file has data-values that represents the output of the total-power as floating-point numbers, which were recorded at every 5 seconds. The first data set of the continuum file is recorded in UTC time whilst the second data set is recorded in LMST time. In addition, the PARAMS line contains parameters such as the frequency (Hz), detector bandwidth (Hz), Declination and Julian date, Right Ascension, UTC, and LMST. All the parameters in the PARAMS line of the recorded file depends on the parameters that were selected in the command line at the start of the observation recording with the simple_ra receiver.

```
PARAMS 1578597000.00000 2500000.00000 -99.00000 2457914 12.00 0
13:46:30.0 01:54:54 0.0129076 0.0129076 0.0111509 0.0000000
13:46:35.0 01:54:59 0.0125835 0.0125835 0.0125025 0.0000000
13:46:40.0 01:55:04 0.0124015 0.0124015 0.0124168 0.0000000
13:46:45.0 01:55:09 0.0122152 0.0122152 0.0122553 0.0000000
13:46:50.0 01:55:14 0.0121518 0.0121518 0.0121368 0.0000000
13:46:55.0 01:55:19 0.0121339 0.0121339 0.0120272 0.0000000
PARAMS 1578597000.00000 2500000.00000 -99.00000 2457914 12.00 0
13:47:00.0 01:55:24 0.0121069 0.0121069 0.0119497 0.0000000
13:47:05.0 01:55:29 0.0120703 0.0120703 0.0118820 0.0000000
13:47:10.0 01:55:34 0.0120345 0.0120345 0.0118353 0.0000000
13:47:15.0 01:55:39 0.0119948 0.0119948 0.0117749 0.0000000
13:47:20.0 01:55:43 0.0119528 0.0119528 0.0117271 0.0000000
13:47:25.0 01:55:49 0.0119095 0.0119095 0.0116753 0.0000000
PARAMS 1578597000.00000 2500000.00000 -99.00000 2457914 12.00 0
13:47:30.0 01:55:54 0.0118635 0.0118635 0.0116243 0.0000000
13:47:35.0 01:55:59 0.0118221 0.0118221 0.0115955 0.0000000
13:47:40.0 01:56:04 0.0117823 0.0117823 0.0115754 0.0000000
13:47:45.0 01:56:09 0.0117436 0.0117436 0.0115400 0.0000000
13:47:50.0 01:56:13 0.0117088 0.0117088 0.0115232 0.0000000
13:47:55.0 01:56:19 0.0116743 0.0116743 0.0114948 0.0000000
PARAMS 1578597000.00000 2500000.00000 -99.00000 2457914 12.00 0
13:48:00.0 01:56:24 0.0116380 0.0116380 0.0114711 0.0000000
13:48:05.0 01:56:29 0.0116135 0.0116135 0.0114411 0.0000000
13:48:10.0 01:56:34 0.0115822 0.0115822 0.0114128 0.0000000
13:48:15.0 01:56:39 0.0115515 0.0115515 0.0113912 0.0000000
13:48:20.0 01:56:44 0.0115227 0.0115227 0.0113595 0.0000000
13:48:25.0 01:56:49 0.0114926 0.0114926 0.0113385 0.0000000
PARAMS 1578597000.00000 2500000.00000 -99.00000 2457914 12.00 0
13:48:30.0 01:56:54 0.0114623 0.0114623 0.0112989 0.0000000
13:48:35.0 01:56:59 0.0114326 0.0114326 0.0112737 0.0000000
13:48:40.0 01:57:04 0.0114068 0.0114068 0.0112590 0.0000000
13:48:45.0 01:57:09 0.0113771 0.0113771 0.0112116 0.0000000
13:48:50.0 01:57:14 0.0113489 0.0113489 0.0111921 0.0000000
13:48:55.0 01:57:19 0.0113204 0.0113204 0.0111804 0.0000000
```

PARAMS 1578597000.00000 2500000.00000	-99.00000	2457914	12.00	0
13:49:00.0 01:57:24	0.0112972	0.0112972	0.0111608	0.0000000
13:49:05.0 01:57:30	0.0112728	0.0112728	0.0111443	0.0000000
13:49:10.0 01:57:35	0.0112522	0.0112522	0.0111384	0.0000000
13:49:15.0 01:57:40	0.0112341	0.0112341	0.0111338	0.0000000
13:49:20.0 01:57:45	0.0112166	0.0112166	0.0111244	0.0000000
13:49:25.0 01:57:50	0.0112010	0.0112010	0.0111174	0.0000000
PARAMS 1578597000.00000 2500000.00000	-99.00000	2457914	12.00	0
13:49:30.0 01:57:55	0.0111847	0.0111847	0.0110934	0.0000000
13:49:35.0 01:58:00	0.0111651	0.0111651	0.0110630	0.0000000
13:49:40.0 01:58:05	0.0111650	0.0111650	0.0111493	0.0000000
13:49:45.0 01:58:10	0.0112099	0.0112099	0.0114291	0.0000000
13:49:50.0 01:58:15	0.0112389	0.0112389	0.0113997	0.0000000
13:49:55.0 01:58:20	0.0112578	0.0112578	0.0113886	0.0000000
PARAMS 1578597000.00000 2500000.00000	-99.00000	2457914	12.00	0
13:50:00.0 01:58:25	0.0112776	0.0112776	0.0113789	0.0000000
13:50:05.0 01:58:30	0.0112967	0.0112967	0.0113698	0.0000000
13:50:10.0 01:58:35	0.0113036	0.0113036	0.0113572	0.0000000
13:50:15.0 01:58:40	0.0113121	0.0113121	0.0113566	0.0000000
13:50:20.0 01:58:45	0.0113175	0.0113175	0.0113501	0.0000000
13:50:25.0 01:58:50	0.0113199	0.0113199	0.0113417	0.0000000
PARAMS 1578597000.00000 2500000.00000	-99.00000	2457914	12.00	0
13:50:30.0 01:58:55	0.0113245	0.0113245	0.0113370	0.0000000
13:50:35.0 01:59:00	0.0113256	0.0113256	0.0113186	0.0000000
13:50:40.0 01:59:05	0.0113226	0.0113226	0.0113101	0.0000000
13:50:45.0 01:59:10	0.0113177	0.0113177	0.0112906	0.0000000
13:50:50.0 01:59:15	0.0113120	0.0113120	0.0112827	0.0000000
13:50:55.0 01:59:20	0.0113068	0.0113068	0.0112897	0.0000000
PARAMS 1578597000.00000 2500000.00000	-99.00000	2457914	12.00	0
13:51:00.0 01:59:25	0.0113046	0.0113046	0.0112845	0.0000000
13:51:05.0 01:59:30	0.0112985	0.0112985	0.0112619	0.0000000
13:51:10.0 01:59:35	0.0112899	0.0112899	0.0112534	0.0000000
13:51:15.0 01:59:40	0.0112852	0.0112852	0.0112550	0.0000000
13:51:20.0 01:59:45	0.0112797	0.0112797	0.0112555	0.0000000
13:51:25.0 01:59:50	0.0112742	0.0112742	0.0112325	0.0000000
PARAMS 1578597000.00000 2500000.00000	-99.00000	2457914	12.00	0
13:51:30.0 01:59:55	0.0112662	0.0112662	0.0112259	0.0000000
13:51:35.0 02:00:00	0.0112611	0.0112611	0.0112401	0.0000000
13:51:40.0 02:00:05	0.0112560	0.0112560	0.0112320	0.0000000
13:51:45.0 02:00:10	0.0112525	0.0112525	0.0112299	0.0000000
13:51:50.0 02:00:15	0.0112487	0.0112487	0.0112190	0.0000000
13:51:55.0 02:00:20	0.0112435	0.0112435	0.0112070	0.0000000
PARAMS 1578597000.00000 2500000.00000	-99.00000	2457914	12.00	0
13:52:00.0 02:00:25	0.0112371	0.0112371	0.0112121	0.0000000
13:52:05.0 02:00:30	0.0112303	0.0112303	0.0111994	0.0000000
13:52:10.0 02:00:35	0.0112254	0.0112254	0.0112082	0.0000000

13:52:15.0 02:00:40	0.0112215	0.0112215	0.0111948	0.0000000
13:52:20.0 02:00:45	0.0112146	0.0112146	0.0111851	0.0000000
13:52:25.0 02:00:50	0.0112087	0.0112087	0.0111695	0.0000000
PARAMS 1578597000.00000 2500000.00000	-99.00000	2457914	12.00 0	
13:52:30.0 02:00:55	0.0112018	0.0112018	0.0111723	0.0000000
13:52:35.0 02:01:00	0.0111969	0.0111969	0.0111774	0.0000000
13:52:40.0 02:01:05	0.0111939	0.0111939	0.0111777	0.0000000
13:52:45.0 02:01:10	0.0111950	0.0111950	0.0112120	0.0000000
13:52:50.0 02:01:15	0.0111934	0.0111934	0.0111872	0.0000000
13:52:55.0 02:01:20	0.0111894	0.0111894	0.0111774	0.0000000
PARAMS 1578597000.00000 2500000.00000	-99.00000	2457914	12.00 0	
13:53:00.0 02:01:25	0.0111914	0.0111914	0.0112086	0.0000000
13:53:05.0 02:01:30	0.0111974	0.0111974	0.0112368	0.0000000
13:53:10.0 02:01:35	0.0112113	0.0112113	0.0112895	0.0000000
13:53:15.0 02:01:40	0.0112289	0.0112289	0.0113244	0.0000000
13:53:20.0 02:01:45	0.0112476	0.0112476	0.0113453	0.0000000
13:53:25.0 02:01:50	0.0112669	0.0112669	0.0113688	0.0000000
PARAMS 1578597000.00000 2500000.00000	-99.00000	2457914	12.00 0	
13:53:30.0 02:01:55	0.0112834	0.0112834	0.0113763	0.0000000
13:53:35.0 02:02:00	0.0113060	0.0113060	0.0114307	0.0000000
13:53:40.0 02:02:05	0.0113300	0.0113300	0.0114506	0.0000000
13:53:45.0 02:02:10	0.0113550	0.0113550	0.0115002	0.0000000
13:53:50.0 02:02:15	0.0113920	0.0113920	0.0115615	0.0000000
13:53:55.0 02:02:20	0.0114206	0.0114206	0.0115830	0.0000000
PARAMS 1578597000.00000 2500000.00000	-99.00000	2457914	12.00 0	
13:54:00.0 02:02:25	0.0114467	0.0114467	0.0115814	0.0000000
13:54:05.0 02:02:30	0.0114777	0.0114777	0.0116430	0.0000000
13:54:10.0 02:02:35	0.0115053	0.0115053	0.0116644	0.0000000
13:54:15.0 02:02:40	0.0115445	0.0115445	0.0117563	0.0000000
13:54:20.0 02:02:45	0.0115878	0.0115878	0.0118262	0.0000000
13:54:25.0 02:02:50	0.0116373	0.0116373	0.0119224	0.0000000
PARAMS 1578597000.00000 2500000.00000	-99.00000	2457914	12.00 0	
13:54:30.0 02:02:55	0.0116946	0.0116946	0.0119906	0.0000000
13:54:35.0 02:03:00	0.0117488	0.0117488	0.0120622	0.0000000
13:54:40.0 02:03:05	0.0118149	0.0118149	0.0121836	0.0000000
13:54:45.0 02:03:10	0.0118784	0.0118784	0.0122340	0.0000000
13:54:50.0 02:03:15	0.0119434	0.0119434	0.0122759	0.0000000
13:54:55.0 02:03:20	0.0120069	0.0120069	0.0123428	0.0000000
PARAMS 1578597000.00000 2500000.00000	-99.00000	2457914	12.00 0	
13:55:00.0 02:03:25	0.0120705	0.0120705	0.0124238	0.0000000
13:55:05.0 02:03:30	0.0121366	0.0121366	0.0125029	0.0000000
13:55:10.0 02:03:36	0.0122064	0.0122064	0.0125872	0.0000000
13:55:15.0 02:03:41	0.0122815	0.0122815	0.0126987	0.0000000
13:55:20.0 02:03:46	0.0123616	0.0123616	0.0128152	0.0000000
13:55:25.0 02:03:51	0.0124576	0.0124576	0.0129823	0.0000000
PARAMS 1578597000.00000 2500000.00000	-99.00000	2457914	12.00 0	

13:55:30.0 02:03:56	0.0125576	0.0125576	0.0131191	0.0000000
13:55:35.0 02:04:01	0.0126754	0.0126754	0.0133215	0.0000000
13:55:40.0 02:04:06	0.0127971	0.0127971	0.0135070	0.0000000
13:55:45.0 02:04:11	0.0129313	0.0129313	0.0136467	0.0000000
13:55:50.0 02:04:16	0.0130596	0.0130596	0.0137937	0.0000000
13:55:55.0 02:04:21	0.0132143	0.0132143	0.0139822	0.0000000
PARAMS 1578597000.00000 2500000.00000 -99.00000 2457914	12.00 0			
13:56:00.0 02:04:26	0.0133922	0.0133922	0.0142931	0.0000000
13:56:05.0 02:04:31	0.0135212	0.0135212	0.0142959	0.0000000
13:56:10.0 02:04:36	0.0136781	0.0136781	0.0144618	0.0000000
13:56:15.0 02:04:41	0.0138185	0.0138185	0.0145992	0.0000000
13:56:20.0 02:04:46	0.0139744	0.0139744	0.0148883	0.0000000
13:56:25.0 02:04:51	0.0141745	0.0141745	0.0152053	0.0000000
PARAMS 1578597000.00000 2500000.00000 -99.00000 2457914	12.00 0			
13:56:30.0 02:04:56	0.0143360	0.0143360	0.0152183	0.0000000
13:56:35.0 02:05:01	0.0145387	0.0145387	0.0156854	0.0000000
13:56:40.0 02:05:06	0.0147374	0.0147374	0.0157968	0.0000000
13:56:45.0 02:05:11	0.0149317	0.0149317	0.0159941	0.0000000
13:56:50.0 02:05:16	0.0151612	0.0151612	0.0164102	0.0000000
13:56:55.0 02:05:21	0.0153430	0.0153430	0.0163762	0.0000000
PARAMS 1578597000.00000 2500000.00000 -99.00000 2457914	12.00 0			
13:57:00.0 02:05:26	0.0155539	0.0155539	0.0166970	0.0000000
13:57:05.0 02:05:31	0.0158353	0.0158353	0.0171264	0.0000000
13:57:10.0 02:05:36	0.0160754	0.0160754	0.0173630	0.0000000
13:57:15.0 02:05:41	0.0163288	0.0163288	0.0176304	0.0000000
13:57:20.0 02:05:46	0.0166146	0.0166146	0.0180932	0.0000000
13:57:25.0 02:05:51	0.0169008	0.0169008	0.0184044	0.0000000
PARAMS 1578597000.00000 2500000.00000 -99.00000 2457914	12.00 0			
13:57:30.0 02:05:56	0.0171467	0.0171467	0.0187229	0.0000000
13:57:35.0 02:06:01	0.0175304	0.0175304	0.0191560	0.0000000
13:57:40.0 02:06:06	0.0178508	0.0178508	0.0194906	0.0000000
13:57:45.0 02:06:11	0.0181767	0.0181767	0.0198840	0.0000000
13:57:50.0 02:06:16	0.0184058	0.0184058	0.0200445	0.0000000
13:57:55.0 02:06:21	0.0187650	0.0187650	0.0202778	0.0000000
PARAMS 1578597000.00000 2500000.00000 -99.00000 2457914	12.00 0			
13:58:00.0 02:06:26	0.0190514	0.0190514	0.0204978	0.0000000
13:58:05.0 02:06:31	0.0193512	0.0193512	0.0208868	0.0000000
13:58:10.0 02:06:36	0.0196616	0.0196616	0.0212584	0.0000000
13:58:15.0 02:06:41	0.0199444	0.0199444	0.0213909	0.0000000
13:58:20.0 02:06:46	0.0202881	0.0202881	0.0220569	0.0000000
13:58:25.0 02:06:51	0.0206362	0.0206362	0.0223176	0.0000000
PARAMS 1578597000.00000 2500000.00000 -99.00000 2457914	12.00 0			
13:58:30.0 02:06:56	0.0209842	0.0209842	0.0227463	0.0000000
13:58:35.0 02:07:01	0.0213123	0.0213123	0.0230237	0.0000000
13:58:40.0 02:07:06	0.0215887	0.0215887	0.0233973	0.0000000
13:58:45.0 02:07:11	0.0219330	0.0219330	0.0238080	0.0000000

13:58:50.0	02:07:16	0.0223076	0.0223076	0.0243296	0.0000000
13:58:55.0	02:07:21	0.0227205	0.0227205	0.0248162	0.0000000
PARAMS	1578597000.00000	2500000.00000	-99.00000	2457914	12.00 0
13:59:00.0	02:07:26	0.0231095	0.0231095	0.0252305	0.0000000
13:59:05.0	02:07:31	0.0234833	0.0234833	0.0254904	0.0000000
13:59:10.0	02:07:36	0.0239041	0.0239041	0.0262127	0.0000000
13:59:15.0	02:07:41	0.0243269	0.0243269	0.0265255	0.0000000
13:59:20.0	02:07:46	0.0247192	0.0247192	0.0267926	0.0000000
13:59:25.0	02:07:51	0.0251194	0.0251194	0.0273184	0.0000000
PARAMS	1578597000.00000	2500000.00000	-99.00000	2457914	12.00 0
13:59:30.0	02:07:56	0.0256482	0.0256482	0.0285007	0.0000000
13:59:35.0	02:08:01	0.0261819	0.0261819	0.0288740	0.0000000
13:59:40.0	02:08:06	0.0267450	0.0267450	0.0296552	0.0000000
13:59:45.0	02:08:11	0.0272041	0.0272041	0.0296936	0.0000000
13:59:50.0	02:08:16	0.0275957	0.0275957	0.0297837	0.0000000
13:59:55.0	02:08:21	0.0281997	0.0281997	0.0317305	0.0000000
PARAMS	1578597000.00000	2500000.00000	-99.00000	2457914	12.00 0
14:00:00.0	02:08:26	0.0287236	0.0287236	0.0314133	0.0000000
14:00:05.0	02:08:31	0.0292122	0.0292122	0.0317653	0.0000000
14:00:10.0	02:08:36	0.0296148	0.0296148	0.0318639	0.0000000
14:00:15.0	02:08:41	0.0300420	0.0300420	0.0322535	0.0000000
14:00:20.0	02:08:46	0.0304618	0.0304618	0.0327871	0.0000000
14:00:25.0	02:08:51	0.0308733	0.0308733	0.0331407	0.0000000
PARAMS	1578597000.00000	2500000.00000	-99.00000	2457914	12.00 0
14:00:30.0	02:08:56	0.0313918	0.0313918	0.0346283	0.0000000
14:00:35.0	02:09:01	0.0320106	0.0320106	0.0350385	0.0000000
14:00:40.0	02:09:06	0.0325162	0.0325162	0.0351164	0.0000000
14:00:45.0	02:09:11	0.0329440	0.0329440	0.0352598	0.0000000
14:00:50.0	02:09:16	0.0334226	0.0334226	0.0359070	0.0000000
14:00:55.0	02:09:21	0.0338467	0.0338467	0.0360453	0.0000000
PARAMS	1578597000.00000	2500000.00000	-99.00000	2457914	12.00 0
14:01:00.0	02:09:26	0.0343601	0.0343601	0.0371081	0.0000000
14:01:05.0	02:09:31	0.0348075	0.0348075	0.0373000	0.0000000
14:01:10.0	02:09:36	0.0353627	0.0353627	0.0382618	0.0000000
14:01:15.0	02:09:42	0.0357311	0.0357311	0.0377112	0.0000000
14:01:20.0	02:09:47	0.0362992	0.0362992	0.0393213	0.0000000
14:01:25.0	02:09:52	0.0367968	0.0367968	0.0392608	0.0000000
PARAMS	1578597000.00000	2500000.00000	-99.00000	2457914	12.00 0
14:01:30.0	02:09:57	0.0372564	0.0372564	0.0396864	0.0000000
14:01:35.0	02:10:02	0.0377090	0.0377090	0.0403395	0.0000000
14:01:40.0	02:10:07	0.0381450	0.0381450	0.0404115	0.0000000
14:01:45.0	02:10:12	0.0386300	0.0386300	0.0412300	0.0000000
14:01:50.0	02:10:17	0.0392261	0.0392261	0.0421593	0.0000000
14:01:55.0	02:10:22	0.0397779	0.0397779	0.0424923	0.0000000
PARAMS	1578597000.00000	2500000.00000	-99.00000	2457914	12.00 0
14:02:00.0	02:10:27	0.0403052	0.0403052	0.0430809	0.0000000

14:02:05.0	02:10:32	0.0407669	0.0407669	0.0433137	0.0000000
14:02:10.0	02:10:37	0.0412240	0.0412240	0.0438166	0.0000000
14:02:15.0	02:10:42	0.0415781	0.0415781	0.0432868	0.0000000
14:02:20.0	02:10:47	0.0419149	0.0419149	0.0438306	0.0000000
14:02:25.0	02:10:52	0.0422911	0.0422911	0.0442183	0.0000000
PARAMS	1578597000.00000	2500000.00000	-99.00000	2457914	12.00 0
14:02:30.0	02:10:57	0.0426210	0.0426210	0.0442734	0.0000000
14:02:35.0	02:11:02	0.0429909	0.0429909	0.0448592	0.0000000
14:02:40.0	02:11:07	0.0433179	0.0433179	0.0450548	0.0000000
14:02:45.0	02:11:12	0.0436771	0.0436771	0.0455662	0.0000000
14:02:50.0	02:11:17	0.0440762	0.0440762	0.0461042	0.0000000
14:02:55.0	02:11:22	0.0444267	0.0444267	0.0463255	0.0000000
PARAMS	1578597000.00000	2500000.00000	-99.00000	2457914	12.00 0
14:03:00.0	02:11:27	0.0447693	0.0447693	0.0465705	0.0000000
14:03:05.0	02:11:32	0.0451361	0.0451361	0.0470161	0.0000000
14:03:10.0	02:11:37	0.0454291	0.0454291	0.0468638	0.0000000
14:03:15.0	02:11:42	0.0456472	0.0456472	0.0468952	0.0000000
14:03:20.0	02:11:47	0.0458908	0.0458908	0.0472176	0.0000000
14:03:25.0	02:11:52	0.0461109	0.0461109	0.0473630	0.0000000
PARAMS	1578597000.00000	2500000.00000	-99.00000	2457914	12.00 0
14:03:30.0	02:11:57	0.0463998	0.0463998	0.0479937	0.0000000
14:03:35.0	02:12:02	0.0466247	0.0466247	0.0478469	0.0000000
14:03:40.0	02:12:07	0.0468009	0.0468009	0.0477036	0.0000000
14:03:45.0	02:12:12	0.0469971	0.0469971	0.0480019	0.0000000
14:03:50.0	02:12:17	0.0471361	0.0471361	0.0479705	0.0000000
14:03:55.0	02:12:22	0.0473018	0.0473018	0.0480618	0.0000000
PARAMS	1578597000.00000	2500000.00000	-99.00000	2457914	12.00 0
14:04:00.0	02:12:27	0.0474958	0.0474958	0.0485370	0.0000000
14:04:05.0	02:12:32	0.0476079	0.0476079	0.0481131	0.0000000
14:04:10.0	02:12:37	0.0476979	0.0476979	0.0481954	0.0000000
14:04:15.0	02:12:42	0.0477478	0.0477478	0.0480138	0.0000000
14:04:20.0	02:12:47	0.0477760	0.0477760	0.0478692	0.0000000
14:04:25.0	02:12:52	0.0478390	0.0478390	0.0482890	0.0000000
PARAMS	1578597000.00000	2500000.00000	-99.00000	2457914	12.00 0
14:04:30.0	02:12:57	0.0478848	0.0478848	0.0481595	0.0000000
14:04:35.0	02:13:02	0.0479121	0.0479121	0.0480599	0.0000000
14:04:40.0	02:13:07	0.0478890	0.0478890	0.0477232	0.0000000
14:04:45.0	02:13:12	0.0478659	0.0478659	0.0478417	0.0000000
14:04:50.0	02:13:17	0.0478244	0.0478244	0.0474505	0.0000000
14:04:55.0	02:13:22	0.0477522	0.0477522	0.0473457	0.0000000
PARAMS	1578597000.00000	2500000.00000	-99.00000	2457914	12.00 0
14:05:00.0	02:13:27	0.0476882	0.0476882	0.0473251	0.0000000
14:05:05.0	02:13:32	0.0476118	0.0476118	0.0471309	0.0000000
14:05:10.0	02:13:37	0.0475163	0.0475163	0.0469952	0.0000000
14:05:15.0	02:13:42	0.0473947	0.0473947	0.0468207	0.0000000
14:05:20.0	02:13:47	0.0472506	0.0472506	0.0463549	0.0000000

14:05:25.0	02:13:52	0.0470815	0.0470815	0.0461891	0.0000000
PARAMS	1578597000.00000	2500000.00000	-99.00000	2457914	12.00 0
14:05:30.0	02:13:57	0.0468957	0.0468957	0.0458940	0.0000000
14:05:35.0	02:14:02	0.0467134	0.0467134	0.0456678	0.0000000
14:05:40.0	02:14:07	0.0465125	0.0465125	0.0454275	0.0000000
14:05:45.0	02:14:12	0.0462733	0.0462733	0.0449441	0.0000000
14:05:50.0	02:14:17	0.0460371	0.0460371	0.0447737	0.0000000
14:05:55.0	02:14:22	0.0457830	0.0457830	0.0444744	0.0000000
PARAMS	1578597000.00000	2500000.00000	-99.00000	2457914	12.00 0
14:06:00.0	02:14:27	0.0455110	0.0455110	0.0441141	0.0000000
14:06:05.0	02:14:32	0.0452461	0.0452461	0.0437746	0.0000000
14:06:10.0	02:14:37	0.0449761	0.0449761	0.0435757	0.0000000
14:06:15.0	02:14:42	0.0446852	0.0446852	0.0431067	0.0000000
14:06:20.0	02:14:47	0.0443419	0.0443419	0.0424963	0.0000000
14:06:25.0	02:14:52	0.0439622	0.0439622	0.0421015	0.0000000
PARAMS	1578597000.00000	2500000.00000	-99.00000	2457914	12.00 0
14:06:30.0	02:14:57	0.0436090	0.0436090	0.0418497	0.0000000
14:06:35.0	02:15:02	0.0432999	0.0432999	0.0416276	0.0000000
14:06:40.0	02:15:07	0.0429702	0.0429702	0.0412170	0.0000000
14:06:45.0	02:15:12	0.0426150	0.0426150	0.0407739	0.0000000
14:06:50.0	02:15:17	0.0422039	0.0422039	0.0399493	0.0000000
14:06:55.0	02:15:22	0.0418421	0.0418421	0.0399901	0.0000000
PARAMS	1578597000.00000	2500000.00000	-99.00000	2457914	12.00 0
14:07:00.0	02:15:27	0.0415252	0.0415252	0.0397786	0.0000000
14:07:05.0	02:15:32	0.0411534	0.0411534	0.0391545	0.0000000
14:07:10.0	02:15:37	0.0407816	0.0407816	0.0387560	0.0000000
14:07:15.0	02:15:42	0.0403599	0.0403599	0.0382061	0.0000000
14:07:20.0	02:15:48	0.0399830	0.0399830	0.0380561	0.0000000
14:07:25.0	02:15:53	0.0395740	0.0395740	0.0375746	0.0000000
PARAMS	1578597000.00000	2500000.00000	-99.00000	2457914	12.00 0
14:07:30.0	02:15:58	0.0392203	0.0392203	0.0372900	0.0000000
14:07:35.0	02:16:03	0.0387982	0.0387982	0.0365115	0.0000000
14:07:40.0	02:16:08	0.0383514	0.0383514	0.0359057	0.0000000
14:07:45.0	02:16:12	0.0379954	0.0379954	0.0355587	0.0000000
14:07:50.0	02:16:18	0.0375621	0.0375621	0.0348614	0.0000000
14:07:55.0	02:16:23	0.0370753	0.0370753	0.0344503	0.0000000
PARAMS	1578597000.00000	2500000.00000	-99.00000	2457914	12.00 0
14:08:00.0	02:16:28	0.0366596	0.0366596	0.0345818	0.0000000
14:08:05.0	02:16:33	0.0362220	0.0362220	0.0337531	0.0000000
14:08:10.0	02:16:38	0.0357880	0.0357880	0.0332957	0.0000000
14:08:15.0	02:16:43	0.0353383	0.0353383	0.0327931	0.0000000
14:08:20.0	02:16:48	0.0349164	0.0349164	0.0327198	0.0000000
14:08:25.0	02:16:53	0.0344505	0.0344505	0.0320077	0.0000000
PARAMS	1578597000.00000	2500000.00000	-99.00000	2457914	12.00 0
14:08:30.0	02:16:58	0.0340196	0.0340196	0.0317066	0.0000000
14:08:35.0	02:17:03	0.0335749	0.0335749	0.0312303	0.0000000

14:08:40.0 02:17:08	0.0331280	0.0331280	0.0306957	0.0000000
14:08:45.0 02:17:13	0.0326865	0.0326865	0.0302065	0.0000000
14:08:50.0 02:17:18	0.0322262	0.0322262	0.0296727	0.0000000
14:08:55.0 02:17:23	0.0317619	0.0317619	0.0292299	0.0000000
PARAMS 1578597000.00000 2500000.00000 -99.00000 2457914	12.00	0		
14:09:00.0 02:17:28	0.0313077	0.0313077	0.0287152	0.0000000
14:09:05.0 02:17:33	0.0308362	0.0308362	0.0280535	0.0000000
14:09:10.0 02:17:38	0.0303672	0.0303672	0.0276968	0.0000000
14:09:15.0 02:17:43	0.0298693	0.0298693	0.0271957	0.0000000
14:09:20.0 02:17:48	0.0294041	0.0294041	0.0268753	0.0000000
14:09:25.0 02:17:53	0.0289007	0.0289007	0.0261308	0.0000000
PARAMS 1578597000.00000 2500000.00000 -99.00000 2457914	12.00	0		
14:09:30.0 02:17:58	0.0284200	0.0284200	0.0255541	0.0000000
14:09:35.0 02:18:03	0.0278744	0.0278744	0.0250695	0.0000000
14:09:40.0 02:18:08	0.0273948	0.0273948	0.0248395	0.0000000
14:09:45.0 02:18:13	0.0269420	0.0269420	0.0244824	0.0000000
14:09:50.0 02:18:18	0.0265104	0.0265104	0.0241568	0.0000000
14:09:55.0 02:18:23	0.0260659	0.0260659	0.0235024	0.0000000
PARAMS 1578597000.00000 2500000.00000 -99.00000 2457914	12.00	0		
14:10:00.0 02:18:28	0.0255529	0.0255529	0.0225320	0.0000000
14:10:05.0 02:18:33	0.0250620	0.0250620	0.0225809	0.0000000
14:10:10.0 02:18:38	0.0246304	0.0246304	0.0221567	0.0000000
14:10:15.0 02:18:43	0.0241943	0.0241943	0.0218298	0.0000000
14:10:20.0 02:18:48	0.0238161	0.0238161	0.0217334	0.0000000
14:10:25.0 02:18:53	0.0234240	0.0234240	0.0213131	0.0000000
PARAMS 1578597000.00000 2500000.00000 -99.00000 2457914	12.00	0		
14:10:30.0 02:18:58	0.0230262	0.0230262	0.0209301	0.0000000
14:10:35.0 02:19:03	0.0226250	0.0226250	0.0204169	0.0000000
14:10:40.0 02:19:08	0.0221982	0.0221982	0.0199953	0.0000000
14:10:45.0 02:19:13	0.0217530	0.0217530	0.0194853	0.0000000
14:10:50.0 02:19:18	0.0213236	0.0213236	0.0192390	0.0000000
14:10:55.0 02:19:23	0.0209714	0.0209714	0.0191093	0.0000000
PARAMS 1578597000.00000 2500000.00000 -99.00000 2457914	12.00	0		
14:11:00.0 02:19:28	0.0206441	0.0206441	0.0189455	0.0000000
14:11:05.0 02:19:33	0.0203213	0.0203213	0.0186256	0.0000000
14:11:10.0 02:19:38	0.0199939	0.0199939	0.0182840	0.0000000
14:11:15.0 02:19:43	0.0196625	0.0196625	0.0179313	0.0000000
14:11:20.0 02:19:48	0.0193347	0.0193347	0.0176246	0.0000000
14:11:25.0 02:19:53	0.0190175	0.0190175	0.0173538	0.0000000
PARAMS 1578597000.00000 2500000.00000 -99.00000 2457914	12.00	0		
14:11:30.0 02:19:58	0.0187103	0.0187103	0.0170626	0.0000000
14:11:35.0 02:20:03	0.0183923	0.0183923	0.0167532	0.0000000
14:11:40.0 02:20:08	0.0180973	0.0180973	0.0165483	0.0000000
14:11:45.0 02:20:13	0.0177353	0.0177353	0.0158061	0.0000000
14:11:50.0 02:20:18	0.0174185	0.0174185	0.0157713	0.0000000
14:11:55.0 02:20:23	0.0171289	0.0171289	0.0156037	0.0000000

PARAMS 1578597000.00000 2500000.00000	-99.00000	2457914	12.00	0
14:12:00.0 02:20:28	0.0168389	0.0168389	0.0152762	0.0000000
14:12:05.0 02:20:33	0.0165743	0.0165743	0.0151531	0.0000000
14:12:10.0 02:20:38	0.0162807	0.0162807	0.0147250	0.0000000
14:12:15.0 02:20:43	0.0158566	0.0158566	0.0136855	0.0000000
14:12:20.0 02:20:48	0.0154812	0.0154812	0.0135678	0.0000000
14:12:25.0 02:20:53	0.0152218	0.0152218	0.0138035	0.0000000
PARAMS 1578597000.00000 2500000.00000	-99.00000	2457914	12.00	0
14:12:30.0 02:20:58	0.0149892	0.0149892	0.0137364	0.0000000
14:12:35.0 02:21:03	0.0147667	0.0147667	0.0135894	0.0000000
14:12:40.0 02:21:08	0.0145571	0.0145571	0.0134619	0.0000000
14:12:45.0 02:21:13	0.0143578	0.0143578	0.0132946	0.0000000
14:12:50.0 02:21:18	0.0141565	0.0141565	0.0130799	0.0000000
14:12:55.0 02:21:23	0.0139649	0.0139649	0.0129609	0.0000000
PARAMS 1578597000.00000 2500000.00000	-99.00000	2457914	12.00	0
14:13:00.0 02:21:28	0.0137656	0.0137656	0.0126995	0.0000000
14:13:05.0 02:21:33	0.0135736	0.0135736	0.0125824	0.0000000
14:13:10.0 02:21:38	0.0134097	0.0134097	0.0125390	0.0000000
14:13:15.0 02:21:43	0.0132576	0.0132576	0.0124418	0.0000000
14:13:20.0 02:21:48	0.0130883	0.0130883	0.0122179	0.0000000
14:13:25.0 02:21:54	0.0129276	0.0129276	0.0120568	0.0000000
PARAMS 1578597000.00000 2500000.00000	-99.00000	2457914	12.00	0
14:13:30.0 02:21:59	0.0127890	0.0127890	0.0120398	0.0000000
14:13:35.0 02:22:04	0.0126782	0.0126782	0.0120983	0.0000000
14:13:40.0 02:22:09	0.0125781	0.0125781	0.0120403	0.0000000
14:13:45.0 02:22:14	0.0124772	0.0124772	0.0119391	0.0000000
14:13:50.0 02:22:19	0.0123805	0.0123805	0.0118562	0.0000000
14:13:55.0 02:22:24	0.0122843	0.0122843	0.0117657	0.0000000
PARAMS 1578597000.00000 2500000.00000	-99.00000	2457914	12.00	0
14:14:00.0 02:22:29	0.0121831	0.0121831	0.0116312	0.0000000
14:14:05.0 02:22:34	0.0120833	0.0120833	0.0115284	0.0000000
14:14:10.0 02:22:39	0.0119841	0.0119841	0.0114562	0.0000000
14:14:15.0 02:22:44	0.0118935	0.0118935	0.0114394	0.0000000
14:14:20.0 02:22:49	0.0118141	0.0118141	0.0113928	0.0000000
14:14:25.0 02:22:54	0.0117412	0.0117412	0.0113339	0.0000000
PARAMS 1578597000.00000 2500000.00000	-99.00000	2457914	12.00	0
14:14:30.0 02:22:59	0.0116682	0.0116682	0.0112770	0.0000000
14:14:35.0 02:23:04	0.0115926	0.0115926	0.0112095	0.0000000
14:14:40.0 02:23:09	0.0115236	0.0115236	0.0111766	0.0000000
14:14:45.0 02:23:14	0.0114646	0.0114646	0.0111406	0.0000000
14:14:50.0 02:23:19	0.0114075	0.0114075	0.0111030	0.0000000
14:14:55.0 02:23:24	0.0113510	0.0113510	0.0110814	0.0000000
PARAMS 1578597000.00000 2500000.00000	-99.00000	2457914	12.00	0
14:15:00.0 02:23:29	0.0112983	0.0112983	0.0110313	0.0000000
14:15:05.0 02:23:34	0.0112531	0.0112531	0.0110014	0.0000000
14:15:10.0 02:23:39	0.0112066	0.0112066	0.0109560	0.0000000

14:15:15.0 02:23:44	0.0111616	0.0111616	0.0109249	0.0000000
14:15:20.0 02:23:49	0.0111208	0.0111208	0.0109040	0.0000000
14:15:25.0 02:23:54	0.0110765	0.0110765	0.0108244	0.0000000
PARAMS 1578597000.00000 2500000.00000 -99.00000 2457914	12.00 0			
14:15:30.0 02:23:59	0.0110318	0.0110318	0.0108084	0.0000000
14:15:35.0 02:24:04	0.0109921	0.0109921	0.0107725	0.0000000
14:15:40.0 02:24:09	0.0109452	0.0109452	0.0107296	0.0000000
14:15:45.0 02:24:14	0.0109204	0.0109204	0.0107730	0.0000000
14:15:50.0 02:24:19	0.0108926	0.0108926	0.0107382	0.0000000
14:15:55.0 02:24:24	0.0108639	0.0108639	0.0107022	0.0000000
PARAMS 1578597000.00000 2500000.00000 -99.00000 2457914	12.00 0			
14:16:00.0 02:24:29	0.0108375	0.0108375	0.0106981	0.0000000
14:16:05.0 02:24:34	0.0108177	0.0108177	0.0106959	0.0000000
14:16:10.0 02:24:39	0.0107941	0.0107941	0.0106645	0.0000000
14:16:15.0 02:24:44	0.0107741	0.0107741	0.0106718	0.0000000
14:16:20.0 02:24:49	0.0107575	0.0107575	0.0106675	0.0000000
14:16:25.0 02:24:54	0.0107375	0.0107375	0.0106384	0.0000000
PARAMS 1578597000.00000 2500000.00000 -99.00000 2457914	12.00 0			
14:16:30.0 02:24:59	0.0107193	0.0107193	0.0106349	0.0000000
14:16:35.0 02:25:04	0.0107029	0.0107029	0.0106189	0.0000000
14:16:40.0 02:25:09	0.0106881	0.0106881	0.0106208	0.0000000
14:16:45.0 02:25:14	0.0106695	0.0106695	0.0105634	0.0000000
14:16:50.0 02:25:19	0.0106558	0.0106558	0.0105799	0.0000000
14:16:55.0 02:25:24	0.0106371	0.0106371	0.0105199	0.0000000
PARAMS 1578597000.00000 2500000.00000 -99.00000 2457914	12.00 0			
14:17:00.0 02:25:29	0.0106226	0.0106226	0.0105339	0.0000000
14:17:05.0 02:25:34	0.0106067	0.0106067	0.0105264	0.0000000
14:17:10.0 02:25:39	0.0105964	0.0105964	0.0105347	0.0000000
14:17:15.0 02:25:44	0.0105881	0.0105881	0.0105192	0.0000000
14:17:20.0 02:25:49	0.0105776	0.0105776	0.0105248	0.0000000
14:17:25.0 02:25:54	0.0105668	0.0105668	0.0105059	0.0000000
PARAMS 1578597000.00000 2500000.00000 -99.00000 2457914	12.00 0			
14:17:30.0 02:25:59	0.0105545	0.0105545	0.0104886	0.0000000
14:17:35.0 02:26:04	0.0105372	0.0105372	0.0104488	0.0000000
14:17:40.0 02:26:09	0.0105264	0.0105264	0.0104715	0.0000000
14:17:45.0 02:26:14	0.0105190	0.0105190	0.0104811	0.0000000
14:17:50.0 02:26:19	0.0105112	0.0105112	0.0104620	0.0000000
14:17:55.0 02:26:24	0.0105005	0.0105005	0.0104361	0.0000000
PARAMS 1578597000.00000 2500000.00000 -99.00000 2457914	12.00 0			
14:18:00.0 02:26:29	0.0104919	0.0104919	0.0104523	0.0000000
14:18:05.0 02:26:34	0.0104833	0.0104833	0.0104348	0.0000000
14:18:10.0 02:26:39	0.0104742	0.0104742	0.0104226	0.0000000
14:18:15.0 02:26:44	0.0104665	0.0104665	0.0104305	0.0000000
14:18:20.0 02:26:49	0.0104582	0.0104582	0.0104050	0.0000000
14:18:25.0 02:26:54	0.0104499	0.0104499	0.0104032	0.0000000
PARAMS 1578597000.00000 2500000.00000 -99.00000 2457914	12.00 0			

14:18:30.0 02:26:59	0.0104436	0.0104436	0.0104364	0.0000000
14:18:35.0 02:27:04	0.0104430	0.0104430	0.0104178	0.0000000
14:18:40.0 02:27:09	0.0104367	0.0104367	0.0104102	0.0000000
14:18:45.0 02:27:14	0.0104318	0.0104318	0.0103975	0.0000000
14:18:50.0 02:27:19	0.0104265	0.0104265	0.0103879	0.0000000
14:18:55.0 02:27:24	0.0104177	0.0104177	0.0103789	0.0000000
PARAMS 1578597000.00000 2500000.00000 -99.00000 2457914 12.00 0				
14:19:00.0 02:27:29	0.0104091	0.0104091	0.0103487	0.0000000
14:19:05.0 02:27:34	0.0103987	0.0103987	0.0103469	0.0000000
14:19:10.0 02:27:39	0.0103890	0.0103890	0.0103306	0.0000000
14:19:15.0 02:27:44	0.0103775	0.0103775	0.0103199	0.0000000
14:19:20.0 02:27:49	0.0103673	0.0103673	0.0102713	0.0000000
14:19:25.0 02:27:54	0.0103455	0.0103455	0.0102317	0.0000000
PARAMS 1578597000.00000 2500000.00000 -99.00000 2457914 12.00 0				
14:19:30.0 02:28:00	0.0103314	0.0103314	0.0102527	0.0000000
14:19:35.0 02:28:05	0.0103169	0.0103169	0.0102509	0.0000000
14:19:40.0 02:28:10	0.0103087	0.0103087	0.0102557	0.0000000
14:19:45.0 02:28:15	0.0102968	0.0102968	0.0102308	0.0000000
14:19:50.0 02:28:20	0.0102868	0.0102868	0.0102283	0.0000000
14:19:55.0 02:28:25	0.0102728	0.0102728	0.0101852	0.0000000
PARAMS 1578597000.00000 2500000.00000 -99.00000 2457914 12.00 0				
14:20:00.0 02:28:30	0.0102601	0.0102601	0.0101947	0.0000000
14:20:05.0 02:28:35	0.0102499	0.0102499	0.0102007	0.0000000
14:20:10.0 02:28:40	0.0102424	0.0102424	0.0102109	0.0000000
14:20:15.0 02:28:45	0.0102408	0.0102408	0.0102258	0.0000000
14:20:20.0 02:28:50	0.0102381	0.0102381	0.0102239	0.0000000
14:20:25.0 02:28:55	0.0102374	0.0102374	0.0102299	0.0000000
PARAMS 1578597000.00000 2500000.00000 -99.00000 2457914 12.00 0				
14:20:30.0 02:29:00	0.0102390	0.0102390	0.0102458	0.0000000
14:20:35.0 02:29:05	0.0102392	0.0102392	0.0102298	0.0000000
14:20:40.0 02:29:10	0.0102376	0.0102376	0.0102343	0.0000000
14:20:45.0 02:29:15	0.0102401	0.0102401	0.0102478	0.0000000
14:20:50.0 02:29:20	0.0102411	0.0102411	0.0102472	0.0000000
14:20:55.0 02:29:25	0.0102422	0.0102422	0.0102427	0.0000000
PARAMS 1578597000.00000 2500000.00000 -99.00000 2457914 12.00 0				
14:21:00.0 02:29:30	0.0102432	0.0102432	0.0102454	0.0000000
14:21:05.0 02:29:35	0.0102429	0.0102429	0.0102404	0.0000000
14:21:10.0 02:29:40	0.0102441	0.0102441	0.0102453	0.0000000
14:21:15.0 02:29:45	0.0102465	0.0102465	0.0102599	0.0000000
14:21:20.0 02:29:50	0.0102515	0.0102515	0.0102714	0.0000000
14:21:25.0 02:29:55	0.0102535	0.0102535	0.0102681	0.0000000
PARAMS 1578597000.00000 2500000.00000 -99.00000 2457914 12.00 0				
14:21:30.0 02:30:00	0.0102537	0.0102537	0.0102692	0.0000000
14:21:35.0 02:30:05	0.0102559	0.0102559	0.0102732	0.0000000
14:21:40.0 02:30:10	0.0102613	0.0102613	0.0102971	0.0000000
14:21:45.0 02:30:15	0.0102641	0.0102641	0.0102808	0.0000000

14:21:50.0 02:30:20	0.0102706	0.0102706	0.0103051	0.0000000
14:21:55.0 02:30:25	0.0102808	0.0102808	0.0103291	0.0000000
PARAMS 1578597000.00000 2500000.00000	-99.00000	2457914	12.00	0
14:22:00.0 02:30:30	0.0102883	0.0102883	0.0103187	0.0000000
14:22:05.0 02:30:35	0.0102923	0.0102923	0.0103194	0.0000000
14:22:10.0 02:30:40	0.0102978	0.0102978	0.0103290	0.0000000
14:22:15.0 02:30:45	0.0103036	0.0103036	0.0103343	0.0000000
14:22:20.0 02:30:50	0.0103071	0.0103071	0.0103245	0.0000000
14:22:25.0 02:30:55	0.0103112	0.0103112	0.0103353	0.0000000
PARAMS 1578597000.00000 2500000.00000	-99.00000	2457914	12.00	0
14:22:30.0 02:31:00	0.0103148	0.0103148	0.0103304	0.0000000
14:22:35.0 02:31:05	0.0103191	0.0103191	0.0103349	0.0000000
14:22:40.0 02:31:10	0.0103213	0.0103213	0.0103263	0.0000000
14:22:45.0 02:31:15	0.0103219	0.0103219	0.0103337	0.0000000
14:22:50.0 02:31:20	0.0103225	0.0103225	0.0103262	0.0000000
14:22:55.0 02:31:25	0.0103225	0.0103225	0.0103262	0.0000000

(B.1.3) CSV files in continuum mode

The CSV data file is also recorded in continuum mode by the `simple_ra` receiver in a format of `CR2017060_Drift.csv`, which means `(CR YYYYMMDD experimentname.csv)`. Parameters in the data file `CR20170607_Drift.csv` are defined as follows: the first three columns represents the UTC time, next three columns represents the LMST time, following total power and the last column represents the frequency in MHz at which the telescope was operating.

```
14 3 20 2 3 54 0.0098367 0.0098367 0 0 0 1620000000
14 3 25 2 3 59 0.0106431 0.0106431 0 0 0 1620000000 14 3 30 2 4 4 0.0106117 0.0106117 0 0
0 1620000000 14 3 35 2 4 9 0.0106498 0.0106498 0 0 0 1620000000 14 3 40 2 4 14 0.0106502
0.0106502 0 0 0 1620000000 14 3 45 2 4 19 0.0106552 0.0106552 0 0 0 1620000000
```

14	3	20	2	3	54	0.0098367	0.0098367	0	0	0	1620000000
14	3	25	2	3	59	0.0106431	0.0106431	0	0	0	1620000000
14	3	30	2	4	4	0.0106117	0.0106117	0	0	0	1620000000
14	3	35	2	4	9	0.0106498	0.0106498	0	0	0	1620000000
14	3	40	2	4	14	0.0106502	0.0106502	0	0	0	1620000000
14	3	45	2	4	19	0.0106552	0.0106552	0	0	0	1620000000
14	3	50	2	4	24	0.0106552	0.0106552	0	0	0	1620000000
14	3	55	2	4	29	0.0106581	0.0106581	0	0	0	1620000000
14	4	0	2	4	34	0.0106619	0.0106619	0	0	0	1620000000
14	4	5	2	4	39	0.0106668	0.0106668	0	0	0	1620000000
14	4	10	2	4	44	0.0106715	0.0106715	0	0	0	1620000000
14	4	15	2	4	49	0.0106756	0.0106756	0	0	0	1620000000
14	4	20	2	4	54	0.010683	0.010683	0	0	0	1620000000
14	4	25	2	4	59	0.010691	0.010691	0	0	0	1620000000
14	4	30	2	5	4	0.0107014	0.0107014	0	0	0	1620000000
14	4	35	2	5	9	0.0107086	0.0107086	0	0	0	1620000000
14	4	40	2	5	14	0.0107207	0.0107207	0	0	0	1620000000
14	4	45	2	5	19	0.010733	0.010733	0	0	0	1620000000
14	4	50	2	5	24	0.0107452	0.0107452	0	0	0	1620000000
14	4	55	2	5	29	0.0107577	0.0107577	0	0	0	1620000000
14	5	0	2	5	34	0.0107703	0.0107703	0	0	0	1620000000
14	5	5	2	5	39	0.010783	0.010783	0	0	0	1620000000
14	5	10	2	5	44	0.010799	0.010799	0	0	0	1620000000
14	5	15	2	5	49	0.0108177	0.0108177	0	0	0	1620000000
14	5	20	2	5	54	0.0108351	0.0108351	0	0	0	1620000000
14	5	25	2	5	59	0.0108531	0.0108531	0	0	0	1620000000
14	5	30	2	6	4	0.0108741	0.0108741	0	0	0	1620000000
14	5	35	2	6	9	0.0108968	0.0108968	0	0	0	1620000000
14	5	40	2	6	14	0.0109188	0.0109188	0	0	0	1620000000
14	5	45	2	6	19	0.0109397	0.0109397	0	0	0	1620000000
14	5	50	2	6	24	0.0109665	0.0109665	0	0	0	1620000000
14	5	55	2	6	29	0.0109947	0.0109947	0	0	0	1620000000
14	6	0	2	6	34	0.0110236	0.0110236	0	0	0	1620000000
14	6	5	2	6	38	0.0110477	0.0110477	0	0	0	1620000000
14	6	10	2	6	44	0.0110785	0.0110785	0	0	0	1620000000
14	6	15	2	6	49	0.0111066	0.0111066	0	0	0	1620000000
14	6	20	2	6	54	0.0111134	0.0111134	0	0	0	1620000000
14	6	25	2	6	59	0.0111566	0.0111566	0	0	0	1620000000
14	6	30	2	7	4	0.0111871	0.0111871	0	0	0	1620000000
14	6	35	2	7	9	0.0112187	0.0112187	0	0	0	1620000000
14	6	40	2	7	14	0.0112568	0.0112568	0	0	0	1620000000
14	6	45	2	7	19	0.0112913	0.0112913	0	0	0	1620000000
14	6	50	2	7	24	0.0113928	0.0113928	0	0	0	1620000000
14	6	55	2	7	29	0.011474	0.011474	0	0	0	1620000000
14	7	0	2	7	34	0.0115246	0.0115246	0	0	0	1620000000
14	7	5	2	7	39	0.0115735	0.0115735	0	0	0	1620000000

14	7	10	2	7	44	0.0116123	0.0116123	0	0	0	1620000000
14	7	15	2	7	49	0.0116608	0.0116608	0	0	0	1620000000
14	7	20	2	7	54	0.0117374	0.0117374	0	0	0	1620000000
14	7	25	2	7	59	0.0117882	0.0117882	0	0	0	1620000000
14	7	30	2	8	4	0.0118267	0.0118267	0	0	0	1620000000
14	7	35	2	8	9	0.0118722	0.0118722	0	0	0	1620000000
14	7	40	2	8	14	0.0119264	0.0119264	0	0	0	1620000000
14	7	45	2	8	19	0.0119818	0.0119818	0	0	0	1620000000
14	7	50	2	8	24	0.0120331	0.0120331	0	0	0	1620000000
14	7	55	2	8	29	0.0121032	0.0121032	0	0	0	1620000000
14	8	0	2	8	34	0.0121854	0.0121854	0	0	0	1620000000
14	8	5	2	8	40	0.0122573	0.0122573	0	0	0	1620000000
14	8	10	2	8	45	0.0123177	0.0123177	0	0	0	1620000000
14	8	15	2	8	50	0.0123828	0.0123828	0	0	0	1620000000
14	8	20	2	8	55	0.0124591	0.0124591	0	0	0	1620000000
14	8	25	2	9	0	0.012572	0.012572	0	0	0	1620000000
14	8	30	2	9	5	0.0127089	0.0127089	0	0	0	1620000000
14	8	35	2	9	10	0.0127908	0.0127908	0	0	0	1620000000
14	8	40	2	9	15	0.0128557	0.0128557	0	0	0	1620000000
14	8	45	2	9	20	0.0129322	0.0129322	0	0	0	1620000000
14	8	50	2	9	25	0.0130302	0.0130302	0	0	0	1620000000
14	8	55	2	9	30	0.0131363	0.0131363	0	0	0	1620000000
14	9	0	2	9	35	0.0132176	0.0132176	0	0	0	1620000000
14	9	5	2	9	40	0.0133054	0.0133054	0	0	0	1620000000
14	9	10	2	9	45	0.0134486	0.0134486	0	0	0	1620000000
14	9	15	2	9	50	0.0135743	0.0135743	0	0	0	1620000000
14	9	20	2	9	55	0.0137661	0.0137661	0	0	0	1620000000
14	9	25	2	10	0	0.0139562	0.0139562	0	0	0	1620000000
14	9	30	2	10	5	0.0141771	0.0141771	0	0	0	1620000000
14	9	35	2	10	10	0.0143782	0.0143782	0	0	0	1620000000
14	9	40	2	10	15	0.0145556	0.0145556	0	0	0	1620000000
14	9	45	2	10	20	0.0146911	0.0146911	0	0	0	1620000000
14	9	50	2	10	25	0.0148548	0.0148548	0	0	0	1620000000
14	9	55	2	10	30	0.0151684	0.0151684	0	0	0	1620000000
14	10	0	2	10	35	0.0153112	0.0153112	0	0	0	1620000000
14	10	5	2	10	40	0.0153928	0.0153928	0	0	0	1620000000
14	10	10	2	10	45	0.0155809	0.0155809	0	0	0	1620000000
14	10	15	2	10	50	0.0157849	0.0157849	0	0	0	1620000000
14	10	20	2	10	55	0.0160039	0.0160039	0	0	0	1620000000
14	10	25	2	11	0	0.0162133	0.0162133	0	0	0	1620000000
14	10	30	2	11	5	0.016358	0.016358	0	0	0	1620000000
14	10	35	2	11	10	0.0164633	0.0164633	0	0	0	1620000000
14	10	40	2	11	15	0.0167174	0.0167174	0	0	0	1620000000
14	10	45	2	11	20	0.016828	0.016828	0	0	0	1620000000
14	10	50	2	11	25	0.0169214	0.0169214	0	0	0	1620000000
14	10	55	2	11	30	0.0170201	0.0170201	0	0	0	1620000000

14	11	0	2	11	35	0.0171814	0.0171814	0	0	0	1620000000
14	11	5	2	11	40	0.0173451	0.0173451	0	0	0	1620000000
14	11	10	2	11	45	0.0175186	0.0175186	0	0	0	1620000000
14	11	15	2	11	50	0.017679	0.017679	0	0	0	1620000000
14	11	20	2	11	55	0.0178136	0.0178136	0	0	0	1620000000
14	11	25	2	12	0	0.0180285	0.0180285	0	0	0	1620000000
14	11	30	2	12	5	0.0182557	0.0182557	0	0	0	1620000000
14	11	35	2	12	10	0.0184567	0.0184567	0	0	0	1620000000
14	11	40	2	12	15	0.0186964	0.0186964	0	0	0	1620000000
14	11	45	2	12	20	0.0189372	0.0189372	0	0	0	1620000000
14	11	50	2	12	25	0.0191475	0.0191475	0	0	0	1620000000
14	11	55	2	12	30	0.0193709	0.0193709	0	0	0	1620000000
14	12	0	2	12	35	0.0195663	0.0195663	0	0	0	1620000000
14	12	5	2	12	40	0.0198087	0.0198087	0	0	0	1620000000
14	12	10	2	12	45	0.020171	0.020171	0	0	0	1620000000
14	12	15	2	12	50	0.0204146	0.0204146	0	0	0	1620000000
14	12	20	2	12	55	0.02078	0.02078	0	0	0	1620000000
14	12	25	2	13	0	0.0209684	0.0209684	0	0	0	1620000000
14	12	30	2	13	5	0.0211407	0.0211407	0	0	0	1620000000
14	12	35	2	13	10	0.0213057	0.0213057	0	0	0	1620000000
14	12	40	2	13	15	0.0215138	0.0215138	0	0	0	1620000000
14	12	45	2	13	20	0.0216616	0.0216616	0	0	0	1620000000
14	12	50	2	13	25	0.022099	0.022099	0	0	0	1620000000
14	12	55	2	13	30	0.022346	0.022346	0	0	0	1620000000
14	13	0	2	13	35	0.0226059	0.0226059	0	0	0	1620000000
14	13	5	2	13	40	0.0228246	0.0228246	0	0	0	1620000000
14	13	10	2	13	45	0.0229858	0.0229858	0	0	0	1620000000
14	13	15	2	13	50	0.0232374	0.0232374	0	0	0	1620000000
14	13	20	2	13	55	0.0234806	0.0234806	0	0	0	1620000000
14	13	25	2	14	0	0.0238966	0.0238966	0	0	0	1620000000
14	13	30	2	14	5	0.0240285	0.0240285	0	0	0	1620000000
14	13	35	2	14	10	0.0240721	0.0240721	0	0	0	1620000000
14	13	40	2	14	15	0.024253	0.024253	0	0	0	1620000000
14	13	45	2	14	20	0.024437	0.024437	0	0	0	1620000000
14	13	50	2	14	25	0.0246195	0.0246195	0	0	0	1620000000
14	13	55	2	14	30	0.0249227	0.0249227	0	0	0	1620000000
14	14	0	2	14	35	0.0250429	0.0250429	0	0	0	1620000000
14	14	5	2	14	40	0.0250747	0.0250747	0	0	0	1620000000
14	14	10	2	14	46	0.0251919	0.0251919	0	0	0	1620000000
14	14	15	2	14	51	0.0254099	0.0254099	0	0	0	1620000000
14	14	20	2	14	56	0.0255152	0.0255152	0	0	0	1620000000
14	14	25	2	15	1	0.0259199	0.0259199	0	0	0	1620000000
14	14	30	2	15	6	0.0262997	0.0262997	0	0	0	1620000000
14	14	35	2	15	11	0.0264591	0.0264591	0	0	0	1620000000
14	14	40	2	15	16	0.0268191	0.0268191	0	0	0	1620000000
14	14	45	2	15	20	0.0268384	0.0268384	0	0	0	1620000000

14	14	50	2	15	26	0.0271103	0.0271103	0	0	0	1620000000
14	14	55	2	15	31	0.0270994	0.0270994	0	0	0	1620000000
14	15	0	2	15	36	0.0273123	0.0273123	0	0	0	1620000000
14	15	5	2	15	41	0.027253	0.027253	0	0	0	1620000000
14	15	10	2	15	46	0.0273125	0.0273125	0	0	0	1620000000
14	15	15	2	15	51	0.0274494	0.0274494	0	0	0	1620000000
14	15	20	2	15	56	0.0274199	0.0274199	0	0	0	1620000000
14	15	25	2	16	1	0.0275915	0.0275915	0	0	0	1620000000
14	15	30	2	16	6	0.0280965	0.0280965	0	0	0	1620000000
14	15	35	2	16	11	0.0284924	0.0284924	0	0	0	1620000000
14	15	40	2	16	16	0.0289715	0.0289715	0	0	0	1620000000
14	15	45	2	16	21	0.0291811	0.0291811	0	0	0	1620000000
14	15	50	2	16	26	0.0294996	0.0294996	0	0	0	1620000000
14	15	55	2	16	31	0.0296787	0.0296787	0	0	0	1620000000
14	16	0	2	16	36	0.0300234	0.0300234	0	0	0	1620000000
14	16	5	2	16	41	0.0299203	0.0299203	0	0	0	1620000000
14	16	10	2	16	46	0.0298414	0.0298414	0	0	0	1620000000
14	16	15	2	16	51	0.0298073	0.0298073	0	0	0	1620000000
14	16	20	2	16	56	0.0298745	0.0298745	0	0	0	1620000000
14	16	25	2	17	1	0.029827	0.029827	0	0	0	1620000000
14	16	30	2	17	5	0.0299605	0.0299605	0	0	0	1620000000
14	16	35	2	17	11	0.0298786	0.0298786	0	0	0	1620000000
14	16	40	2	17	16	0.0298758	0.0298758	0	0	0	1620000000
14	16	45	2	17	21	0.029777	0.029777	0	0	0	1620000000
14	16	50	2	17	26	0.0297024	0.0297024	0	0	0	1620000000
14	16	55	2	17	31	0.0295813	0.0295813	0	0	0	1620000000
14	17	0	2	17	35	0.0295943	0.0295943	0	0	0	1620000000
14	17	5	2	17	41	0.0295685	0.0295685	0	0	0	1620000000
14	17	10	2	17	46	0.0294032	0.0294032	0	0	0	1620000000
14	17	15	2	17	51	0.0292163	0.0292163	0	0	0	1620000000
14	17	20	2	17	56	0.0290213	0.0290213	0	0	0	1620000000
14	17	25	2	18	1	0.0289102	0.0289102	0	0	0	1620000000
14	17	30	2	18	6	0.0289708	0.0289708	0	0	0	1620000000
14	17	35	2	18	11	0.0290105	0.0290105	0	0	0	1620000000
14	17	40	2	18	16	0.0289363	0.0289363	0	0	0	1620000000
14	17	45	2	18	21	0.0288693	0.0288693	0	0	0	1620000000
14	17	50	2	18	26	0.0285957	0.0285957	0	0	0	1620000000
14	17	55	2	18	31	0.0283781	0.0283781	0	0	0	1620000000
14	18	0	2	18	36	0.0282075	0.0282075	0	0	0	1620000000
14	18	5	2	18	41	0.0280029	0.0280029	0	0	0	1620000000
14	18	10	2	18	46	0.0278174	0.0278174	0	0	0	1620000000
14	18	15	2	18	51	0.0276557	0.0276557	0	0	0	1620000000
14	18	20	2	18	56	0.0275636	0.0275636	0	0	0	1620000000
14	18	25	2	19	1	0.0274716	0.0274716	0	0	0	1620000000
14	18	30	2	19	6	0.0273117	0.0273117	0	0	0	1620000000
14	18	35	2	19	11	0.0270815	0.0270815	0	0	0	1620000000

14	18	40	2	19	16	0.026854	0.026854	0	0	0	1620000000
14	18	45	2	19	21	0.0266415	0.0266415	0	0	0	1620000000
14	18	50	2	19	26	0.0264545	0.0264545	0	0	0	1620000000
14	18	55	2	19	31	0.0263306	0.0263306	0	0	0	1620000000
14	19	0	2	19	36	0.0264908	0.0264908	0	0	0	1620000000
14	19	5	2	19	41	0.0262735	0.0262735	0	0	0	1620000000
14	19	10	2	19	46	0.0261154	0.0261154	0	0	0	1620000000
14	19	15	2	19	51	0.0261644	0.0261644	0	0	0	1620000000
14	19	20	2	19	56	0.0259924	0.0259924	0	0	0	1620000000
14	19	25	2	20	1	0.025903	0.025903	0	0	0	1620000000
14	19	30	2	20	6	0.0255316	0.0255316	0	0	0	1620000000
14	19	35	2	20	11	0.0252809	0.0252809	0	0	0	1620000000
14	19	40	2	20	16	0.0249219	0.0249219	0	0	0	1620000000
14	19	45	2	20	21	0.0246035	0.0246035	0	0	0	1620000000
14	19	50	2	20	26	0.0243331	0.0243331	0	0	0	1620000000
14	19	55	2	20	31	0.0240914	0.0240914	0	0	0	1620000000
14	20	0	2	20	36	0.0238176	0.0238176	0	0	0	1620000000
14	20	5	2	20	41	0.0235963	0.0235963	0	0	0	1620000000
14	20	10	2	20	46	0.0233278	0.0233278	0	0	0	1620000000
14	20	15	2	20	52	0.0231806	0.0231806	0	0	0	1620000000
14	20	20	2	20	57	0.0230438	0.0230438	0	0	0	1620000000
14	20	25	2	21	2	0.0228054	0.0228054	0	0	0	1620000000
14	20	30	2	21	7	0.0225693	0.0225693	0	0	0	1620000000
14	20	35	2	21	12	0.022259	0.022259	0	0	0	1620000000
14	20	40	2	21	17	0.0220915	0.0220915	0	0	0	1620000000
14	20	45	2	21	22	0.0218919	0.0218919	0	0	0	1620000000
14	20	50	2	21	27	0.0216465	0.0216465	0	0	0	1620000000
14	20	55	2	21	32	0.0214411	0.0214411	0	0	0	1620000000
14	21	0	2	21	37	0.0212186	0.0212186	0	0	0	1620000000
14	21	5	2	21	42	0.0210353	0.0210353	0	0	0	1620000000
14	21	10	2	21	47	0.0207693	0.0207693	0	0	0	1620000000
14	21	15	2	21	52	0.0205009	0.0205009	0	0	0	1620000000
14	21	20	2	21	57	0.0202784	0.0202784	0	0	0	1620000000
14	21	25	2	22	2	0.0200681	0.0200681	0	0	0	1620000000
14	21	30	2	22	7	0.019806	0.019806	0	0	0	1620000000
14	21	35	2	22	12	0.0195781	0.0195781	0	0	0	1620000000
14	21	40	2	22	17	0.0193509	0.0193509	0	0	0	1620000000
14	21	45	2	22	22	0.0191434	0.0191434	0	0	0	1620000000
14	21	50	2	22	27	0.0188725	0.0188725	0	0	0	1620000000
14	21	55	2	22	32	0.0185888	0.0185888	0	0	0	1620000000
14	22	0	2	22	37	0.0183732	0.0183732	0	0	0	1620000000
14	22	5	2	22	42	0.0181471	0.0181471	0	0	0	1620000000
14	22	10	2	22	47	0.017918	0.017918	0	0	0	1620000000
14	22	15	2	22	52	0.0177289	0.0177289	0	0	0	1620000000
14	22	20	2	22	57	0.0175961	0.0175961	0	0	0	1620000000
14	22	25	2	23	2	0.0173773	0.0173773	0	0	0	1620000000

14	22	30	2	23	7	0.017187	0.017187	0	0	0	1620000000
14	22	35	2	23	12	0.0169828	0.0169828	0	0	0	1620000000
14	22	40	2	23	17	0.0167778	0.0167778	0	0	0	1620000000
14	22	45	2	23	22	0.0165884	0.0165884	0	0	0	1620000000
14	22	50	2	23	27	0.0163928	0.0163928	0	0	0	1620000000
14	22	55	2	23	32	0.016202	0.016202	0	0	0	1620000000
14	23	0	2	23	37	0.0160455	0.0160455	0	0	0	1620000000
14	23	5	2	23	42	0.0159153	0.0159153	0	0	0	1620000000
14	23	10	2	23	46	0.0158077	0.0158077	0	0	0	1620000000
14	23	15	2	23	52	0.0156826	0.0156826	0	0	0	1620000000
14	23	20	2	23	57	0.0155363	0.0155363	0	0	0	1620000000
14	23	25	2	24	2	0.0153777	0.0153777	0	0	0	1620000000
14	23	30	2	24	7	0.0152424	0.0152424	0	0	0	1620000000
14	23	35	2	24	12	0.0151187	0.0151187	0	0	0	1620000000
14	23	40	2	24	17	0.014994	0.014994	0	0	0	1620000000
14	23	45	2	24	22	0.0148522	0.0148522	0	0	0	1620000000
14	23	50	2	24	27	0.0147389	0.0147389	0	0	0	1620000000
14	23	55	2	24	32	0.0146109	0.0146109	0	0	0	1620000000
14	24	0	2	24	37	0.0144527	0.0144527	0	0	0	1620000000
14	24	5	2	24	42	0.0143405	0.0143405	0	0	0	1620000000
14	24	10	2	24	47	0.014247	0.014247	0	0	0	1620000000
14	24	15	2	24	52	0.0141209	0.0141209	0	0	0	1620000000
14	24	20	2	24	57	0.014003	0.014003	0	0	0	1620000000
14	24	25	2	25	2	0.013891	0.013891	0	0	0	1620000000
14	24	30	2	25	7	0.0138088	0.0138088	0	0	0	1620000000
14	24	35	2	25	12	0.0137057	0.0137057	0	0	0	1620000000
14	24	40	2	25	17	0.0136075	0.0136075	0	0	0	1620000000
14	24	45	2	25	22	0.0135204	0.0135204	0	0	0	1620000000
14	24	50	2	25	26	0.0134475	0.0134475	0	0	0	1620000000
14	24	55	2	25	32	0.0133578	0.0133578	0	0	0	1620000000
14	25	0	2	25	37	0.0132676	0.0132676	0	0	0	1620000000
14	25	5	2	25	42	0.0131847	0.0131847	0	0	0	1620000000
14	25	10	2	25	47	0.0130975	0.0130975	0	0	0	1620000000
14	25	15	2	25	52	0.0130072	0.0130072	0	0	0	1620000000
14	25	20	2	25	57	0.0129171	0.0129171	0	0	0	1620000000
14	25	25	2	26	2	0.0128365	0.0128365	0	0	0	1620000000
14	25	30	2	26	7	0.0127523	0.0127523	0	0	0	1620000000
14	25	35	2	26	12	0.0126763	0.0126763	0	0	0	1620000000
14	25	40	2	26	17	0.0126055	0.0126055	0	0	0	1620000000
14	25	45	2	26	22	0.0125419	0.0125419	0	0	0	1620000000
14	25	50	2	26	27	0.0124843	0.0124843	0	0	0	1620000000
14	25	55	2	26	32	0.0124281	0.0124281	0	0	0	1620000000
14	26	0	2	26	37	0.0123747	0.0123747	0	0	0	1620000000
14	26	5	2	26	42	0.0123251	0.0123251	0	0	0	1620000000
14	26	10	2	26	47	0.0122887	0.0122887	0	0	0	1620000000
14	26	15	2	26	51	0.0122423	0.0122423	0	0	0	1620000000

14	26	20	2	26	58	0.0121974	0.0121974	0	0	0	1620000000
14	26	25	2	27	3	0.0121675	0.0121675	0	0	0	1620000000
14	26	30	2	27	8	0.0121382	0.0121382	0	0	0	1620000000
14	26	35	2	27	13	0.0121002	0.0121002	0	0	0	1620000000
14	26	40	2	27	18	0.012065	0.012065	0	0	0	1620000000
14	26	45	2	27	23	0.0120357	0.0120357	0	0	0	1620000000
14	26	50	2	27	28	0.0120004	0.0120004	0	0	0	1620000000
14	26	55	2	27	33	0.011977	0.011977	0	0	0	1620000000
14	27	0	2	27	38	0.011952	0.011952	0	0	0	1620000000
14	27	5	2	27	43	0.0119231	0.0119231	0	0	0	1620000000
14	27	10	2	27	48	0.0118928	0.0118928	0	0	0	1620000000
14	27	15	2	27	53	0.0118647	0.0118647	0	0	0	1620000000
14	27	20	2	27	58	0.011833	0.011833	0	0	0	1620000000
14	27	25	2	28	3	0.0118054	0.0118054	0	0	0	1620000000
14	27	30	2	28	8	0.0117804	0.0117804	0	0	0	1620000000
14	27	35	2	28	13	0.011758	0.011758	0	0	0	1620000000
14	27	40	2	28	18	0.0117396	0.0117396	0	0	0	1620000000
14	27	45	2	28	23	0.0117149	0.0117149	0	0	0	1620000000
14	27	50	2	28	28	0.0116915	0.0116915	0	0	0	1620000000
14	27	55	2	28	33	0.0116614	0.0116614	0	0	0	1620000000
14	28	0	2	28	38	0.0116407	0.0116407	0	0	0	1620000000
14	28	5	2	28	43	0.0116228	0.0116228	0	0	0	1620000000
14	28	10	2	28	48	0.0115961	0.0115961	0	0	0	1620000000
14	28	15	2	28	53	0.0115763	0.0115763	0	0	0	1620000000
14	28	20	2	28	58	0.0115581	0.0115581	0	0	0	1620000000
14	28	25	2	29	3	0.0115449	0.0115449	0	0	0	1620000000
14	28	30	2	29	8	0.0115313	0.0115313	0	0	0	1620000000
14	28	35	2	29	13	0.0115183	0.0115183	0	0	0	1620000000
14	28	40	2	29	18	0.011504	0.011504	0	0	0	1620000000
14	28	45	2	29	23	0.0114871	0.0114871	0	0	0	1620000000
14	28	50	2	29	28	0.0114699	0.0114699	0	0	0	1620000000
14	28	55	2	29	33	0.0114532	0.0114532	0	0	0	1620000000
14	29	0	2	29	38	0.011438	0.011438	0	0	0	1620000000
14	29	5	2	29	43	0.0114204	0.0114204	0	0	0	1620000000
14	29	10	2	29	48	0.0114009	0.0114009	0	0	0	1620000000
14	29	15	2	29	53	0.011375	0.011375	0	0	0	1620000000
14	29	20	2	29	58	0.0113545	0.0113545	0	0	0	1620000000
14	29	25	2	30	3	0.0113346	0.0113346	0	0	0	1620000000
14	29	30	2	30	8	0.0113154	0.0113154	0	0	0	1620000000
14	29	35	2	30	13	0.0112943	0.0112943	0	0	0	1620000000
14	29	40	2	30	18	0.0112752	0.0112752	0	0	0	1620000000
14	29	45	2	30	23	0.0112556	0.0112556	0	0	0	1620000000
14	29	50	2	30	28	0.0112322	0.0112322	0	0	0	1620000000
14	29	55	2	30	33	0.0112143	0.0112143	0	0	0	1620000000
14	30	0	2	30	38	0.0111989	0.0111989	0	0	0	1620000000
14	30	5	2	30	43	0.0111812	0.0111812	0	0	0	1620000000

14	30	10	2	30	48	0.0111632	0.0111632	0	0	0	1620000000
14	30	15	2	30	53	0.0111443	0.0111443	0	0	0	1620000000
14	30	20	2	30	58	0.0111231	0.0111231	0	0	0	1620000000
14	30	25	2	31	3	0.0111064	0.0111064	0	0	0	1620000000
14	30	30	2	31	8	0.0110909	0.0110909	0	0	0	1620000000
14	30	35	2	31	13	0.0110678	0.0110678	0	0	0	1620000000
14	30	40	2	31	18	0.0110497	0.0110497	0	0	0	1620000000
14	30	45	2	31	23	0.0110345	0.0110345	0	0	0	1620000000
14	30	50	2	31	28	0.0110193	0.0110193	0	0	0	1620000000
14	30	55	2	31	33	0.0110086	0.0110086	0	0	0	1620000000
14	31	0	2	31	38	0.0109967	0.0109967	0	0	0	1620000000
14	31	5	2	31	43	0.0109856	0.0109856	0	0	0	1620000000
14	31	10	2	31	48	0.0109735	0.0109735	0	0	0	1620000000
14	31	15	2	31	53	0.0109633	0.0109633	0	0	0	1620000000
14	31	20	2	31	58	0.0109493	0.0109493	0	0	0	1620000000
14	31	25	2	32	3	0.0109342	0.0109342	0	0	0	1620000000
14	31	30	2	32	8	0.0109197	0.0109197	0	0	0	1620000000
14	31	35	2	32	13	0.010906	0.010906	0	0	0	1620000000
14	31	40	2	32	18	0.0108904	0.0108904	0	0	0	1620000000
14	31	45	2	32	23	0.0108733	0.0108733	0	0	0	1620000000
14	31	50	2	32	28	0.0108648	0.0108648	0	0	0	1620000000
14	31	55	2	32	33	0.0108547	0.0108547	0	0	0	1620000000
14	32	0	2	32	38	0.0108434	0.0108434	0	0	0	1620000000
14	32	5	2	32	43	0.0108313	0.0108313	0	0	0	1620000000
14	32	10	2	32	48	0.0108172	0.0108172	0	0	0	1620000000
14	32	15	2	32	53	0.0108051	0.0108051	0	0	0	1620000000
14	32	20	2	32	58	0.0107956	0.0107956	0	0	0	1620000000
14	32	25	2	33	4	0.0107872	0.0107872	0	0	0	1620000000
14	32	30	2	33	9	0.0107791	0.0107791	0	0	0	1620000000
14	32	35	2	33	14	0.0107705	0.0107705	0	0	0	1620000000
14	32	40	2	33	19	0.0107604	0.0107604	0	0	0	1620000000
14	32	45	2	33	24	0.0107515	0.0107515	0	0	0	1620000000
14	32	50	2	33	29	0.0107463	0.0107463	0	0	0	1620000000
14	32	55	2	33	34	0.0107396	0.0107396	0	0	0	1620000000
14	33	0	2	33	39	0.0107332	0.0107332	0	0	0	1620000000
14	33	5	2	33	44	0.0107285	0.0107285	0	0	0	1620000000
14	33	10	2	33	49	0.0107266	0.0107266	0	0	0	1620000000
14	33	15	2	33	54	0.0107253	0.0107253	0	0	0	1620000000
14	33	20	2	33	59	0.0107225	0.0107225	0	0	0	1620000000
14	33	25	2	34	4	0.0107207	0.0107207	0	0	0	1620000000
14	33	30	2	34	9	0.0107195	0.0107195	0	0	0	1620000000
14	33	35	2	34	14	0.0107199	0.0107199	0	0	0	1620000000
14	33	40	2	34	19	0.0107216	0.0107216	0	0	0	1620000000
14	33	45	2	34	24	0.0107216	0.0107216	0	0	0	1620000000
14	33	50	2	34	29	0.0107212	0.0107212	0	0	0	1620000000
14	33	55	2	34	34	0.0107237	0.0107237	0	0	0	1620000000

14	34	0	2	34	39	0.0107296	0.0107296	0	0	0	1620000000
14	34	5	2	34	44	0.0107316	0.0107316	0	0	0	1620000000
14	34	10	2	34	49	0.0107323	0.0107323	0	0	0	1620000000
14	34	15	2	34	53	0.0107325	0.0107325	0	0	0	1620000000
14	34	20	2	34	59	0.0107343	0.0107343	0	0	0	1620000000
14	34	25	2	35	4	0.010735	0.010735	0	0	0	1620000000
14	34	30	2	35	9	0.0107358	0.0107358	0	0	0	1620000000
14	34	35	2	35	14	0.0107347	0.0107347	0	0	0	1620000000
14	34	40	2	35	19	0.0107318	0.0107318	0	0	0	1620000000
14	34	45	2	35	24	0.0107339	0.0107339	0	0	0	1620000000
14	34	50	2	35	29	0.0107342	0.0107342	0	0	0	1620000000
14	34	55	2	35	34	0.0107344	0.0107344	0	0	0	1620000000
14	35	0	2	35	39	0.010733	0.010733	0	0	0	1620000000
14	35	5	2	35	44	0.0107336	0.0107336	0	0	0	1620000000
14	35	10	2	35	49	0.0107351	0.0107351	0	0	0	1620000000
14	35	15	2	35	54	0.0107341	0.0107341	0	0	0	1620000000
14	35	20	2	35	59	0.0107333	0.0107333	0	0	0	1620000000
14	35	25	2	36	4	0.0107322	0.0107322	0	0	0	1620000000
14	35	30	2	36	9	0.0107337	0.0107337	0	0	0	1620000000
14	35	35	2	36	14	0.0107341	0.0107341	0	0	0	1620000000
14	35	40	2	36	19	0.0107364	0.0107364	0	0	0	1620000000
14	35	45	2	36	24	0.0107379	0.0107379	0	0	0	1620000000
14	35	50	2	36	29	0.0107412	0.0107412	0	0	0	1620000000
14	35	55	2	36	34	0.0107443	0.0107443	0	0	0	1620000000
14	36	0	2	36	39	0.0107466	0.0107466	0	0	0	1620000000
14	36	5	2	36	44	0.0107467	0.0107467	0	0	0	1620000000
14	36	10	2	36	49	0.0107448	0.0107448	0	0	0	1620000000
14	36	15	2	36	54	0.0107424	0.0107424	0	0	0	1620000000
14	36	20	2	36	59	0.0107411	0.0107411	0	0	0	1620000000
14	36	25	2	37	4	0.0107383	0.0107383	0	0	0	1620000000
14	36	30	2	37	8	0.0107374	0.0107374	0	0	0	1620000000
14	36	35	2	37	14	0.0107404	0.0107404	0	0	0	1620000000
14	36	40	2	37	19	0.0107436	0.0107436	0	0	0	1620000000
14	36	45	2	37	24	0.010743	0.010743	0	0	0	1620000000
14	36	50	2	37	29	0.0107452	0.0107452	0	0	0	1620000000
14	36	55	2	37	34	0.0107444	0.0107444	0	0	0	1620000000
14	37	0	2	37	39	0.0107438	0.0107438	0	0	0	1620000000
14	37	5	2	37	44	0.0107444	0.0107444	0	0	0	1620000000
14	37	10	2	37	49	0.0107394	0.0107394	0	0	0	1620000000
14	37	15	2	37	54	0.0107333	0.0107333	0	0	0	1620000000
14	37	20	2	37	59	0.0107254	0.0107254	0	0	0	1620000000
14	37	25	2	38	4	0.0107209	0.0107209	0	0	0	1620000000
14	37	30	2	38	9	0.0107171	0.0107171	0	0	0	1620000000
14	37	35	2	38	14	0.0107116	0.0107116	0	0	0	1620000000
14	37	40	2	38	19	0.01071	0.01071	0	0	0	1620000000
14	37	45	2	38	24	0.0107076	0.0107076	0	0	0	1620000000

14	37	50	2	38	29	0.010705	0.010705	0	0	0	1620000000
14	37	55	2	38	33	0.0107015	0.0107015	0	0	0	1620000000
14	38	0	2	38	38	0.010698	0.010698	0	0	0	1620000000
14	38	5	2	38	44	0.0106907	0.0106907	0	0	0	1620000000
14	38	10	2	38	49	0.0106867	0.0106867	0	0	0	1620000000
14	38	15	2	38	54	0.0106831	0.0106831	0	0	0	1620000000
14	38	20	2	38	59	0.0106773	0.0106773	0	0	0	1620000000
14	38	25	2	39	4	0.0106713	0.0106713	0	0	0	1620000000
14	38	30	2	39	10	0.0106647	0.0106647	0	0	0	1620000000
14	38	35	2	39	15	0.0106579	0.0106579	0	0	0	1620000000
14	38	40	2	39	20	0.0106527	0.0106527	0	0	0	1620000000
14	38	45	2	39	25	0.0106472	0.0106472	0	0	0	1620000000
14	38	50	2	39	30	0.0106374	0.0106374	0	0	0	1620000000
14	38	55	2	39	35	0.0106316	0.0106316	0	0	0	1620000000
14	39	0	2	39	40	0.010627	0.010627	0	0	0	1620000000
14	39	5	2	39	45	0.0106222	0.0106222	0	0	0	1620000000
14	39	10	2	39	50	0.0106182	0.0106182	0	0	0	1620000000
14	39	15	2	39	55	0.0106135	0.0106135	0	0	0	1620000000
14	39	20	2	40	0	0.010608	0.010608	0	0	0	1620000000
14	39	25	2	40	5	0.0106057	0.0106057	0	0	0	1620000000
14	39	30	2	40	10	0.0106011	0.0106011	0	0	0	1620000000
14	39	35	2	40	15	0.0105972	0.0105972	0	0	0	1620000000
14	39	40	2	40	20	0.0105964	0.0105964	0	0	0	1620000000
14	39	45	2	40	25	0.0105945	0.0105945	0	0	0	1620000000
14	39	50	2	40	30	0.0105887	0.0105887	0	0	0	1620000000
14	39	55	2	40	35	0.0105848	0.0105848	0	0	0	1620000000
14	40	0	2	40	40	0.0105838	0.0105838	0	0	0	1620000000
14	40	5	2	40	45	0.0105841	0.0105841	0	0	0	1620000000
14	40	10	2	40	50	0.0105833	0.0105833	0	0	0	1620000000
14	40	15	2	40	55	0.010581	0.010581	0	0	0	1620000000
14	40	20	2	41	0	0.0105815	0.0105815	0	0	0	1620000000
14	40	25	2	41	5	0.0105813	0.0105813	0	0	0	1620000000
14	40	30	2	41	10	0.0105794	0.0105794	0	0	0	1620000000
14	40	35	2	41	15	0.0105784	0.0105784	0	0	0	1620000000
14	40	40	2	41	20	0.0105788	0.0105788	0	0	0	1620000000
14	40	45	2	41	25	0.0105778	0.0105778	0	0	0	1620000000
14	40	50	2	41	30	0.0105769	0.0105769	0	0	0	1620000000
14	40	55	2	41	35	0.0105743	0.0105743	0	0	0	1620000000
14	41	0	2	41	40	0.0105742	0.0105742	0	0	0	1620000000
14	41	5	2	41	45	0.0105771	0.0105771	0	0	0	1620000000
14	41	10	2	41	50	0.0105793	0.0105793	0	0	0	1620000000
14	41	15	2	41	55	0.0105785	0.0105785	0	0	0	1620000000
14	41	20	2	42	0	0.010579	0.010579	0	0	0	1620000000
14	41	25	2	42	5	0.01058	0.01058	0	0	0	1620000000
14	41	30	2	42	10	0.0105806	0.0105806	0	0	0	1620000000
14	41	35	2	42	15	0.0105814	0.0105814	0	0	0	1620000000

14	41	40	2	42	20	0.0105768	0.0105768	0	0	0	1620000000
14	41	45	2	42	25	0.0105743	0.0105743	0	0	0	1620000000
14	41	50	2	42	30	0.0105743	0.0105743	0	0	0	1620000000
14	41	55	2	42	35	0.0105695	0.0105695	0	0	0	1620000000
14	42	0	2	42	40	0.0105682	0.0105682	0	0	0	1620000000
14	42	5	2	42	45	0.0105644	0.0105644	0	0	0	1620000000
14	42	10	2	42	50	0.0105618	0.0105618	0	0	0	1620000000
14	42	15	2	42	55	0.0105603	0.0105603	0	0	0	1620000000
14	42	20	2	43	0	0.0105583	0.0105583	0	0	0	1620000000
14	42	25	2	43	5	0.0105544	0.0105544	0	0	0	1620000000
14	42	30	2	43	10	0.0105535	0.0105535	0	0	0	1620000000
14	42	35	2	43	15	0.0105493	0.0105493	0	0	0	1620000000
14	42	40	2	43	20	0.0105407	0.0105407	0	0	0	1620000000
14	42	45	2	43	25	0.0105344	0.0105344	0	0	0	1620000000
14	42	50	2	43	30	0.0105327	0.0105327	0	0	0	1620000000
14	42	55	2	43	35	0.0105324	0.0105324	0	0	0	1620000000
14	43	0	2	43	40	0.010529	0.010529	0	0	0	1620000000
14	43	5	2	43	45	0.0105315	0.0105315	0	0	0	1620000000
14	43	10	2	43	50	0.0105347	0.0105347	0	0	0	1620000000
14	43	15	2	43	55	0.0105386	0.0105386	0	0	0	1620000000
14	43	20	2	44	0	0.0105428	0.0105428	0	0	0	1620000000
14	43	25	2	44	5	0.010549	0.010549	0	0	0	1620000000
14	43	30	2	44	10	0.0105561	0.0105561	0	0	0	1620000000
14	43	35	2	44	15	0.0105619	0.0105619	0	0	0	1620000000
14	43	40	2	44	20	0.0105664	0.0105664	0	0	0	1620000000
14	43	45	2	44	25	0.01057	0.01057	0	0	0	1620000000
14	43	50	2	44	30	0.0105716	0.0105716	0	0	0	1620000000
14	43	55	2	44	35	0.0105706	0.0105706	0	0	0	1620000000
14	44	0	2	44	40	0.0105717	0.0105717	0	0	0	1620000000
14	44	5	2	44	45	0.0105707	0.0105707	0	0	0	1620000000
14	44	10	2	44	50	0.0105718	0.0105718	0	0	0	1620000000
14	44	15	2	44	55	0.0105735	0.0105735	0	0	0	1620000000
14	44	20	2	45	0	0.0105738	0.0105738	0	0	0	1620000000
14	44	25	2	45	5	0.0105726	0.0105726	0	0	0	1620000000
14	44	30	2	45	10	0.0105727	0.0105727	0	0	0	1620000000
14	44	35	2	45	16	0.0105744	0.0105744	0	0	0	1620000000
14	44	40	2	45	21	0.0105716	0.0105716	0	0	0	1620000000
14	44	45	2	45	26	0.0105703	0.0105703	0	0	0	1620000000
14	44	50	2	45	31	0.0105672	0.0105672	0	0	0	1620000000
14	44	55	2	45	36	0.0105678	0.0105678	0	0	0	1620000000
14	45	0	2	45	41	0.0105671	0.0105671	0	0	0	1620000000
14	45	5	2	45	46	0.0105658	0.0105658	0	0	0	1620000000
14	45	10	2	45	51	0.0105631	0.0105631	0	0	0	1620000000
14	45	15	2	45	56	0.0105604	0.0105604	0	0	0	1620000000
14	45	20	2	46	1	0.0105609	0.0105609	0	0	0	1620000000
14	45	25	2	46	6	0.0105597	0.0105597	0	0	0	1620000000

14	45	30	2	46	11	0.0105615	0.0105615	0	0	0	1620000000
14	45	35	2	46	16	0.0105591	0.0105591	0	0	0	1620000000
14	45	40	2	46	21	0.0105566	0.0105566	0	0	0	1620000000
14	45	45	2	46	25	0.0105546	0.0105546	0	0	0	1620000000
14	45	50	2	46	31	0.0105532	0.0105532	0	0	0	1620000000
14	45	55	2	46	36	0.0105516	0.0105516	0	0	0	1620000000
14	46	0	2	46	41	0.0105486	0.0105486	0	0	0	1620000000
14	46	5	2	46	46	0.0105478	0.0105478	0	0	0	1620000000
14	46	10	2	46	51	0.0105464	0.0105464	0	0	0	1620000000
14	46	15	2	46	56	0.0105444	0.0105444	0	0	0	1620000000
14	46	20	2	47	1	0.0105451	0.0105451	0	0	0	1620000000
14	46	25	2	47	6	0.0105438	0.0105438	0	0	0	1620000000
14	46	30	2	47	11	0.0105415	0.0105415	0	0	0	1620000000
14	46	35	2	47	16	0.0105395	0.0105395	0	0	0	1620000000
14	46	40	2	47	21	0.0105371	0.0105371	0	0	0	1620000000
14	46	45	2	47	26	0.0105345	0.0105345	0	0	0	1620000000
14	46	50	2	47	31	0.0105333	0.0105333	0	0	0	1620000000
14	46	55	2	47	36	0.0105325	0.0105325	0	0	0	1620000000
14	47	0	2	47	41	0.0105293	0.0105293	0	0	0	1620000000
14	47	5	2	47	46	0.010529	0.010529	0	0	0	1620000000

Appendix C

Appendix C, shares some of the images that were captured to illustrate the effects of bad weather during experimental observations with our small radio telescope.

(C.1.0) Effects of heavy rains and wind

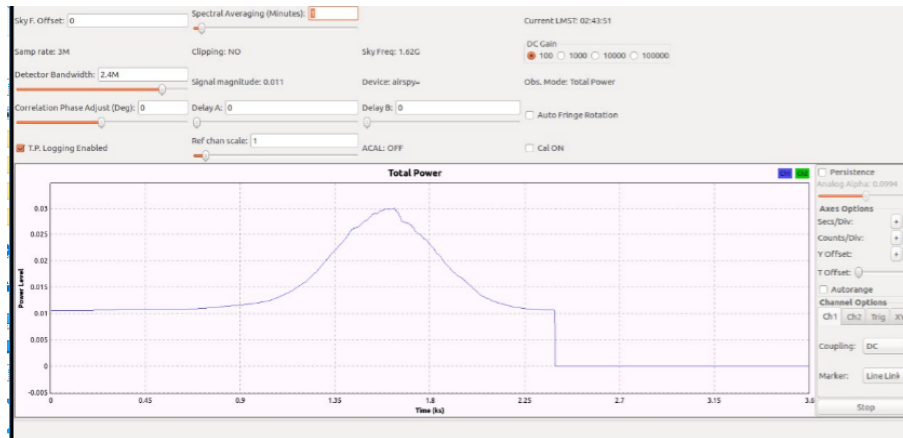


Figure 6.1: Shows the effects of heavy rains and wind during the drift scan of the Sun with a small radio telescope, in the beginning of the observation we could see that the weather was good for the observation. But after sometime the weather became windy and the telescope was being shaken.

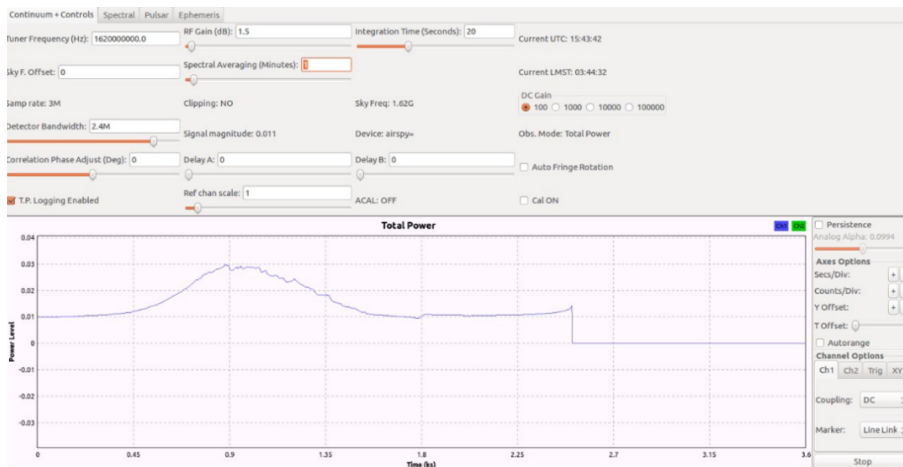


Figure 6.2: Shows the effects of heavy rains and wind during the observation of the Sun with a small radio telescope. Heavy rains and wind could lead to poor observation of the source as shown above. The full solar drift scan shared here, can not be compared to other solar drift scans that were done in good weather with the same small radio telescope.

Appendix C

(C.2.0) Observation site



Figure 6.3: Shows the observation site for the off-the shelf methanol maser radio telescope on the roof of the STRI building at the University of Hertfordshire. The site is surrounded by building walls, roofing metals and glasses that could also contribute to poor observations by the telescope

(C.2.1) Observation site

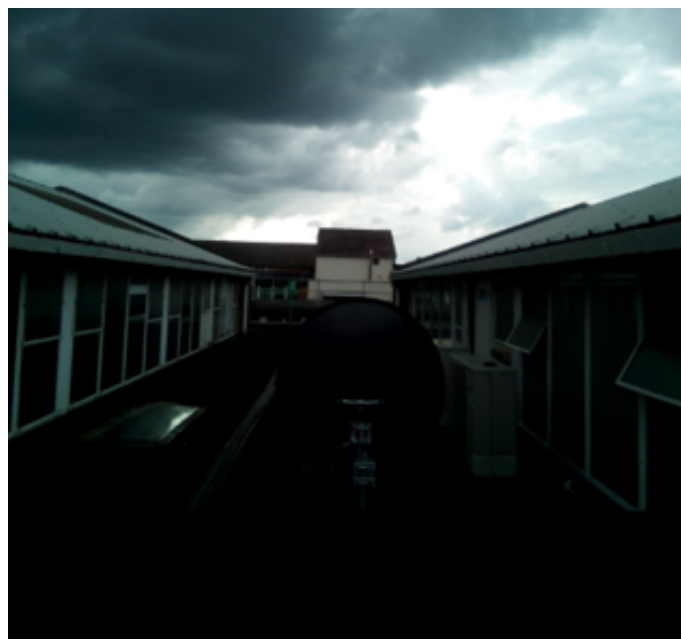


Figure 6.4: Shows the observation site for the off-the shelf methanol maser radio telescope during an observation on a rainy and stormy day at the University of Hertfordshire.

Bibliography

- Alexandru, C. (2016). Gqrx. *Software Defined Radio Powered by GNUradio and Qt* [Online], Available:www.github.com/csete/gqrx.
- Antenna, S. (2017). Satellite antenna alignment 2.99.0.0.
- Batrla, W., Matthews, H. E., Menten, K. M., and Walmsley, C. M. (1987). *Nature*,326,931.
- Blattenberger, K. (2016). Rf cafe. noise temperature. [Online], Available :<http://www.rfcafe.com>.
- Bogusław, M. and Szymon, M. (2012). Build your own radio telescope. *Science in School*. [Online], Available:<http://www.scienceinschool.org/2012/issue23/telescope>.
- Breen, S. L.and et, a. (2016). 12.2 ghz methanol maser mmb follow-up catalogue-iv.longitude range $20^{\circ} - 60^{\circ}$. *MNRAS* 459, 4066–4087.
- Breen, S., Ellingsen, S. P., L., C., Green, J. A., Fuller, G. A., Voronkov, M. A., Quinn, L. J., and Avison, A. (2011). Statistical properties of 12.2 ghz methanol masers associated with a complete sample of 6.7 ghz methanol masers. *The Astrophysical Journal*, 733(2):80.
- Caswell, J. L., Gardner, F. F., R., N., Wellington, K. J., McCutcheon, W. H., and Peng, R. S. (1993). Methanol masers at 12 ghz. *Royal Astronomical Society ,Provided by the NASA Astrophysics Data System*.
- Cragg, D. M., Johns, K. P., Godfrey, P. D., and Brown, R. D. (1992). *MNRAS*,259,203.
- Crockett, C. (2012). Astronomy essentials. [Online], Available :<http://earthsky.org/astronomy-essentials/what-is-sidereal-time>.
- Dale, E. G. (2014). Physics 728, radio astronomy: Lecture #5,. *Front End Receiving System*, [Online] Available: <https://web.njit.edu/~gary/728/Lecture5.html>.
- David, E. F., Allan, E. R., Preethi, P., and Philip, S. (2008). Tamke-allan observatory, undergraduate laboratory experiments in ku-band radio astronomy: A very small radio telescope interferometer. *Haystack Observatory Massachusetts Institute of Technology*.
- DeWitt, A. (2017). Introduction to dstv dish observations. *AVN/Newton-Fund 2017 Observational and Technical Training Har-tebeesthoek Radio Astronomy Observatory*. [Online], Available: http://avntraining.hartrao.ac.za/images/Schools/2017March/AVN2017_DSTVdish.pdf.
- Ellingsen, S. P. (2005). Methanol masers: Reliable tracers of the early stages of high-mass star formation. *The American Astronomical Society*.
- Eric, J. (2016). Low noise block downconverter (lnb). *Satellite LNB: What is it, how does it work and where do I buy one?* [Online],Available:<http://www.satsig.net/lnb/explanation-description-lnb.htm>.
- Fish, L. V. and Rogers, A. E. (2009). On the feasibility of a low-cost methanol radio telescope. VSRT Memo Num 065. [Online], Available:<https://www.google.com/url?url=https://www.haystack.mit.edu/edu/undergrad/VVRT/VVRT>

- Gaylard, M. (2012). Radio astronomy with a single dish radio telescope. *Hartebeesthoek Radio Astronomy Observatory (HarTRAO) South-Africa*. [Online], Available: http://avntraining.hartrao.ac.za/images/radio_astronomy_theory.pdf.
- Gaylard, M. J. (2006). Practical radio astronomy with a hi-math introduction. *Hartebeesthoek Radio Astronomy Observatory South-Africa*. [Online], Available: https://ir.dut.ac.za/bitstream/10321/1067/1/PILLAY_2012.pd.
- Gnuradio.org (2016). Gnu radio. *The GNU radio Foundation* [Online], Available: www.gnuradio.org/.
- Jean, M. P. (2016). Amateur radio astronomy..how to start. *F5VLB-EA4EOZ- 2016 Amateur Radio Astronomy*. [Online], Available: <http://www.astrosurf.com/luxorion/Documents/amateur-radioastronomy-f5vlb-jm-polard.pdf>.
- Joardar, S., Bhattacharyya, S., Bhattacharya, A. B., and Datta, C. R. (2010). Radio astronomy and super-synthesis survey. *Tata Institute of Fundamental Research Giant Meter wave Radio Telescope Narayagaon, Pune 410504, India*, Progress In Electromagnetics Research B, Vol. 22, 73102.
- Joshi, B. C. (2014). Teaching radio astronomy with affordable small radio telescope (as-rt). 40th COSPAR Scientific Assembly, Provided by the SAO/NASA Astrophysics Data System, [Online] Available: <http://adsabs.harvard.edu/abs/2014cosp...40E1346J>.
- Koo, B. C., Williams, D. R., Hellies, C., and Backer, D. C. (1988). *ApJ*, 326, 931.
- Koppen, J. (2007). Report on the experiences with the esa-dresden radio telescope. *Observational Astronomiqui, Strasbourg, International Space University, IIIkirch*.
- Koppen, J. (2010). Solar observation with esa-haystack. *Solar Drift Scans*. [Online], Available :<http://astro.u-strasbg.fr/koppen/Haystack/solar.html>.
- Koppen, J. (2011a). Determining the system temperature. *Solar Drift Scans*. [Online], Available :<http://astro.u-strasbg.fr/koppen/ue7e/sundrift.html>.
- Koppen, J. (2011b). Introduction to radio astronomy data reduction and analysis (1). *Solar Drift Scan*. [Online], Available :<http://astro.u-strasbg.fr/koppen/JKHome.html>.
- Kraus, J. D. (1966). *Radio Astronomy*. McGraw- Hill.
- Kraus, J. D. (1986). *Radio astronomy*. Cygnus-Quasar, 2nd ed edition.
- Kurtz, S., Hofner, P., and Alvarez, C. V. (2004). *ApJS*, 155, 149.
- Lashley, J. (2010). Microwave radio telescope projects. *The Radio Sky and How to Observe It, Astronomers' Observing Guides*. Springer Science+ Business Media, LLC, 10.1007/978-1-4419-0883-4_10.
- Laufer, C. (2015). *The Hobbyist's Guide to The RTL-SDR: Really Cheap SDR*, volume 1. Printed in Great Britain by Amazon, 2nd ed edition.
- MacRobert, A. (2006). The essential guide to astronomy. [Online], available: <http://www.skyandtelescope.com/astronomy>.

- MacRobert, A. (2017). Equatorial coordinates. COSMOS The SAO Encyclopedia of Astronomy [online], available: <http://astronomy.swin.edu.au/cms/cpg15x/albums/userpics/equatorialcoordinatesystem2.gif>.
- Mandal, P., Agarwal, D., Kumar, P., Yelikar, A., Soni, K., and Krishna, V. (2016). Everyday radio telescope. pages 1–13.
- Marcus, D. L. (2013). Simple_ra a collection of tools for amateur radio astronomy observations. *Science Radio Laboratories, Inc.*
- Marcus, L. (2012). A 21cm radio telescope for the cost-conscious. *Science Radio Laboratories, Inc*[Online], Available:<https://www.sbrac.org>.
- Menten, K. M. (1991). The discovery of a new very strong and widespread interstellar methanol maser line. *The American Astrophysical Society*. 1991ApJ...380L..75M.
- Michael, L. (2003). Horizon coordinate. [online], available:<http://www.google.co.zm/search?q=horizon+coordinate+system>.
- Millar, W. (2006). *The Amateur Astronomer's Introduction to the Celestial Sphere*. Cambridge University Press.
- O'Neil, K. K. (2001). Single dish calibration techniques at radio wavelengths. ASP Conference Series, Vol. , 2001:1–21.
- Pestalozz.R.M. (2007). Methanol masers as tools to study high-mass star formation. *2008 International Astronomical Union*.
- Pillay, A. (2012). The development of a transit radio telescope at the hydrogen line frequency. Available: *Department of Electronic Engineering in the Faculty of Engineering and The Built Environment at the Durban University of Technology*.
- Preethi, P. (2016). molecular lines in radio astronomy. haystack observatory. [Online], Available:<http://www.haystack.mit.edu>.
- Preethi, P., Shute, P. A., Thomas, C. K., Battersby, C., and Sterling, S. (2008). Class i methanol masers: Signposts of star formation? *The Astronomical Journal*, 135(5):1718.
- Primesat.eu/lbns (2017). Lbns. lnb universal lbns, single, twin, quad, quatro and octo lbns. [Online], Available:http://www.primesat.eu/lbns_satellite_lnb.php.
- Rohlfs, K., Wilson, T. L., and Huttemeister, S. (2009). *Tools of radio astronomy*, volume Astronomy and astrophysics library. Springer, 5th ed edition.
- Rouse, M. (June, 2017). Azimuth-and-elevation. [Online] Available:<http://searchcio-midmarket.techtargt.com/definition/azimuth-and-elevation>.
- Sanna, A., Menten, K., Carrasco, G. C., Reid, M. J., Ellingsen, S. P., Brunthaler, A., Moscadelli, L., Cesaroni, R., and Krishnan, V. (2015). The environment of the strongest galactic methanol maser. *The Astrophysical Journal*, 804(1).
- Seeber, B. (2014). Gnu radio tutorials, ettus research. [Online], Available: https://files.ettus.com/tutorials/labs/Lab_1-5.pdf.

- Sobolev, A. M. (2007). Astrophysical masers and their environments, *proc. iau. IAU Symposium, 242, 81*.
- Sourav, K. S. and Joydeep, B. (2011). Portable radio telescope. *Indian Institute of Science Education and Research – Kolkata* [Online], Available : <http://www.researchgate.net>.
- Storey, J. V. and Lloyd, J. P. (1993). A radio telescope for undergraduate teaching. *Proceedings of the Astronomical Society of Australia*, Vol. 10, Issue 3(p.225):163–166.
- Tarif, R. (2016). Solar drift scan technique. [Online], available :<http://astronomylog.wordpress.com/Solar-drift-scans-technique/>.
- www.airspy.com (2017). Airspy mini – the ultimate performance in a dongle form factor.
- Zubair, M., Haider, Z., Khan, S. A., and Naisir, J. (2011). Atmospheric influences on satellite communications. *COMSATS Institute of Information Technology, Islamabad (1,2,3)*, *COMSATS Institute of Information Technology, Abbott Abad (4)*, ISSN 0033-2097, R. 87 NR 5/2011(p.264).